INFLUENCE OF CLIMATE AND RESERVOIR OPERATIONS ON THE THERMAL STRUCTURE AND RELEASED WATER TEMPERATURES OF A MONOMICTIC RESERVOIR

Maurice Alfonso Duka

September 2021

Department of Civil and Environmental Engineering
Graduate School of Urban Environmental Sciences
Tokyo Metropolitan University

INFLUENCE OF CLIMATE AND RESERVOIR OPERATIONS ON THE THERMAL STRUCTURE AND RELEASED WATER TEMPERATURES OF A MONOMICTIC RESERVOIR

By

Maurice Alfonso Duka

A dissertation submitted in partial fulfillment of the requirements for the degree of
Doctor of Philosophy in Civil and Environmental Engineering

Department of Civil and Environmental Engineering
Graduate School of Urban Environmental Sciences
Tokyo Metropolitan University

Tokyo, Japan

September 2021

GUIDANCE COMMITTEE:

Dr. Katsuhide YOKOYAMA
Advisor/Chair of Guidance Committee
Professor, Environmental Hydraulics Laboratory
Department of Civil and Environmental Engineering
Graduate School of Urban Environmental Sciences
Tokyo Metropolitan University

Dr. Yoshiyuki IMAMURA
Professor, Hydrology Laboratory
Department of Civil and Environmental Engineering
Graduate School of Urban Environmental Sciences
Tokyo Metropolitan University

Dr. Tadaharu ISHIKAWA
Professor Emeritus
Department of Environmental Science and Technology
Interdisciplinary Graduate School of Science and Engineering
Tokyo Institute of Technology

Dr. Tetsuya SHINTANI
Associate Professor, Coastal Engineering Laboratory
Department of Civil and Environmental Engineering
Graduate School of Urban Environmental Sciences
Tokyo Metropolitan University

ABSTRACT

The temperature and thermal structure of the reservoir govern the turbidity current dynamics and phytoplankton movement, which are greatly related to sedimentation and eutrophication of the water body and its water quality status. Understanding therefore the factors affecting the thermal conditions of the reservoir such as climate and reservoir operation is key to water quality management. Climate warming poses serious impacts such as surface water warming, increased rates of evaporation and enhanced resistance to vertical mixing. On the other hand, reservoir operations as controlled by hydraulic facilities can vary the thermal responses of the water body. For example, conventional deep penstock withdrawal (DPW) promotes warming of the water profile while shallow releases from the selective withdrawal (SW) can strengthen the thermocline. Additionally, vertical curtains (VC) can be installed in the upstream reaches of the reservoir, which can promote surface cooling.

The Ogouchi Reservoir in Japan was chosen as the study site as it had apparently experienced climate warming between 1959 and 2016 and its operation had transitioned into three periods namely, Periods A (DPW, 1957-1991), B (SW and no VC, 1992-2001) and C (SW and VC, 2002-2016). The general objective of the study is to clarify the effects of climate and the different operations on the thermal structure and outflow temperatures of the reservoir. The long-term data of reservoir temperatures were analyzed in comparison with climate parameters and several thermal indices were quantified to describe the thermal stratification. Furthermore, numerical simulation was carried out to determine the effects of the facilities on both the in-reservoir and outflow temperatures, in the hope to evaluate the necessary method of management for these thermal properties.

This dissertation is composed of six chapters.

Chapter 1 is the introduction that provides the research background, which includes the thermal mechanisms in lakes and reservoirs, thermal classification of lakes, seasonal stratification of a monomictic reservoir and the issues and problems faced by water supply reservoirs. Literatures related to thermal structure and outflow temperatures of reservoirs as affected by climate and management were also reviewed.

Chapter 2 provides the methodology, which comprises the study area and the data analysis and numerical simulation. For the data analysis, the climate and reservoir properties were subjected to statistical tests such as Mann-Kendall, Kruskal-Wallis, rank-

sum and correlation. Different stratification parameters were also computed to quantitatively describe the reservoir's thermal condition such as Heat Content (Q), Brunt-Väisälä Frequency (N^2), Thermocline Strength Index (TSI) and Schmidt Stability Index (SSI). For the simulation, Fantom Refined was used to analyze the thermo-hydrodynamics of the reservoir. This simulator uses the equations of continuity and 3-D Navier-Stokes with incompressible and Boussinesq approximation alongside temperature transport, which were discretized based on a collocated finite-volume method. The k-ω was adopted for the turbulence closure model based on the Generic Length Scale Model. Uniform grids were set in the horizontal and the vertical. The time step was set at 20 s. The hourly river and weather data served as the boundary conditions. The vertical temperature profile and the water level were set as the initial condition. The VC was modeled as an impermeable cell face with its upper edge moving with water level.

Chapter 3 presents the long-term trends of climatic parameters such as air temperature, rainfall and wind speed, together with the results of the analysis of the distribution of water temperatures during the three periods. Although annual temperatures were increasing, the surface water temperatures were decreasing due to the shift in facilities. Period A produced warmer profiles and exhibited higher heat content (Q), in comparison with Periods B and C. It was found that the varying operations bear a stronger influence on the reservoir's water temperatures than climate change itself.

Chapter 4 discusses the seasonal variation of thermal stratification under different operating schemes. The N^2 plots show that Periods B and C have higher stability and stronger thermocline than Period A. Highest stability in terms of SSI is found in Period C (SW and VC) for Aug-Sep and Oct-Nov while the strongest thermocline in terms of TSI is observed in Period B (purely SW) for Apr-Jul and Aug-Sep. Period A (DPW) exhibited large thermal dispersion while Periods B and C showed narrower epilimnion. Longer duration of stratification is associated with shallow withdrawals (B and C). The shift in operation has caused the significant differences of stratification characteristics among periods.

Chapter 5 covers the application in the three-dimensional simulation of in-reservoir and outflow temperatures. For setting up the outflow for the SW, the Modified Gaussian Method Distribution (MGDM) is tested and compared with conventional Uniform Distribution Method (UDM). Results showed that MGDM can reproduce the two thermal properties more reasonably than UDM. The simulation results of three cases

corresponding to the three periods of operations have confirmed the significant differences in thermal distribution among the periods, as shown in Chapter 3 and 4. Furthermore, the SW case without and with the curtain, representing Periods B and C, respectively can mitigate the cold water pollution, which is rather manifested in the case of DPW, representing Period A. Lastly, with the application of MGDM to the 3-D model, sensitivity analyses were carried out by varying the SW intake levels considering the scenarios of with and without the VC, in order to evaluate the necessary combined operation method to regulate the reservoir temperatures. On average, lowering the intake gate of the SW results in a temperature drop of outflows by 1.6 to 1.9°C.

Chapter 6 provides the summary, conclusions and recommendations for future studies.

PREFACE

The completion of this dissertation would not be possible without the assistance and support of the people who have been with me throughout this Ph.D. journey.

I offer my sincerest thanks to my supervisor, Yokoyama-Sensei who has patiently guided me for three years. I am forever indebted for the opportunity to study under you. I thought at first I already had enough writing and analytical skills necessary for a doctorate degree. But I realized that I have to improve more, work harder and think more critically. I promised during my application for scholarship that I will be do my very best as your Ph.D. student and I hope that I did not disappoint you as I end this chapter in my study. Thank you for always accommodating the students from UPLB to study and learn at TMU. I am excited to work with you again in the future, do study together and write more journal papers. This Ph.D. journey has been the most productive so far in my academic life.

To Shintani-Sensei, I am grateful for your guidance and constant encouragement. I truly appreciate the moments where I learned a lot from your wisdom and compassionate words. I had thoughts of quitting my Ph.D. many times but your words comforted me. I am hoping to work with you in the future so that I could learn more about numerical simulation. I will do my best so that my students would appreciate the wonders of numerical simulation through Fantom Refined.

Likewise, I thank Imamura-Sensei and Ishikawa-Sensei for the constructive comments and suggestions that definitely helped improve my thesis. It was a great honor to be under your guidance.

I would like to thank the Tokyo Metropolitan Government for my scholarship-The Tokyo Human Resources Fund for City Development. Thanks also to the Bureau of Waterworks for entrusting the data of the Ogouchi Reservoir.

To the people at the International Office, especially Mayu-san and Suzuki-san, thanks for helping me out in my concerns as a foreign student.

To Ueno-Sensei and Gubash-Sensei, thank you for your support and encouragement.

To Masuzaki-san, I am always indebted for your patience to help me out despite the language barrier. I should have put more effort into learning Japanese so that I could have interacted with you more and heard your joyful stories.

To Ryohei, thanks for the many memories during our travels and dinners. I could have not survived in Japan without you being my tutor, my classmate and my bestfriend.

To Yuta, Hiroo and Ryuta, thank you for making time for me here in Japan.

To Neri and Charles, my pseudo-batchmates, thanks for all the wonderful memories, stories and late night talks. I am very happy that our relationship has evolved from you being my students before to being my colleagues and friends now.

To the members of the hydraulics and coastal laboratories: Iwamoto-san, Iguchi, Li-san, Shou-chan, Yuto, Koki, Kazuma, Chika-chan, Kota, Li-kun, Haruka, Satoshi, Iwama, Gen, Tsubasa, Reden, Hieu, Kirana, JC, Veera, Lett-san, Nay-kun, Pan-san,

Hashimoto-san, Toru and Katsunori, thank you for the friendship and all the wonderful memories.

To my fellow Filipino scholars: Jean, Lyndon, Mike, Ken, John, Lance, Daryl and Joval, thank you for the memories especially in Live Square.

To my colleagues at the LWRD: Mam Rose, Ate Mona, Sir Roger, Sir Ella, Sir Rory, Sir Ruben, Sir Tony, Jeric, Telle, Jeff, Jeph, Ann and Boyet, thank you for the constant encouragement and assistance to me.

To Jonathan Lasco, thank you for the friendship as we shared our struggles in our Ph.D. I am excited to work with you as soon as we finish our studies. Thanks for helping me out a lot, especially for the statistical analysis of my data. My thesis could have not improved without your suggestions. I wish you all the best in your career and your married life.

To my vegetarian friends both in Japan and in my home country, thank you for being my second family, who inspired and supported me.

To my family: Mama, Papa, Ate Nene, Roy, Rap-Rap, Law-Law and Clark, uncles, aunties, cousins and my dearly departed ancestors, Lolo Indo, Lola Piding, Lolo Amo and Lola Loleng, this dissertation is dedicated to them, the source of my strength. I hope I made our family happy and proud.

Lastly, to the Almighty, thank you for gracing me with light and brightness. I may not be Your best child, but I promise to be Your most filial and diligent one.

Maurice Alfonso Duka

September 2021

PUBLICATIONS

2019

1. Duka, M.A., Yokoyama, K., Shintani, T., Iguchi, K., Iwasaki, H., Ueno, T., Chiba, T., 2019. Influence of water control facilities on thermal stratification of Ogouchi Reservoir for 58 years. J. JSCE, Ser. B1 (Hydraul. Eng.) 75, 685–690. https://doi.org/https://doi.org/10.2208/jscejhe.75.2_I_685

2020

1. Duka, M.A., Shintani, T., Yokoyama, K., 2020. Thermal stratification responses of a monomictic reservoir under different seasons and operation schemes. Sci. Total Environ. 767, 1–15. https://doi.org/10.1016/j.scitotenv.2020.144423

2. Somsook, K., Duka, M.A., Olap, N.A., Casila, J.C.C., Yokoyama, K., 2020. Direct measurement of secondary circulation in a meandering macrotidal estuary. Science of the Total Environment. Vol. 739, pp. 139503. https://doi.org/10.1016/ j.scitotenv.2020.139503.

2021

1. Duka, M.A., Shintani, T., Yokoyama, K., 2021. Mediating the effects of climate on the temperature and thermal structure of a monomictic reservoir through use of hydraulic facilities. Water (Switzerland) 13, 1128. https://doi.org/10.3390/w13081128

2. Somsook, K., Azhikodan, G., Duka, M.A., Yokoyama, K., 2021. Riverbed fluctuation and erosion property of cohesive sediment based on long-term topographic surveys in a macrotidal estuary. Reg. Stud. Mar. Sci. 45, 101848. https://doi.org/10.1016/j.rsma.2021.101848

3. Somsook, K., Olap, N.A., Duka, M.A., Veerapaga, N., Shintani, T., Yokoyama, K., 2021. Analysis of interaction between morphology and flow structure in a meandering macro-tidal estuary using 3-D hydrodynamic modeling. Estuarine Coastal and Shelf Science, Under Review.

4. Duka, M.A., Yokoyama, K., Shintani, T., Sakai, H., Koizumi, A., 2021. Application of the modified Gaussian distribution method to reproduce the water temperatures of the Ogouchi Reservoir. J. JSCE, Ser. B1 (Hydraul. Eng.), Accepted.

5. Gunay, C.J.C., Duka, M.A., Yokoyama, K., Sakai, H., Koizumi, A., Sakai, K., Kuroki, N., 2021. Half-century analysis of climate trends and soil water storage in a steep forested catchment in Kanto Metropolitan Area. J. JSCE, Ser. B1 (Hydraul. Eng.), Accepted.

CONFERENCE PRESENTATIONS

2019

1. Duka, M.A., Yokoyama, K., Shintani, T., Iguchi, K., 2019. Effect of selective withdrawal and vertical curtain on reservoir sedimentation: a 3-D numerical simulation approach. Proc. of the 11th River, Coastal and Estuarine Morphodynamics (RCEM) Symposium. p. 54.

2. Gunay, C.J.C., Duka, M.A., Yokoyama, K., 2019. Long-term analysis of sediment yield in Ogouchi Watershed. Proc. of the 11th River, Coastal and Estuarine Morphodynamics (RCEM) Symposium. p. 125.

3. Iwamoto, N., Duka, M.A., Shintani, T., Yokoyama, K., 2019. Three-dimensional numerical simulation for a developing Asian country: a case study for Pasig River estuary linking Laguna Lake and Manila Bay, Philippines. JSCE Kanto Region.

TABLE OF CONTENTS

LIST OF FIGURES

LIST OF TABLES

CHAPTER 1

Introduction

1.1 Background of the Study

1.1.1 Thermal Mechanisms of Inland Water Bodies

The total heat content of inland water bodies such as lakes and reservoirs is the sum of the net radiation, latent heat, sensible heat and other heat components (**Fig. 1.1**). Radiation components include the net shortwave radiation from the sun and the net longwave radiation from the water body and the atmosphere. Sensible heat transfer between the water body and the atmosphere occurs with the combined processes of conduction and convection, which are affected by the wind. Latent heat transfer, on the other hand, is the thermal process associated with phase change during evaporation. Other heat components include the advection through the inflow and outflow processes of streamflow, precipitation and groundwater flow (Ragotzkie, 1978). For the ground and sediment heat flux, the thermal energy is absorbed in summer but released during winter.

Retention time also influences the heat content of lakes and reservoirs. Higher retention time means more opportunity for the heat to be stored in the water body. On the other hand, lower values of retention time as characterized by large inflows and outflows is associated with higher degree of mixing.

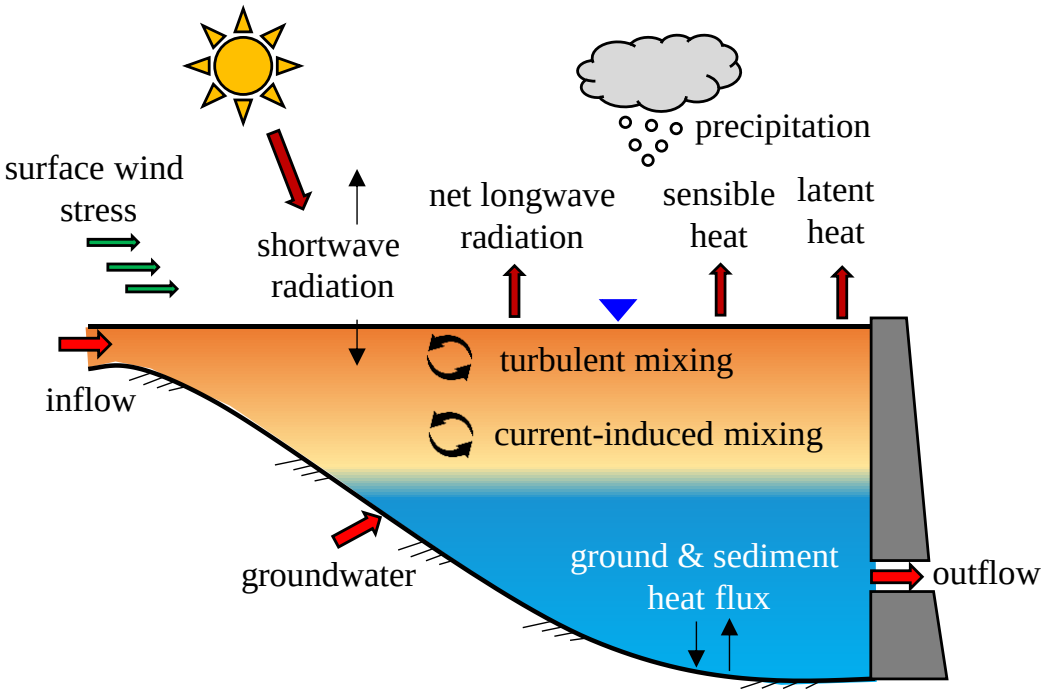

Figure 1.1. Heat balance components in a reservoir.

1.1.2 Thermal Classifications of Lakes

The incoming solar radiation is the main driver of thermal responses of inland waters. The solar radiation received by earth varies with season and latitude; hence, the thermal stratification and circulation processes of lakes and reservoirs also vary. As a result, these water bodies can be thermally classified as shown in **Fig. 1.2**. Located in the Tropical Region, the high-altitude polymictic and the low-altitude oligomictic lakes exhibit several mixing episodes throughout the year. On the other hand, amictic lakes, which are located in Polar Regions, are ice-covered all year round. Further, dimictic inland waters circulate two times a year, specifically in spring and autumn. Cold monomictic water bodies in the Arctic Region mix during summer while warm monomictic lakes and reservoirs in the Temperate Region are fully mixed during winter but stratified during summer (Wetzel, 2001).

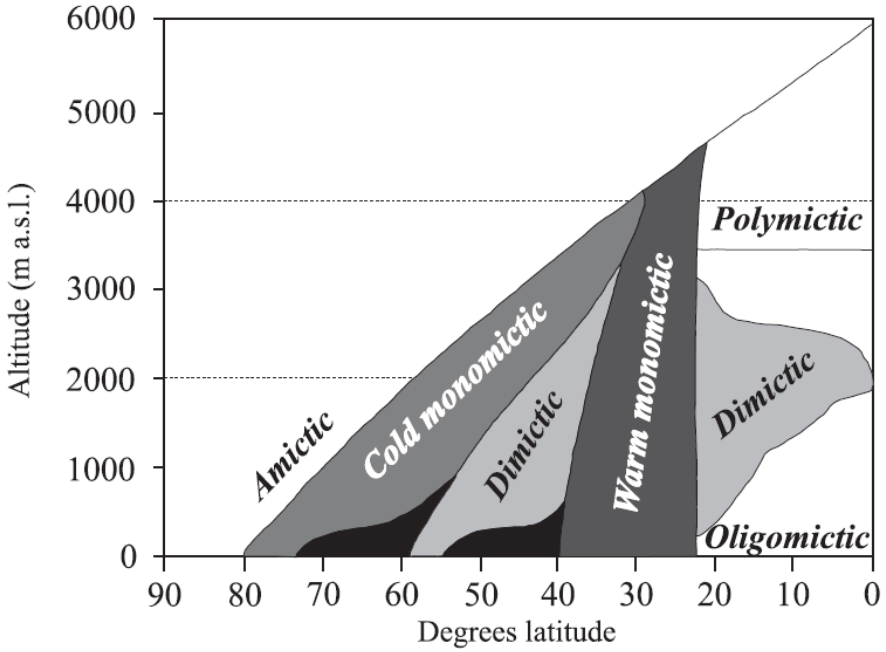

Figure 1.2. Wetzel's lake thermal classification based on latitude and altitude and the lake's mixing condition. (Skowron, 2009).

1.1.3 Seasonal Cycle of Stratification

For a warm monomictic reservoir, the seasonal cycle of stratification, overturn and mixing are shown in **Fig. 1.3**. During spring and summer where solar heating intensifies, the reservoir becomes thermally stratified. The difference of heating received

vertically through the reservoir results in density differences, with the upper layer being less dense than the bottom. Wind plays an important role in inducing the mixing in the upper layer of the reservoir. The warm upper layer is called the epilimnion while the cold bottom one is the hypolimnion. These two layers are separated by the strong density gradients of the thermocline or metalimnion (middle layer) that prevents the transport of materials between them. As the temperature drops during autumn, the epilimnion becomes colder and denser than the hypolimnion, hence overturn occurs as induced by cold water mixing. During winter, isothermal conditions exist in the water body and full mixing is observed as further facilitated by the wind.

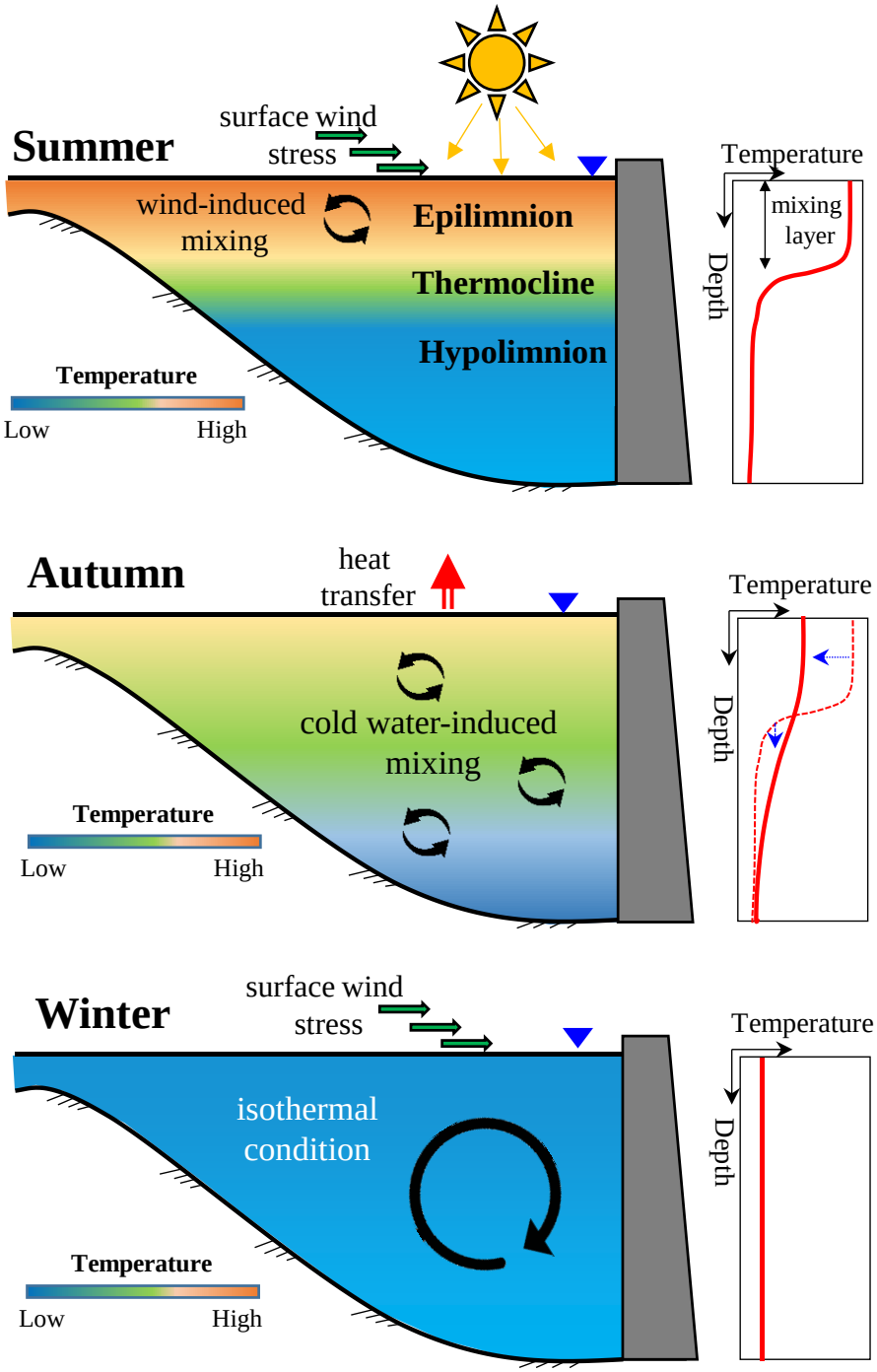

Figure 1.3. Seasonal cycle of stratification in a warm monomictic reservoir.

1.1.4 Problems and Issues in Water Supply Reservoirs

Water supply reservoirs currently face several water quality problems such as what is illustrated in **Fig. 1.4**. For example, eutrophication or the proliferation of phytoplankton is detrimental to the water purification system as this entails an additional load for the water treatment process (Smith et al., 2002). These filtered organic materials

also need to be managed properly in order to prevent problems on foul odor. Reservoir managers should therefore implement some intervention measures, for instance, by controlling the water temperatures and the current flow. With the plethora of studies on eutrophication in lakes and reservoirs, plenty of options are also available for mitigating this problem.

Furthermore, sedimentation has become one of the persistent problems of many reservoirs. Highly turbid waters from floods increase the sediment load in the water body, leading to the decrease in water storage capacity. The release of turbid waters with high concentration of fine sediments can also impair the gill functions of fish by clogging into their gill surfaces (Muraoka et al., 2011). Conservation measures in the watershed and some hydraulic interventions in the reservoir are therefore necessary. Likewise, releasing water from the cold and hypoxic hypolimnion may result in the pollution of the downstream ecosystem (Olden and Naiman, 2010). Although warm water releases may be advantageous for recreation purposes downstream of the dam, this may also give rise to warm water pollution affecting fish survival. Counter-measures should therefore be implemented in order to manage the water quality of the released waters.

These existing water quality problems are expected to worsen with the changing climate. With the increase in rainfall intensity and frequency of storm events, the rates of erosion and sedimentation will also likely increase. Further, frequent floods will transport more nutrients in the reservoir, which will aid in the eutrophication process. As the climate continues to warm, the thermal stratification of reservoirs will also intensify. This will exacerbate hypolimnetic hypoxia and the management of released waters could be troublesome. As mentioned previously, many studies have already dealt with the eutrophication of lakes and reservoirs. Climate-change related studies are also abundant specifically in lakes, which were done in terms of long-term data analyses and numerical simulations. For reservoirs however, most of the existing climate-change related studies deal with numerical simulations but long-term analyses based on actual data are limited. This present study therefore focuses on analyzing the actual effect of climate warming on the thermal conditions of the reservoir and in identifying the measures needed to regulate both the in-reservoir and released water temperatures.

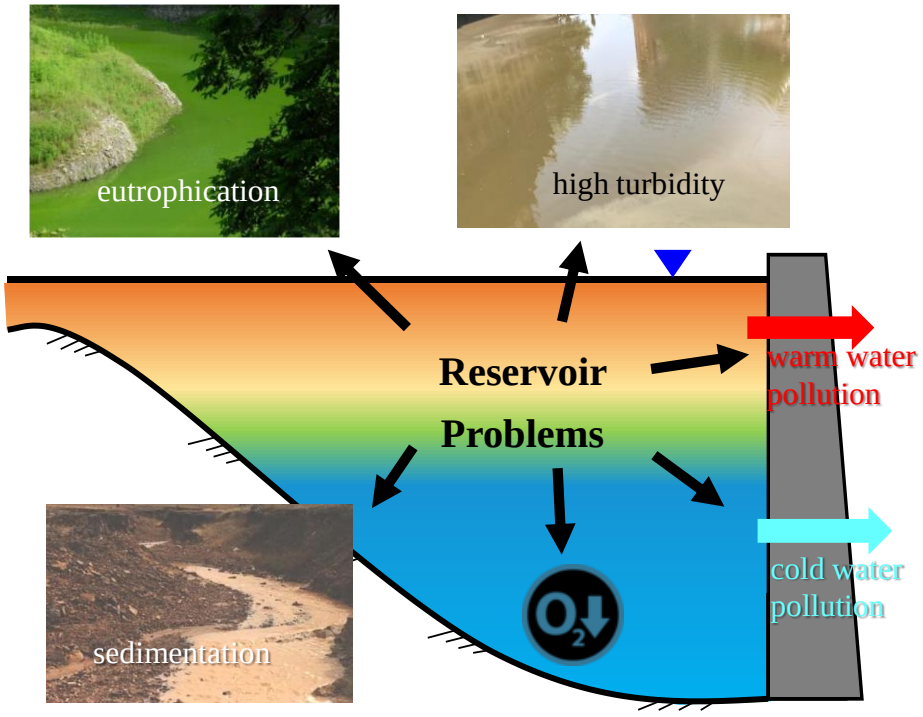

Figure 1.4. Issues and problems faced by water supply reservoirs.

1.2 Previous studies

1.2.1 Introduction

Water temperature plays an essential role in the biological and chemical processes and its overall water quality status of reservoirs. For example, the dissolved oxygen, which is fundamental for the survival and growth of aquatic organisms, is highly dependent on temperature. Furthermore, thermal stratification and circulation characteristics influence nutrient cycling and phytoplankton production. Understanding therefore, the factors affecting the thermal conditions of the reservoir such as climate and reservoir operation is key to water quality management. Climate warming poses serious impacts such as surface water warming, increased rates of evaporation and enhanced resistance to vertical mixing. On the other hand, reservoir operations as controlled by hydraulic facilities can vary the thermal responses of the water body. For instance, conventional deep penstock withdrawal (DPW) promotes warming of the water profile while shallow releases from the selective withdrawal (SW) can strengthen the thermocline. Additionally, vertical curtains (VC) can be installed in the upstream reaches of the reservoir, which can promote surface cooling.

1.2.2 Effect of Climate Warming on Temperatures of Lakes and Reservoirs

Climate warming poses negative impacts on the thermal condition of inland water bodies such as lakes and reservoirs. In terms of surface water temperatures (SWT) for example, long term warming trends in lakes were found to be directly associated with the rising trends in global air temperature (Arvola et al., 2009; Coats et al., 2006; Rose et al., 2016; Schmid et al., 2014). Similar findings were detailed in the studies of Ficker et al. (2017), Schneider & Hook (2010), O'Reilly et al. (2015), Woolway et al. (2019) and Woolway & Merchant (2019) for various lakes worldwide. The rise in SWT could result in: a) increased rates in evaporation (Helfer et al., 2012; Trumpickas et al., 2009), b) elevated rates in bacterial and phytoplankton activities (Woolway et al., 2019), c) enhanced thermal resistance to vertical mixing (Butcher et al., 2015), d) shorter period of ice cover specifically for dimictic lakes (Arvola et al., 2009) and e) proliferation and invasion of warm-water aquatic species (Trumpickas et al., 2009). Climate change studies on lakes have become overly popular in recent years. While long-term analysis of actual data of climate and lake temperatures are highly lauded, a considerable amount of

prudence must be observed especially when making climate projections as some studies produce extremely unrealistic results.

For reservoirs, a number of recent literatures elaborate the responses of this water body to climate change. For example, Lake Dillon in Colorado, USA exhibited notable increase in SWT, heat budget and stability due to climate warming (Lewis et al., 2019). In Lake Qiandahou in China, the increase in air temperature was associated with stronger dissolved oxygen stratification and decrease in oxycline depth (Zhang et al., 2015). Several studies also used 2-D modeling through the CE-QUAL-W2 to evaluate the effect of climate warming on various reservoirs. For instance, the hyper-eutrophic Hodges Reservoir in the USA is projected to experience an increase in evaporation rates, stronger stratification and overall water column warming (Lee et al., 2018). The Aidoghmoush Reservoir in Iran could be subject not only to the increase in both surface and bottom water temperatures but also in its total dissolved solids (TDS) (Azadi et al., 2019). The water quality of the Hsinshan Reservoir in Taiwan is also projected to deteriorate with the reduction of dissolved oxygen concentrations at the bottom layer and the increase in phosphorus concentration (Chang et al., 2015). Interventions are therefore needed to mitigate the effects of climate warming on reservoirs as they are one of the most significant sources of freshwater in the world. It has to be emphasized however that most of these reservoir studies were based from numerical simulations and that long-term analyses are very few.

1.2.3 Effect of Facilities on Reservoir's Thermal Structure

Reservoirs behave differently compared to natural lakes. While lakes are typically restricted by surface outflows, reservoirs can deliberately discharge at several locations throughout its depth (Martin and Arneson, 1978). Lakes also characteristically have lower flushing rates and longer hydraulic retention period than reservoirs (Hayes et al., 2017). The two types of inland water bodies, therefore, generally have considerably different temperature dynamics and respond differently to climate. Reservoirs are predicted from a conceptual model to have a robust capacity in mediating the effects of climate, especially when some water management practices are implemented (Hayes et al., 2017). One type of these management filters involves the use of variable withdrawal techniques and the installation of some hydraulic facilities that can modify the thermal structure of the reservoir. In fact, one study revealed that management operation of reservoir with

multiple outlets is considered to be the main driver of the thermal conditions of this water body (Moreno-Ostos et al., 2008). Another study also showed that dynamic withdrawals in reservoir can potentially mitigate the effects of climate change (Feldbauer et al., 2020). Nowadays, selective withdrawal (SW) systems can be retrofitted in reservoirs by allowing warm water releases from the epilimnion while vertical curtains (VC) can be installed in the upstream reaches to control the direct inflow of river water into the main reservoir body. Determining the combined effects of these two facilities on the reservoir's thermal regime is particularly of high interest, as most available literature deal only with their individual functions.

SW systems are installed primarily to address the problem of cold water pollution. Conventional hydropower dams usually abstract water from the reservoir's deeper layer (hypolimnion) and this process enables the release of cold water, which is detrimental to the downstream aquatic ecosystem (Olden and Naiman, 2010). The installation of SW enables the release of water from the warm layers of the reservoir to counter the effects of cold water pollution and to avoid the low dissolved concentrations downstream. The operation of SW facility in reservoirs needs to be optimized so that suitable water temperatures are maintained downstream (Rheinheimer et al., 2015; Weber et al., 2017), not only during cold periods but also during summer. In terms of the thermal structure of the reservoir, several studies through numerical simulations point out that surface releases through the SW would increase the thermal stability of the reservoir while bottom releases would induce the warming of the entire water column (Çalişkan and Elçi, 2009; Ma et al., 2008; Zouabi-Aloui et al., 2015). One example of a SW facility is a retrofit to an existing water supply and hydropower dam in the Ogouchi Reservoir in Japan, allowing epilimnetic releases only. The function of this facility is not only limited for regulating outflow temperatures but also for releasing the highly turbid water in the reservoir during times of flood. Long-term records of water temperature profiles are available for this reservoir, which can be utilized to evaluate and compare the actual reservoir's thermal responses when operated through hypolimnetic withdrawals by penstock or through epilimnetic releases by SW.

The VC, on the other hand, are structures installed across the river mouths in order to prevent the direct intrusion of river water into the reservoir (Asaeda et al., 2001). The VC can also be installed in some other sections of the reservoirs other than the river mouths. It is called many names such as vertical weir curtain (Park et al., 2017), floating

curtain weirs (Kumar Dutta et al., 2019), flexible curtain (Johnson et al., 1993) and temperature control device (Johnson et al., 1991), among others. Some studies discussed the effectiveness of the curtain for regulating outflow temperature for fishery purposes (Deng et al., 2011), controlling algal blooms 33 (Asaeda et al., 2001; Kumar Dutta et al., 2019) and mitigating the occurrence of cyanobacteria and metabolites (Park et al., 2017). In the Ogouchi Reservoir, the curtains are installed across river mouths and it was found that using them aided in lowering the surface water temperature of the reservoir's upstream section (Takahashi, 2008) and modifying the temperature and velocity distributions before and after the VC (Niiyama et al., 2010). However, the mechanism of this surface cooling phenomenon due to the VC and the effect of combining VC's operation with SW to the reservoir's thermal structure have not yet been elaborated.

1.2.4 Management of In-Reservoir and Outflow Temperatures

Thermal stratification is a phenomenon in water bodies such as lakes and reservoirs where the epilimnion and hypolimnion are separated by strong vertical density gradients (metalimnion or thermocline) as a result of seasonal temperature variations (Boehrer and Schultze, 2008; James et al., 2017). Stratification plays a vital role in reservoir water quality management, as it can significantly influence the hydrodynamics and water quality regimes (Lee et al., 2013), eutrophication and sediment transport processes (Scheu et al., 2015; Zhang et al., 2020) and nutrient and phytoplankton dynamics (Liu et al., 2009). During periods of long and sustained stratification, the hypolimnion could experience anoxia or the depletion of the dissolved oxygen leading to further water quality deterioration (Beutel et al., 2007).

The different modes of reservoir operation do not only influence the reservoir's thermal structure but the outflow temperatures. The creation of dams and reservoirs can significantly alter the conditions of the downstream river environment. For example, if the released temperatures from dams do not match the temperatures of the river downstream, severe impacts will be endured by its aquatic ecosystem. This usually happens across temperate regions in reservoirs that abstract water from deep hypolimnetic layers (Olden and Naiman, 2010). During summer where thermal stratification is at its peak, the dam could discharge very cold waters leading to cold water pollution. The reverse happens during winter where reservoir waters may be warmer than the downstream; hence warm water pollution may occur. This had been the persistent

problem in the case of the Ogouchi Reservoir, which had operated through deep penstock withdrawal (DPW) since its construction in 1957. Until 1992, the Ogouchi Reservoir managers adopted a technology through the use of the selective withdrawal (SW) facility in order to mitigate this problem. The motivation to shift the operation to using SW was rooted from the request of downstream fish farmers whose aquaculture operations were negatively affected by cold water pollution. Presently, the outflow temperatures are well-maintained to match with water temperatures of the Nippara River downstream of the Ogouchi Dam.

Understanding both the thermal structure and the released water temperature of the Ogouchi Reservoir is therefore necessary in order to implement a comprehensive and optimized water quality management.

1.3 Objectives of the Study

The general objective of the study is to clarify the effects of climate and reservoir operation on the thermal structure and the released water temperatures of a monomictic reservoir. Specifically, this study aims to:

1. Determine the influence of climate on the temperatures of the reservoir with varying operation of facilities through long-term data analysis;
2. Provide a long-term and detailed seasonal analysis of the thermal stratification of the reservoir; and
3. Evaluate the effect of the operation of the different facilities on the in-reservoir and released water temperatures through the use of 3-D numerical simulation.

1.4 Outline of the Dissertation

This dissertation is composed of six chapters.

Chapter 1 is composed of the introduction that provides the research background and objectives of the study. Literatures related to thermal structure and outflow temperatures of reservoirs as affected by climate and management are also reviewed.

Chapter 2 provides the methodology, which includes the description of the study area and the data analysis and numerical simulation. For the data analysis, the climate and reservoir properties were subjected to statistical tests such as Mann-Kendall, Kruskal-Wallis, rank-sum and correlation. Different stratification parameters were also computed to describe quantitatively the reservoir's thermal condition, other than water temperature. For the simulation, Fantom Refined was used to analyze the in-reservoir and released water temperatures of the reservoir.

Chapter 3 presents the long-term trends of climatic parameters such as air temperature, rainfall and wind speed, together with the results of the analysis of the distribution of water temperatures during the three periods. Although annual temperatures were increasing, the surface water temperatures were decreasing due to the shift in facilities. Period A produced warmer profiles and exhibited higher heat content (Q), in comparison with Periods B and C. It was found that the varying operations bear a stronger influence on the reservoir's water temperatures than climate change itself.

Chapter 4 discusses the seasonal variation of thermal stratification under different operating schemes. The N^2 plots show that Periods B and C have higher stability and stronger thermocline than Period A. Highest stability in terms of SSI is found in Period C (SW and VC) for Aug-Sep and Oct-Nov while the strongest thermocline in terms of TSI is observed in Period B (purely SW) for Apr-Jul and Aug-Sep. Period A (DPW) exhibited large thermal dispersion while Periods B and C showed narrower epilimnion. Longer duration of stratification is associated with shallow withdrawals (B and C). The shift in operation has caused the significant differences of stratification characteristics among periods.

Chapter 5 covers the application in the three-dimensional simulation of in-reservoir and outflow temperatures. For setting up the outflow for the SW, the Modified Gaussian Method Distribution (MGDM) is tested and compared with conventional Uniform Distribution Method (UDM). Results showed that MGDM can reproduce the

two thermal properties more reasonably than UDM. The simulation results of three cases corresponding to the three periods of operations have confirmed the significant differences in thermal distribution among the periods, as shown in Chapter 4. Furthermore, the SW case without and with the curtain, representing Periods B and C, respectively can mitigate the cold water pollution, which is rather manifested in the case of DPW, representing Period A. Lastly, with the application of MGDM to the 3-D model, sensitivity analyses were carried out by varying the SW intake levels considering the scenarios of with and without the VC, in order to evaluate the necessary combined operation method to regulate the thermal structure and released water temperature of the reservoir.

Chapter 6 provides the summary, conclusions and recommendations for future studies.

CHAPTER 2

Methodology

2.1 Study Area Description

The Ogouchi Reservoir is located in Okutama Town, Tokyo, Japan with a catchment (**Fig. 2.1a**) of an area of 263 km^2. The annual average precipitation is 1,480 mm, where around 34% of this is received during the typhoon season in August and September. Three tributaries drain towards the reservoir, namely the Taba River, the Minetani River and the Kosuge River. A dam with height of 149 m and length of 353 m was constructed, making way for the creation of a monomictic reservoir with an effective storage capacity of 185 Mm^3 and a surface area of 4.25 km^2. The bathymetry of the reservoir is provided in **Fig. 2.1b** where the locations of the water control facilities and water quality observation point are indicated. The longitudinal section of the reservoir is given in **Fig. 2.1c**, showing the VC in the upstream and the SW system and the penstock portal downstream. The VCs at the mouth of the Taba River have depths of 2 and 10 m. Meanwhile, the outlet of the SW facility and the intake of the penstock are located about 40 m and 70 m below the normal water (NWL), respectively.

The Ogouchi Reservoir underwent three distinct periods of management and operation. Deep water releases were made through penstock from 1957 to 1991. Since penstock outflows led to cold water pollution, the operation was shifted to SW (**Fig. 2.2**) starting 1992, with the later addition of the VC (**Fig. 2.3**) in 2002 to mitigate the problem in eutrophication. This study thus highlights the three periods of operation based on the reservoir's data history namely, 1) Period A for the deep penstock withdrawal (DPW) for 1959-1991, 2) Period B for a purely SW operation for 1992-2001 and lastly, 3) Period C the combined operation of SW and VC for 2002-2016. The history of operation of facilities in the reservoir is summarized in **Table 2.1**.

The retention period from 1968 until 2015 is provided in **Fig 2.4**. The retention period of the reservoir is computed as the ratio of the volume of the water body and the annual outflow discharge through the dam. For the Ogouchi Reservoir, this value ranges from 0.40 to 1.24, with an average of 0.70. This means that water in the reservoir is replaced 1.5 times in a year, on average. Generally, the Ogouchi Reservoir would exhibit significantly stronger thermal stratification on years with higher retention period.

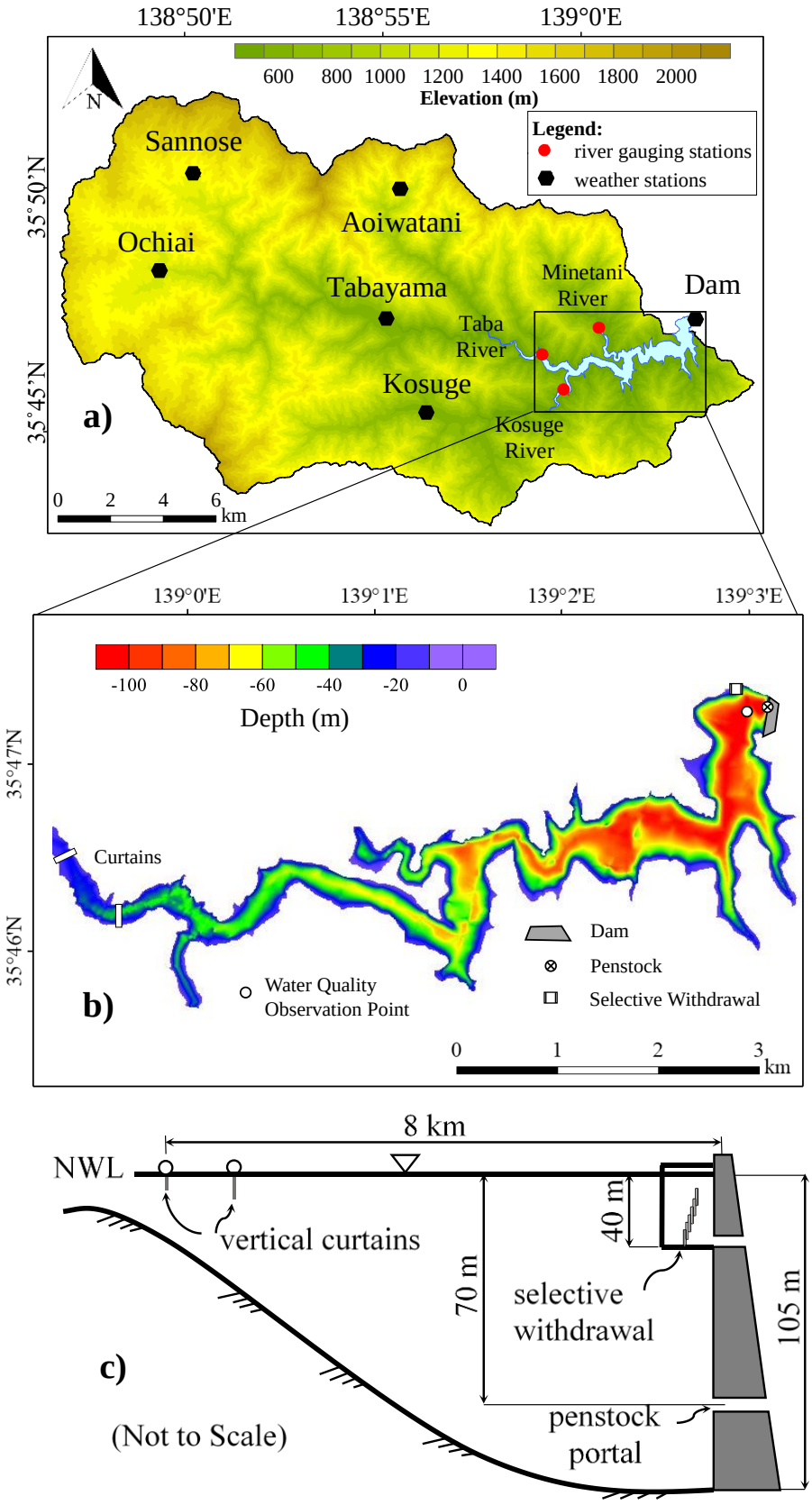

Figure 2.1. Maps of (a) the Ogouchi catchment, (b) reservoir bathymetry, and (c) dam and reservoir profile.

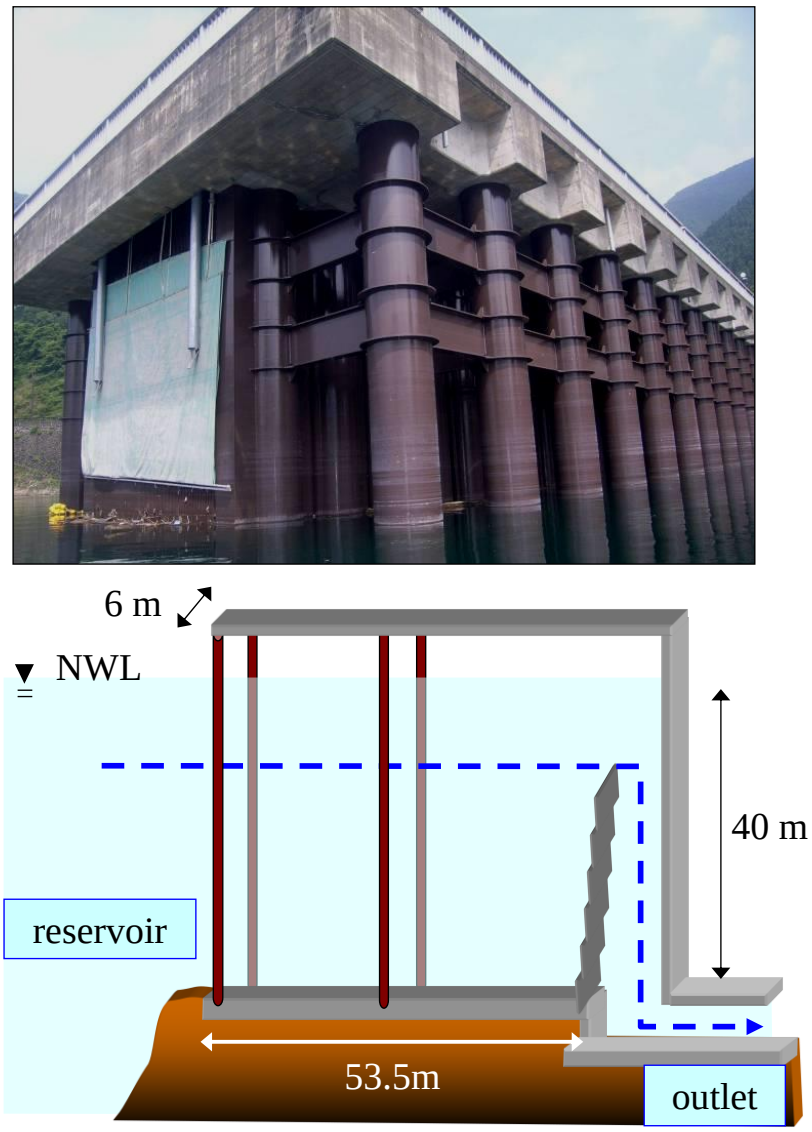

Figure 2.2. The selective withdrawal (SW) facility of the Ogouchi Reservoir (Niiyama, 2010b).

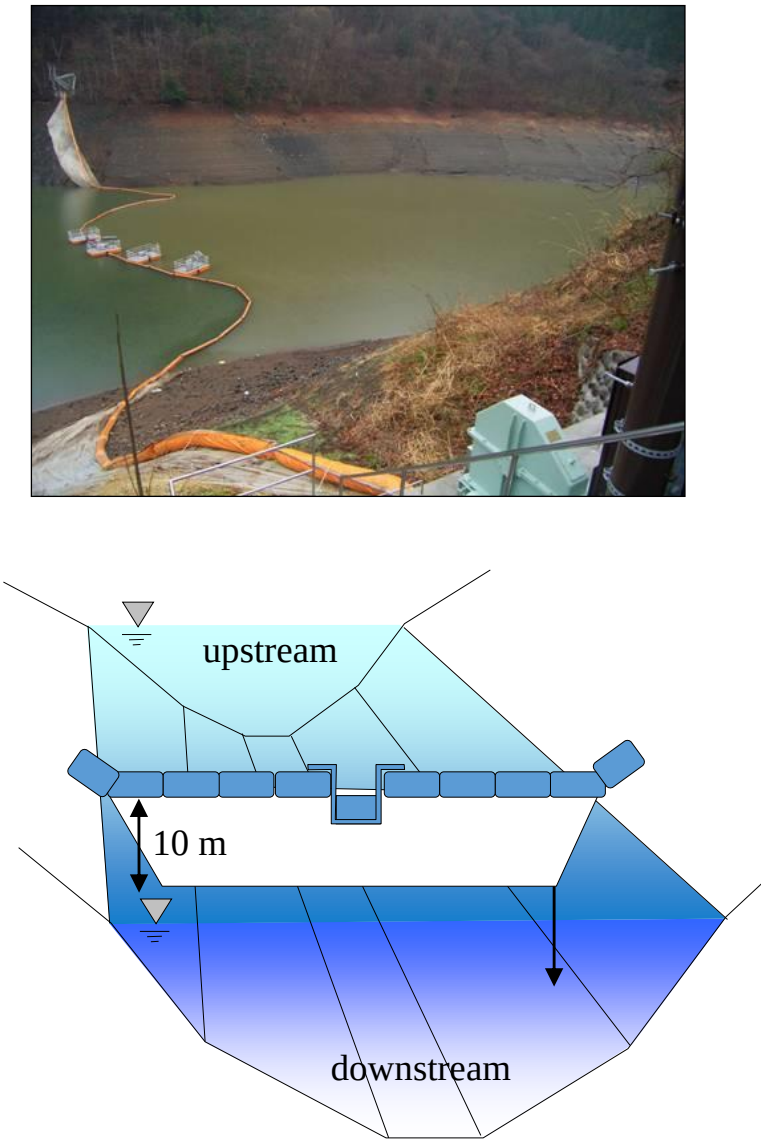

Figure 2.3. The 10-m deep vertical curtain (VC) facility across Taba River (Niiyama, 2010a).

Table 2.1. Description of the three periods of operation in the Ogouchi Reservoir from 1957 until the present.

Period	Years	Mode
A	1957-1991	DPW
B	1992-2001	SW and no VC
C	2002-present	SW and VC

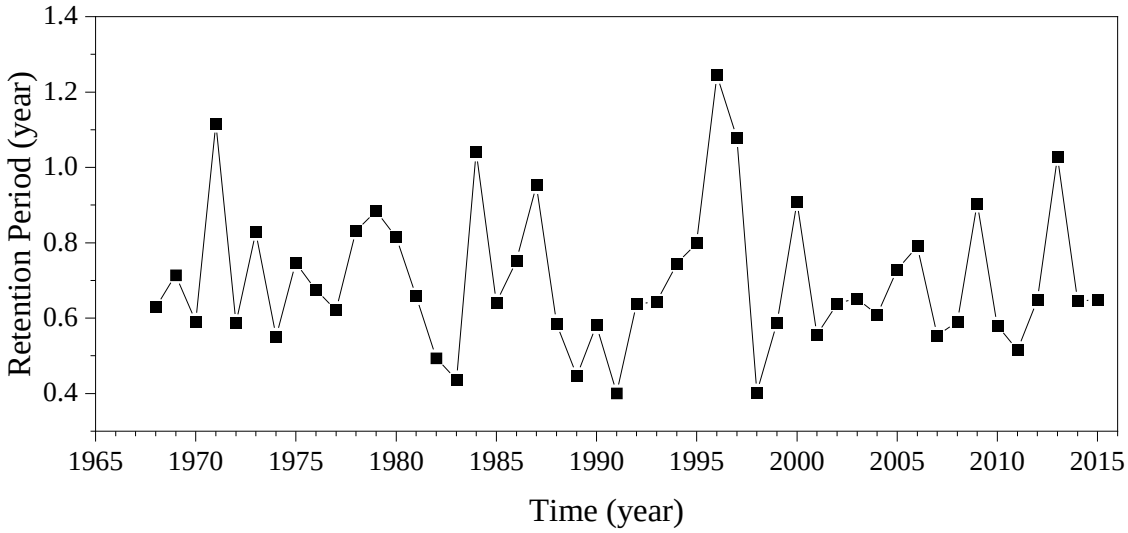

Figure 2.4. Retention period of the Ogouchi Reservoir from 1968 until 2015.

2.2 Data Analysis

2.2.1 Collection of Climate and Reservoir Data

Daily values of air temperature and wind speed were obtained from the dam station, while the rainfall values came from six observation stations (**Table 2.2**). While the dam station contains all three meteorological parameters, the other five stations only have precipitation records. These data are from the Automated Meteorological Data Acquisition System (AMeDAS) by the Japan Meteorological Agency.

Weekly monitoring records of reservoir temperatures are available from 1959 until 2001, while daily records can be accessed from 2003 until 2016 **(Table 2.2)** from the Bureau of Waterworks of the Tokyo Metropolitan Government. Raw temperature values from depths of 0, 10, 20, 30, and 70 m were examined. The temperatures at these depths were averaged.

Table 2.2. Long-term observational data of climate and reservoir temperatures.

Parameters	Station	Elevation (above msl)	Period Covered	Frequency
Air temperature (°C)	Dam	519 m	1959–2016	Daily
Precipitation (mm)	(1) Dam	519 m	1959–2016	Daily
	(2) Ochiai	1113 m	1959–2016	Daily
	(3) Tabayama	611 m	1959–2016	Daily
	(4) Kosuge	656 m	1959–2016	Daily
	(5) Aoiwatani	1217 m	1965–2016	Daily
	(6) Sannose	1268 m	1965–2016	Daily
Wind Speed (m s^{-1})	Dam	519 m	1977–2016	Daily
Water temperature profile (°C)	Upstream of Dam Wall		1959–2001 2003–2016	Weekly Daily

2.2.2 Methods of Statistical Analysis

The climate and reservoir temperature data were evaluated using the Mann-Kendall (M-K) test, Kruskal-Wallis test, Rank-sum test and Correlation test at a significance level α of 0.05.

M-K test (Kendall, 1975; Mann, 1945) is a non-parametric test used to detect long-term monotonic trends. The null hypothesis is that there is absence of a trend while the alternate hypothesis suggests a trend in the two-sided test or an upward or downward trend in the one-sided test (Zaointz, 2019). For the time series $x_1, \dots, x_n$, the M-K calculation begins by estimating the S statistic,

$$S = \sum_{i=1}^{n-1} \sum_{j=k+1}^{n} sgn(x_{j-} x_i) \tag{1}$$

The variance *var* is given by,

$$var = \frac{n(n-1)(2n+5) - \sum_t f_t(f_t-1)(f_t+5)}{18} \tag{2}$$

where *t* varies over the set of tied ranks and f_t is the frequency the rank t appears. The statistic S is standardized using z,

$$z = \begin{cases} \frac{S-1}{\sqrt{var}} & \rightarrow S > 0 \\ 0 & \rightarrow S = 0 \\ \frac{S+1}{\sqrt{var}} & \rightarrow S < 0 \end{cases} \tag{3}$$

Long-term trends were evaluated using the M-K test. A nonparametric estimate of the slope of the trend, called Sen's slope (Sen, 1968), is used in this study rather than that from regression based on the least-squares method. The M–K test was performed for the long-term data; henceforth, the magnitude of the slope is expressed in terms of Sen's slope. For short-term trends, i.e., for every period (A, B, and C), simple linear regression was carried out to determine the slopes of meteorological parameters. The long-term trends of surface water temperature (SWT) were also subjected to the M–K test and the subsequent results were compared with the trends in air temperature. Differences among the three periods of operation were evaluated using Kruskal–Wallis and rank-sum tests.

Kruskal-Wallis (K-W) test is a non-parametric test as an alternative to the one-way analysis of variance (Kruskal and Wallis, 1952). The null hypothesis is that all groups

have identical distribution while the alternative hypothesis is that at least one group has a different distribution. The H-statistic is computed as

$$H = \left[\frac{12}{n_T(n_T+1)}\sum_{i=1}^{k}\frac{R_i^2}{n_i}\right] - 3(n_T+1) \tag{4}$$

where $n_T = \sum_{i=1}^{k} n_i$ = total number of observations in all samples, k is the number of populations, n_i – the number of observations in sample i and R_i is the sum of ranks for sample i. The *H*-statistic is compared with the chi-square value where if *H* is greater than the latter, the null hypothesis is rejected; otherwise fail to reject. K-W test is used to evaluate the similarity or differences among Periods A, B and C.

Rank-sum test or the Mann-Whitney-Wilcoxon test is a non-parametric test to assess if the distribution between two separate groups are systematically different from one another (Mann and Whitney, 1947; Wilcoxon, 1945). For the total number of observations n_1 and n_2 from two groups, respectively, the mean μ_W is calculated as

$$\mu_W = \frac{n_1(n_1+n_2+1)}{2} \tag{5}$$

while the standard deviation σ_W is given by

$$\sigma_W = \sqrt{\frac{n_1 n_2(n_1+n_2+1)}{12}} \tag{6}$$

The *z*-statistic is computed as

$$z = \frac{W-\mu_W}{\sigma_W} \tag{7}$$

where W is the sum of ranks on the observation in the smaller group. The p-value is determined and then compared with the value set for α. Rank-sum test is used to evaluate the similarity or differences between two periods, specifically between Periods B and C.

Lastly, correlation is a measure of closeness of association of the points in the scatter plot to a linear regression line based on those points. The correlation coefficient r is given by

$$r = \frac{Cov(X,Y)}{\sqrt{s_x^2 s_y^2}} \tag{8}$$

where the covariance $Cov(X,\ Y) = \frac{\sum(X-\bar{X})(Y-\bar{Y})}{n-1}$ for the pair $(X,\ Y)$, while $\bar{X}$ and $\bar{Y}$ are the means of X and Y, respectively and s_x^2 and s_y^2 are the sample variances of X and Y, respectively.

2.2.3 Computation of Stratification Indices

To quantitatively define the thermal structure of the reservoir, this study uses several parameters namely, heat content (Q), Brunt-Väisälä Frequency (N^2), Schmidt's Stability Index (SSI) and Thermocline Strength Index (TSI). A schematic diagram of the components of these equations is given in **Fig. 2.5**.

The formula for heat content Q with units of J is

$$Q = \sum_{z_0}^{z_m} mc_v T \tag{9}$$

where m is the mass (kg) of water at each defined layer z, c_v is the specific heat of water (4200 J/kg−K), and T (°C) is the water temperature (Moreno-Ostos et al., 2008).

The Brunt- Väisälä frequency N^2 (s^{-2}) is given by

$$N^2 = -\frac{g}{\bar{\rho}}\frac{\partial \rho}{\partial z} \tag{10}$$

as a measure of the strength of the buoyancy (Durran and Klemp, 1982), where z (m) is the depth of water from the surface, ρ (kg m^{-3}) is water density at a certain layer and temperature, $\bar{\rho}$ (kg m^{-3}) is the vertically averaged potential density, and g (9.80 m s^{-2}) is the acceleration due to gravity.

The Schmidt's Stability Index or SSI (Idso, 1973) is computed using the equation,

$$SSI = \frac{g}{A_0}\sum_{z_0}^{z_m}(z - z_g)(\rho_z - \rho_g)A_z\Delta z \quad (11)$$

where A_0 is surface area of lake (m^2), z_m is maximum depth (m), z_0 is water surface depth (m), A_z is area at depth z (m^2), ρ_z is density at depth z (kg m^{-3}), ρ_g is mean density at depth z_g (kg m^{-3}), z_g is depth to the center of gravity of stratified lake (m). SSI indicates the amount of energy required by wind to mix the heat in the reservoir uniformly over depth, where its value is minimum when the water body is isothermal and maximum when strongly stratified (Sahoo et al., 2016; Yu et al., 2010)**.** The time-series of SSI was generated using the rLakeAnalyzer package.

Lastly, the Thermocline Strength Index or TSI (Yu et al., 2010) is computed using the equation,

$$TSI = \frac{\Delta T}{\Delta h} \quad (12)$$

where ΔT and Δh are the differences of water temperature (˚C) and water depth (m) between intervals. TSI simply indicates the steepness of the thermocline or the average gradient of the thermocline layer (Liu et al., 2019). Since many literatures offer different values where the thermocline starts to appear, this paper adopts a minimum gradient of 0.1˚C m^{-1} in the temperature profile, as this was applied to a study for Lake Biwa, which is also located in Japan (Koue et al., 2018). The temperature gradient per depth interval was computed using actual temperature data, whereas all values equal to or above 0.1 ˚C m^{-1} per depth interval are averaged, hence constituting an average TSI.

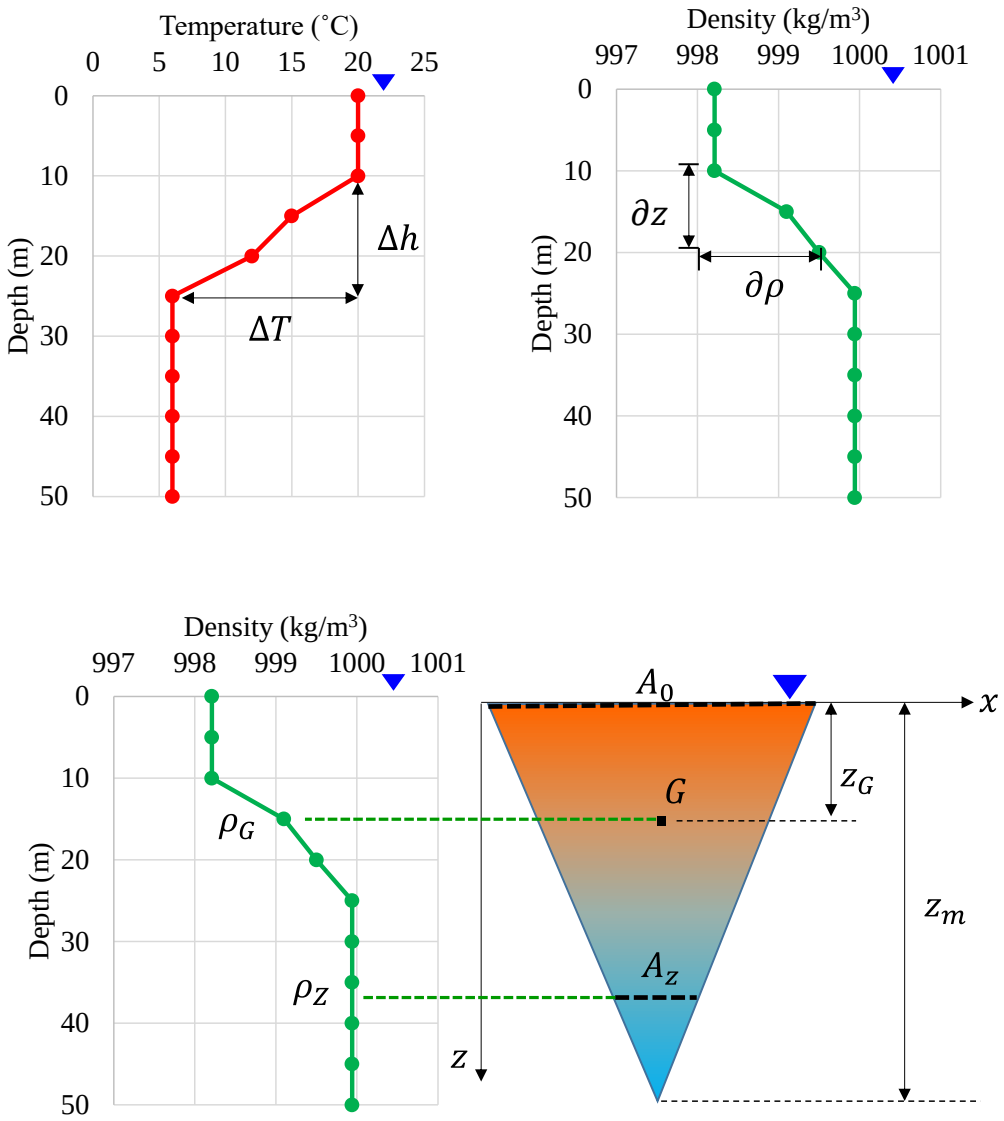

Figure 2.5. Schematic diagram indicating the parameters for the computation of stratification indices.

2.2.4 Difference of SSI and TSI Features

SSI is one of the most widely used metrics that define the thermal stratification of lakes and reservoirs. Recent papers have for instance used SSI to evaluate the effects of climate change on the stratification of these water bodies (Butcher et al., 2015; Ficker et al., 2017; Kobler et al., 2019; Magee and Wu, 2017; Sahoo et al., 2016). On the other hand, TSI can be considered to be the simplest stratification index as it only captures the average thermocline gradient. SSI and TSI were both used in studies for Lake Biwa to relate the chemical and thermal stratifications (Yu et al., 2010) and to evaluate the

interaction of stratification and flow field using numerical simulation (Koue et al., 2018). However, these two papers just calculated the respective values of these indices and discussed them individually. From the authors' knowledge, no paper has yet established a definite relationship between SSI and TSI. Likewise, most papers have utilized SSI to plainly talk about its trends and values and to define the timing of onset and end of stratification, yet the physical features of SSI in relation to other parameters are rarely discussed. For this reason, this paper attempted to analyze more in detail the features of SSI as a function of TSI, thermocline thickness (TT) and surface water temperature (SWT) considering the actual conditions of the Ogouchi Reservoir. Although conceptual in nature, the case analysis can be used to establish definite relationships among the parameters and to determine the strength and weakness of each index.

For the case analysis, some conceptual diagrams are provided in **Fig. 2.6**. The temperature profiles used in the analysis are based on actual data of thermal patterns considering the present operating condition in Period C, with the bottom temperatures fixed at 5˚C for all cases. It is found that SSI and TSI are not linearly related but are rather dependent on the TT and SWT, hence in **Fig. 2.6a**, the temperature profiles are shown to vary in terms of SWT and TT.TSI is temperature-based while SSI is density-based. The SWT ranges from 10 to 30˚C while the TT from 10 to 50 m. TT is defined as the depth of the bottom of the thermocline from the surface considering a threshold thermal gradient of 0.1˚C m^{-1}. In calculating the SSI, the morphometry of the Ogouchi Reservoir was used as indicated by its average areal cross-section in **Fig. 2.6b**.

Using the combinations of SWT and TT, the relationship between SSI and TSI is established in **Fig. 2.6c**. Generally, it shows that the SSI is proportional to ST and TT i.e. thermal stability increases with hotter water surfaces and deeper thermoclines. However, the relationship of TSI with ST, TT and SSI appears to be unclear, specifically where the TSI is increasing. Only by considering constant values of TSI that the increase in ST and TT would correspond to the subsequent increase in SSI. Furthermore, significant inferences can be drawn considering the peak stratification condition in Ogouchi Reservoir where the surface temperature is around 25˚C and the thickness is around 40 m. At this point apparently, a maximum SSI of 10.0 kJ m^{-2} is obtained with a corresponding TSI of around 0.50˚C m^{-1}. But beyond this point considering the 25˚C surface temperature line, having a larger TSI does not necessarily mean having a larger

SSI. This goes to show that TSI alone should not be used in defining the stratification condition of this reservoir specifically during the summer or the peak of heating.

In **Fig. 2.6d**, as warming happens during spring time (left figure), with a constant TT but increasing ST, both the TSI and SSI would increase. For autumn (right figure), with a constant ST but increasing TT, both the TSI and SSI would appear to have constant values during the season. However, during summer (middle figure) where both the ST and TT are increasing, there will be a time where the TSI can be constant but the SSI will continue to increase. This particular situation during summer again highlights the weakness of the TSI to capture the entire stratification condition of the reservoir compared to SSI.

TSI, in terms of long-term average per period, is principally helpful in highlighting the effect of facilities on the thermal stratification of the reservoir. Yet, TSI only captures the average thermal gradient in the reservoir, irrespective of the location of the thermocline and the corresponding thickness of the stratified layer. As such, TSI alone should not be used to define the stratification characteristics of a reservoir. It would be more holistic to consider the Brunt-Väisälä frequency, SSI, heat content and other parameters.

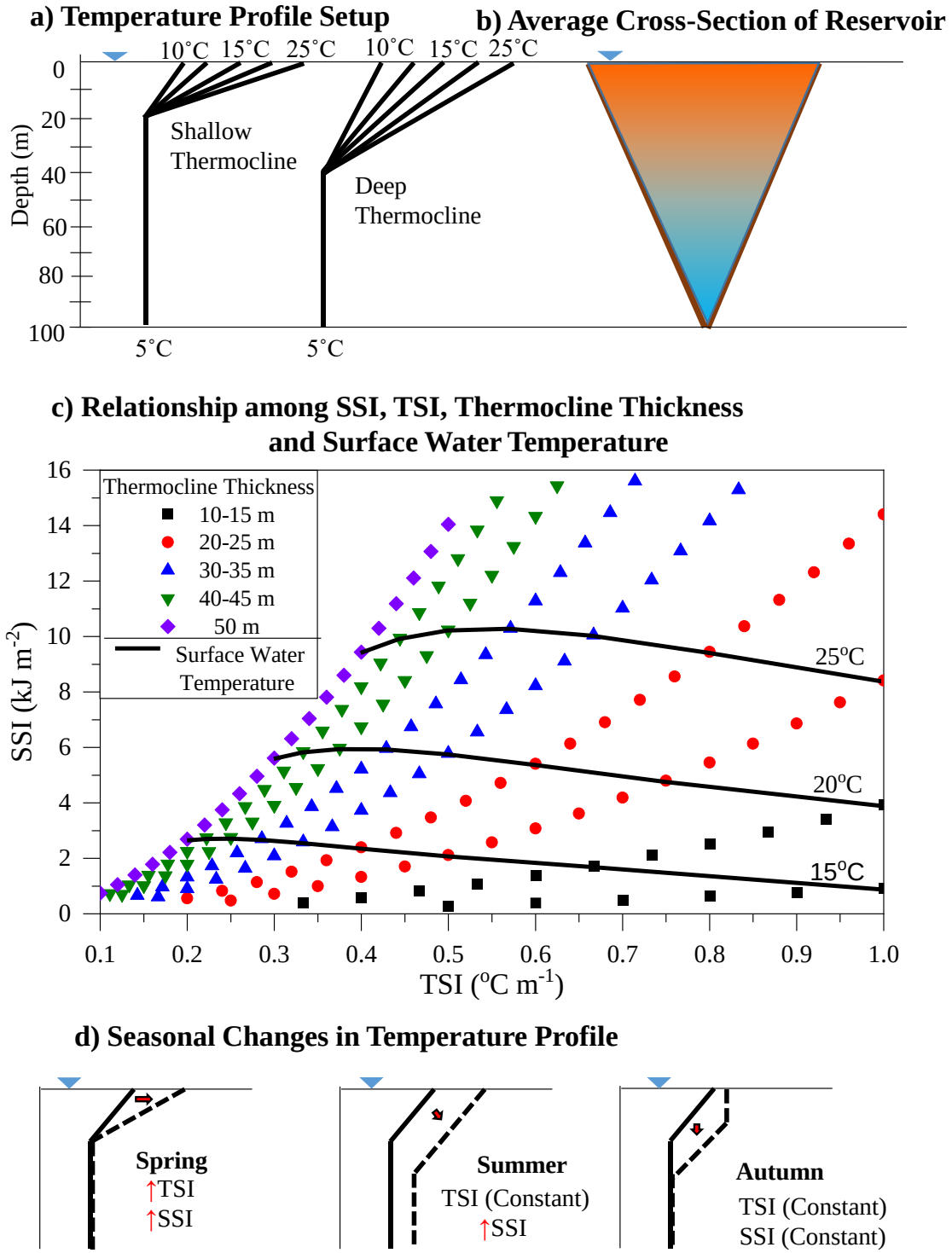

Figure 2.6. Evaluation of the relationship of stratification indices with thermocline thickness (TT) and surface water temperature (SWT). Diagrams are given for a) the setup of temperature profile with varying TT and SWT considering b) the Ogouchi Reservoir morphometry. The c) relationship among the four parameters (SSI, TSI, TT, and ST) is provided in a plot together with the d) diagrams inferring the seasonal changes in profile and indices.

2.3 Numerical Simulation

2.3.1 Model description

A 3-D numerical simulator, Fantom Refined (Veerapaga et al., 2019) was used to analyze the thermo-hydrodynamics of the Ogouchi Reservoir. The model uses the 3-D Navier-Stokes equations with incompressible and Boussinesq approximation,

$$\frac{\partial u}{\partial t}+u\frac{\partial u}{\partial x}+v\frac{\partial u}{\partial y}+w\frac{\partial u}{\partial z}-fu = -\frac{1}{\rho_0}\frac{\partial p}{\partial x}+\frac{\partial}{\partial x}\left(v_H\frac{\partial u}{\partial x}\right)+\frac{\partial}{\partial y}\left(v_H\frac{\partial u}{\partial y}\right)+\frac{\partial}{\partial z}\left(v_V\frac{\partial u}{\partial z}\right) \quad (13)$$

$$\frac{\partial v}{\partial t}+u\frac{\partial v}{\partial x}+v\frac{\partial v}{\partial y}+w\frac{\partial v}{\partial z}-fv = -\frac{1}{\rho_0}\frac{\partial p}{\partial y}+\frac{\partial}{\partial x}\left(v_H\frac{\partial v}{\partial x}\right)+\frac{\partial}{\partial y}\left(v_H\frac{\partial v}{\partial y}\right)+\frac{\partial}{\partial z}\left(v_V\frac{\partial u}{\partial z}\right) \quad (14)$$

$$\frac{\partial w}{\partial t}+u\frac{\partial w}{\partial x}+v\frac{\partial w}{\partial y}+w\frac{\partial w}{\partial z} = -\frac{1}{\rho_0}\frac{\partial p}{\partial z}+\frac{\partial}{\partial x}\left(v_H\frac{\partial w}{\partial x}\right)+\frac{\partial}{\partial y}\left(v_H\frac{\partial w}{\partial y}\right)+\frac{\partial}{\partial z}\left(v_V\frac{\partial w}{\partial z}\right) - \frac{g}{\rho_0}(\rho_0+\rho) \quad (15)$$

subject to incompressibility,

$$\frac{\partial u}{\partial x}+\frac{\partial v}{\partial y}+\frac{\partial w}{\partial z}=0 \quad (16)$$

where u, v and w are the velocities in the x, y and z directions, respectively, p is the pressure, ρ_0 is the reference density, $(\rho_0+\rho)$ is the density, $f(=2\Omega sin\phi)$ is the Coriolis coefficient, ϕ is the latitude, Ω is the angular velocity of the earth, ν_H and ν_V are the horizontal and vertical eddy viscosity coefficients,. The transport equation for temperature is given by,

$$\frac{\partial T}{\partial t}+u\frac{\partial T}{\partial x}+v\frac{\partial T}{\partial y}+w\frac{\partial T}{\partial z}=\frac{\partial}{\partial x}\left(\kappa_H\frac{\partial T}{\partial x}\right)+\frac{\partial}{\partial y}\left(\kappa_H\frac{\partial T}{\partial y}\right)+\frac{\partial}{\partial z}\left(\kappa_V\frac{\partial T}{\partial z}\right) \quad (17)$$

where T is the temperature, κ_H and κ_V are the horizontal and vertical eddy diffusion coefficients.

The equations were discretized based on a collocated finite-volume method. Temporal derivatives were discretized by the second-order Adams-Bashfort method for explicit terms, while for advection terms, by the third-order ULTIMATE-QUICKEST scheme (Leonard, 1991).

2.3.2 Turbulence Closure Model

From the Reynolds-Averaged Navier-Stokes equations, the turbulent eddy viscosity v_v is defined by

$$v_v = c\sqrt{2k}lS_M + v \tag{18}$$

while the turbulent eddy diffusivity is given by

$$K_v = c\sqrt{2k}lS_H + v_\theta \tag{19}$$

where c is a coefficient [=1.0 (Galperin et al., 1988)], v and v_θ are the molecular viscosity and diffusivity, respectively while S_M and S_H are the stability functions describing the effects of shear and stratification. These stability functions are algebraically determined by parameterizing the third-order moments and pressure strain correlation. S_M and S_H account for turbulence damping due to density stratification.

The turbulent kinetic energy k and the turbulent length scale l need to be determined in order to close the set of equations. Fantom Refined adopts the Generic Length Scale (GLS) turbulence closure model, which consists of two equations (Umlauf and Burchard, 2003). The first is the standard equation for turbulent kinetic energy k given by

$$\frac{\partial k}{\partial t} + U_i\frac{\partial k}{\partial x_i} = \frac{\partial}{\partial z}\left(\frac{v_v}{\sigma_k}\frac{\partial k}{\partial z}\right) + P + B + \varepsilon \tag{20}$$

where σ_k is turbulence Schmidt number for k, ε dissipation parameter while P and B represent production by shear and buoyancy. The second equation deals with the generic parameter φ to quantify the turbulence length scale l in the form of

$$\frac{\partial \varphi}{\partial t} + U_i \frac{\partial \varphi}{\partial x_i} = \frac{\partial}{\partial z}\left(\frac{K_M}{\sigma_\psi}\frac{\partial \psi}{\partial z}\right) + \frac{\varphi}{k}(c_1 P + c_3 B + c_2 \varepsilon F_{wall}) \quad (21)$$

where σ_φ is the turbulence Schmidt number for φ, ε is dissipation parameter and F_{wall} is the wall proximity function. The coefficients c_1 and c_2 are related with the von Karman's constant while c_3 is a parameter related to either stably stratified flows or unstable flows.

The parameter φ is determined by

$$\varphi = \left(c_\mu^0\right)^p k^m l^n \quad (22)$$

where c_μ^0 is the stability coefficient derived empirically for unstratified channel flows and *p, m* and *n* are parameters, of which the values vary depending on the type of closure model. For the $k - kl$ model, *p, m* and *n* take the values of 0.0, 1.0 and 1.0, respectively while $k - \varepsilon$ model, 3.0, 1.5 and -1.0, respectively. Additionally, the $k - \omega$ model specifies the values -1.0, 0.5 and -1.0, respectively while the *gen* model, 2.0, 1.0 and -0.67, respectively (Warner et al., 2005).

For this particular study, the $k - \omega$ setting is adopted for the simulation.

2.3.3 Heat Flux Boundaries

The net heat flux across air/water interface Q_{net} is quantified by

$$Q_{net} = Q_{Sn} + Q_L + Q_E + Q_C \quad (23)$$

where Q_{Sn} is the net shortwave solar radiation flux, Q_L is the net long wave radiation flux, Q_E is the latent heat flux due to evaporation and Q_C is the sensible heat flux due to conduction. These heat flux components were computed from air temperature, humidity, cloud cover, radiation and wind speed using the bulk formula (Kondo, 1975).

The net shortwave solar radiation flux is given by

$$Q_{Sn} = Q_{SR}(1 - r)(1 - e^{-\delta}) \quad (24)$$

where Q_{SR} is measured solar radiation, r is reflection coefficient (0.07) and δ is damping coefficient (0.5).

The net long wave radiation flux is computed as

$$Q_L = \varepsilon\sigma\{[9.37x10^{-6}(T_a + 273.16)^6][1 + .17C^2] - (T + 273.16)^4\} \quad (25)$$

where ε is emissivity of the water body (0.96), σ is Stefan-Boltzmann constant (=5.67x10^{-8} W/m^2/K^4), T is water temperature (˚C), T_a is atmospheric temperature (˚C) and C is the cloud fraction.

The latent heat flux due to evaporation is determined using

$$Q_E = L_V \rho_a U_{10}\{q_s - q_a\} \quad (26)$$

where L_V is latent heat of vaporization of water, ρ_a is density of air, U_{10} is wind speed at 10 m above the surface, q_s is the specific humidity of saturated air given by $q_s = \frac{0.622e_s}{P_{atm} - 0.378e_s}$ while q_a is the specific humidity of remote air given by $q_a = \frac{0.622e_a}{P_{atm} - 0.378e_a}$ with e_s as the saturation vapor pressure and e_a as the actual vapor pressure.

Lastly, the sensible heat flux due to conduction is given by

$$Q_C = c_p \rho_a U_{10}\{T - T_a\} \quad (27)$$

where c_P is the specific heat of air.

2.3.4 Initial and Boundary Conditions

Year 2016 was selected for simulation of in-reservoir and outflow temperatures because this year exhibits a long and sustained summer stratification, free from the interference of strong flood events. The reservoir data sets from May 01 to August 31, 2016 were obtained from the Bureau of Waterworks of the Tokyo Metropolitan Government (BW-TMG). Among these data include the hourly levels of water surface and SW intake, outflow from SW and inflow from tributaries, together with the outflow and inflow temperatures and vertical in-reservoir temperatures.

For the weather data, hourly values of air temperature, rainfall, wind speed and direction, relative humidity, solar radiation and cloudiness were downloaded from the website of the Automated Meteorological Data Acquisition System (AMeDAS).

Surface elevation and vertical diffusion were calculated implicitly using the second-order theta method. Uniform grids were set in the horizontal (dx = 50 m, dy = 50 m) and the vertical (dz = 0.5m). The time step, dt was set at 20 s. The hourly river and weather data served as the boundary conditions (**Fig. 2.7)**. The vertical temperature profile and the water level for May 1 were set as the initial condition. The VC was modeled as an impermeable cell face with its upper edge moving with water level.

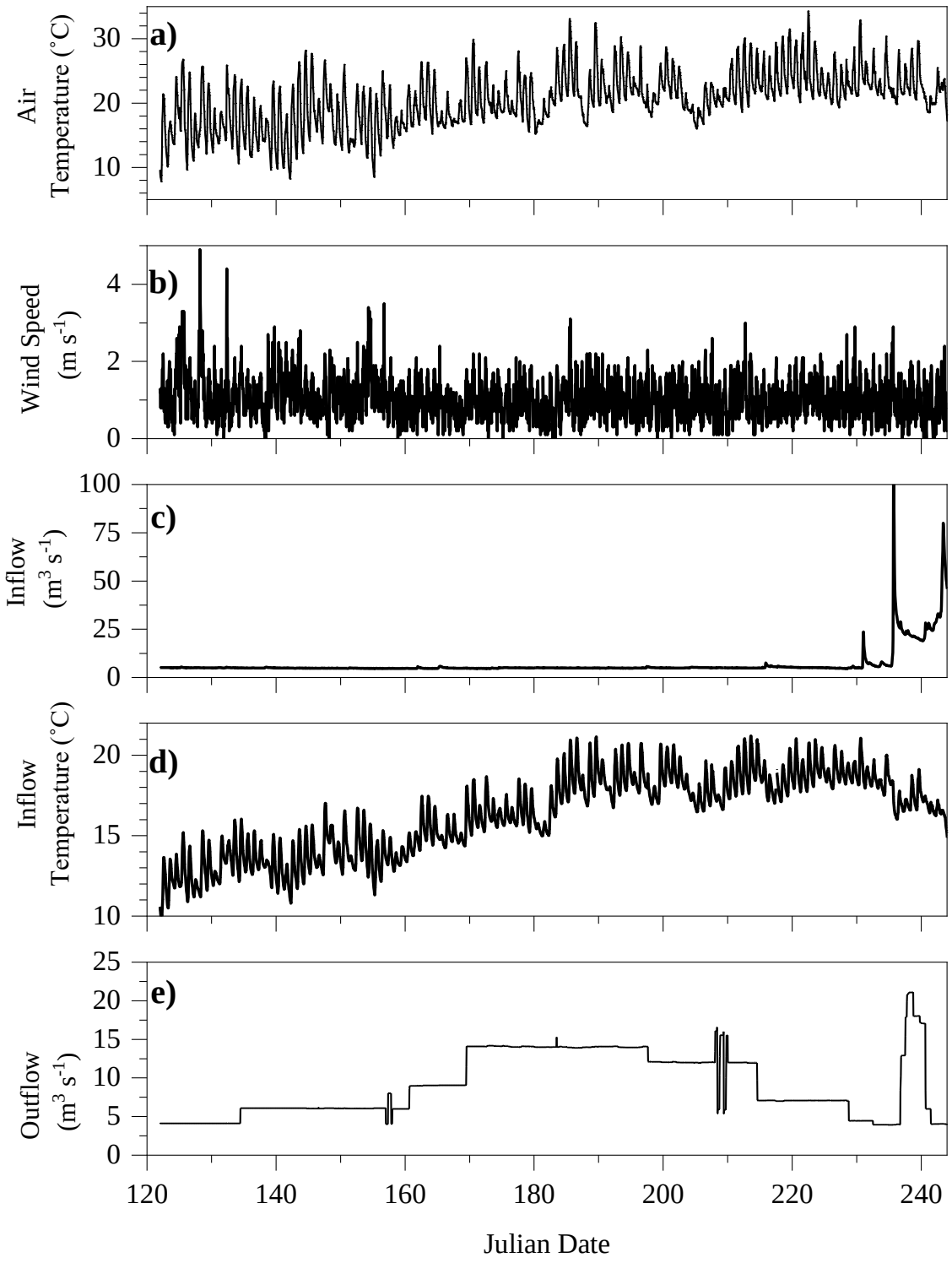

Figure 2.7 Some of the parameters for the boundary conditions for the 2016 simulation: a) air temperature, b) wind speed, c) total inflow, d) average inflow temperature and e) outflow.

2.3.5 Outflow Modeling of Selective Withdrawal

The Modified Gaussian Distribution Method (MGDM) is used to establish the vertical profiles of the outflow passing through the SW. Actual measurements through the SW in the years 2008 and 2009 using the acoustic Doppler turbulent meter yielded the results in **Fig. 2.8**. By applying mathematical modeling, the modified Gaussian distribution was found to provide the better fit to the velocity profile (Niiyama et al., 2010b).

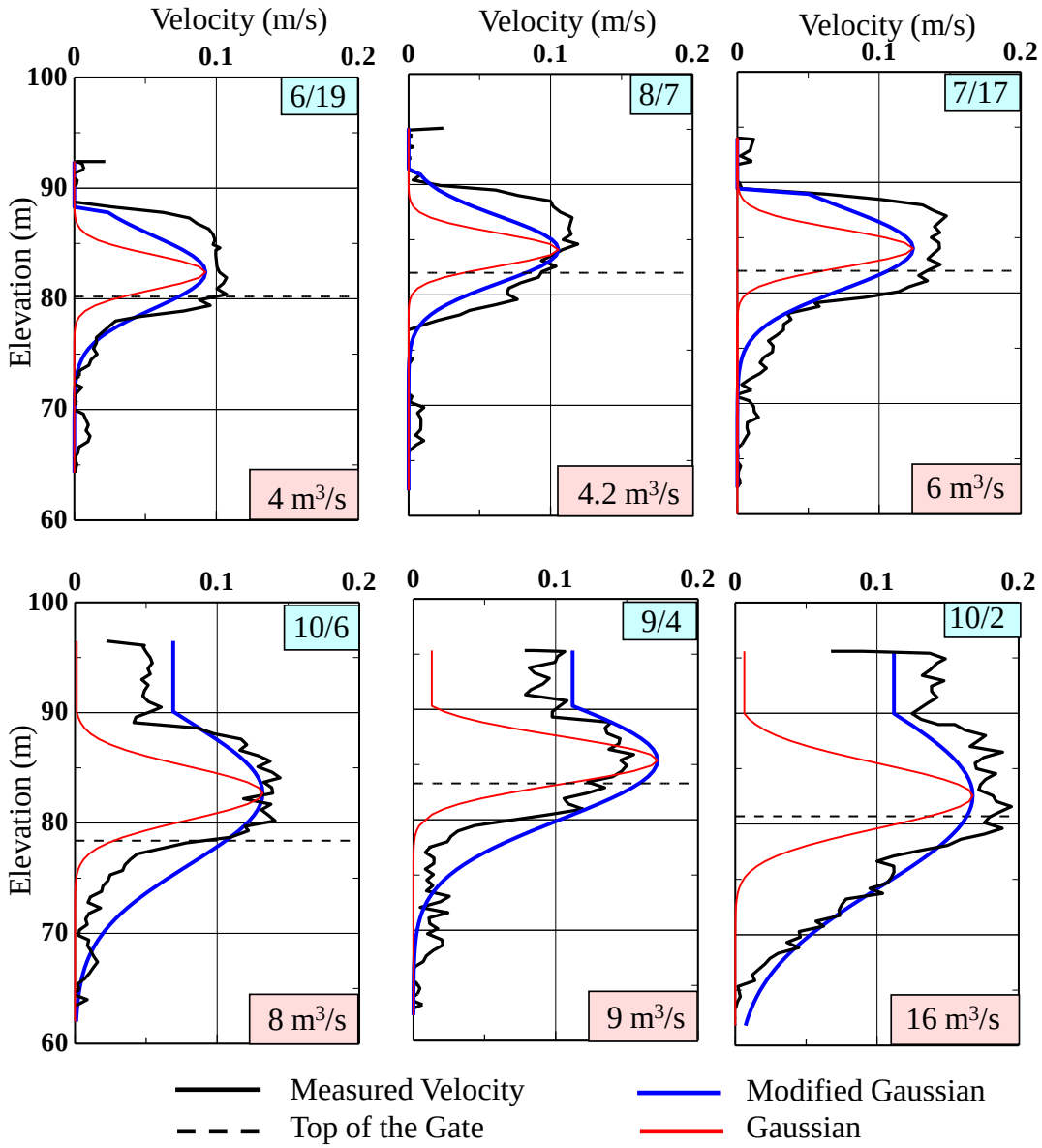

Figure 2.8. Comparison of the measured velocity profiles through the SW with some mathematical models at different outflows and intake levels (Niiyama et al., 2010b).

This modified Gaussian distribution is a function of the discharge, depth of intake level and the density profile of the reservoir (Brooks and Koh, 1969; Niiyama et al., 2010b). The outflow profiles are determined using the formula:

$$f(z) = \frac{1}{\sqrt{2\pi\sigma^2}} e^{\left(-\frac{z^2}{2\sigma^2}\right)} \tag{28}$$

where $f(z)$ is the Gaussian probability density function, σ is the standard deviation (=δ/3.92) and z is the distance from the center and peak of the distribution, which is about 2 m above the gate's intake.

The δ or total depth of the distribution from the water surface is computed as

$$\delta = A\left(\frac{q}{\sqrt{g d_\varepsilon}}\right)^{\frac{1}{2}} \tag{29}$$

where q is the discharge per unit width of the SW, g is acceleration due to gravity and A is a constant (2.7±0.2). The d_ε is the relative density gradient given by

$$d_\varepsilon = \frac{\rho_G - \rho_s}{\rho_G} \frac{1}{Z_G} \tag{30}$$

where ρ_G is the water density along the intake, ρ_s is the surface water density and Z_G is the depth of the gate from the water surface.

The schematic diagram of the Modified Gaussian Distribution for the velocity profile through the SW facility is provided on **Fig. 2.10**. The additional parameter Z_T is the depth of the upper edge of the thermocline. For low flow conditions, the outflow coordinate from the water surface until Z_T is zero while it is a constant non-zero value for high flows.

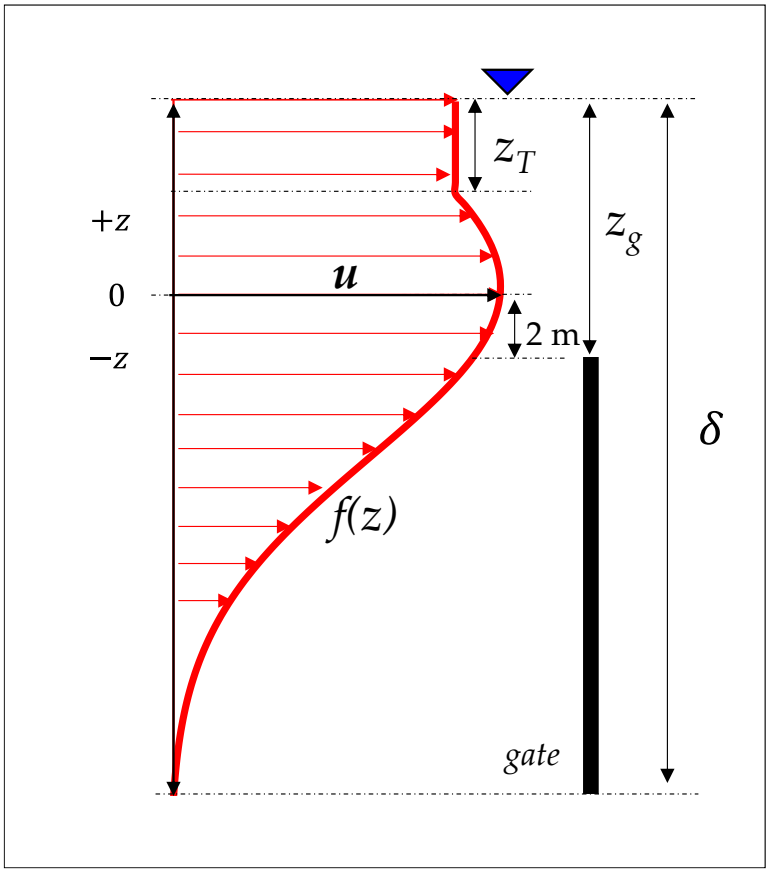

Figure 2.9. Schematic diagram of the modified Gaussian distribution of the outflow through the selective withdrawal facility and the corresponding variables indicated in equations 18-20.

The outflow discharges are first classified to be either low flow (≤6 m^3/s) or high flow (>6 m^3/s). A representative temperature profile for the same value of outflow and SW intake level is selected. Temperature profiles that are located directly after the transition of outflow or intake level are not considered. It is recommended to select a representative temperature profile within the middle of the time range where intake levels and outflows are the same. In **Fig. 2.10a**, the notations of a, b and c (in blue) signify the low-flow distributions while the rest (in red) constitute the high-flow. It is possible that there can be two distinct profiles in a time frame having similar discharge but with shifting intake levels such as in (e) and (f) together with (h) and (i).

Using equations 28-30, ten MGDM profiles were derived. The profiles for low flows are given in **Fig. 2.10b** while the high flows in **Fig. 2.10c**. The areas under the curve for all profiles are equal to unity. Low-flow profiles have more pointed peaks and are shallower while the high flows are relatively flatter and deeper. While low flows have

zero values of coordinates from surface to the top edge of the thermocline, high flows rather have constant non-zero values at this similar location. The theory and application of this method is further discussed in a previous study (Niiyama et al., 2010b).

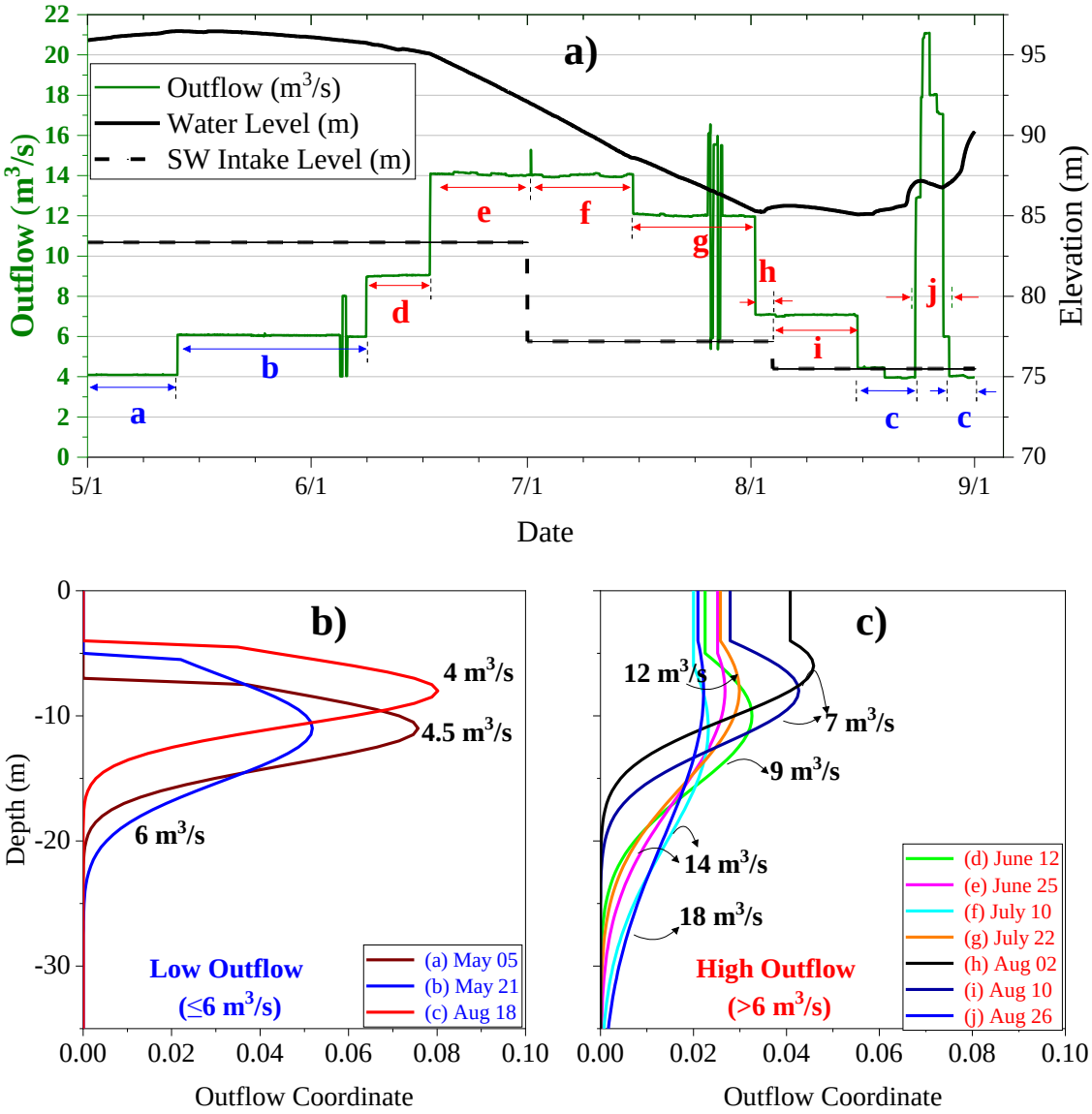

Figure 2.10 Outflow, water level and SW intake level for 2016 (a) and the corresponding modified Gaussian profiles for (b) low flows and (c) high flows.

2.3.6 Development of Simulation Cases

Outflow openings were assigned at vertical cells corresponding to their depth as point flux boundaries. The profiles using MGDM were applied to the vertical profile of

the outflow. The coordinates per profile were multiplied to the total outflow such that the sum of all discharge per layer (dz) is equal to the total value of the outflow.

The Uniform Distribution Method (UDM) was also used to compare the results with the MGDM. The common practice for UDM is to use designated three fixed points that lie along the location of the intake level. The lowering of the SW intake gate was therefore accounted for in the use of UDM for the 2016 simulation.

Simulated water levels were compared with the actual. Furthermore, the actual and simulated profiles were likewise compared, together with the outflow temperatures. This was made for both MGDM and UDM.

After which, three model cases were developed, which correspond to the three periods of operation. For Cases A and B, the VC is removed in the simulation. The outflow method used for Case A is UDM, with the outflow layers corresponding to the location of the 2.8-m diameter penstock at EL 30 m. Meanwhile, both Cases B and C utilized the outflow profiles derived from MGDM.

The resulting outflow temperatures for the three cases were obtained and compared. Vertical temperatures were also determined. To discuss the difference in stratification among the three cases, the Brunt-Väisälä frequency (N^2) was computed for each layer (dz) of the reservoir. The resulting contours of in-reservoir temperatures and N^2 for the three cases were compared.

Simulation was also done for the year 2015 to compare the results in a period where thermal stratification is affected by floods. Year 2015 exhibits an operation where there is no sudden shift in SW intake, i.e. the SW gate is fixed at a certain level from May 01 to August 31.

The simulation cases for 2015 and 2016 are summarized in **Table 2.3** while their intake settings for the calculation are given in **Figs. 2.11** and **2.12** for the sensitivity analysis.

Table 2.3 Description of numerical calculation cases.

Case	Mode of Outflow	Vertical Curtain	Depth of Intake
A	Penstock Withdrawal	No	70 m
B/B1	Selective Withdrawal	No	4 m
B2	Selective Withdrawal	No	7 m
B3	Selective Withdrawal	No	10 m
C1	Selective Withdrawal	Yes	4 m
C2	Selective Withdrawal	Yes	7 m
C/C3	Selective Withdrawal	Yes	10 m

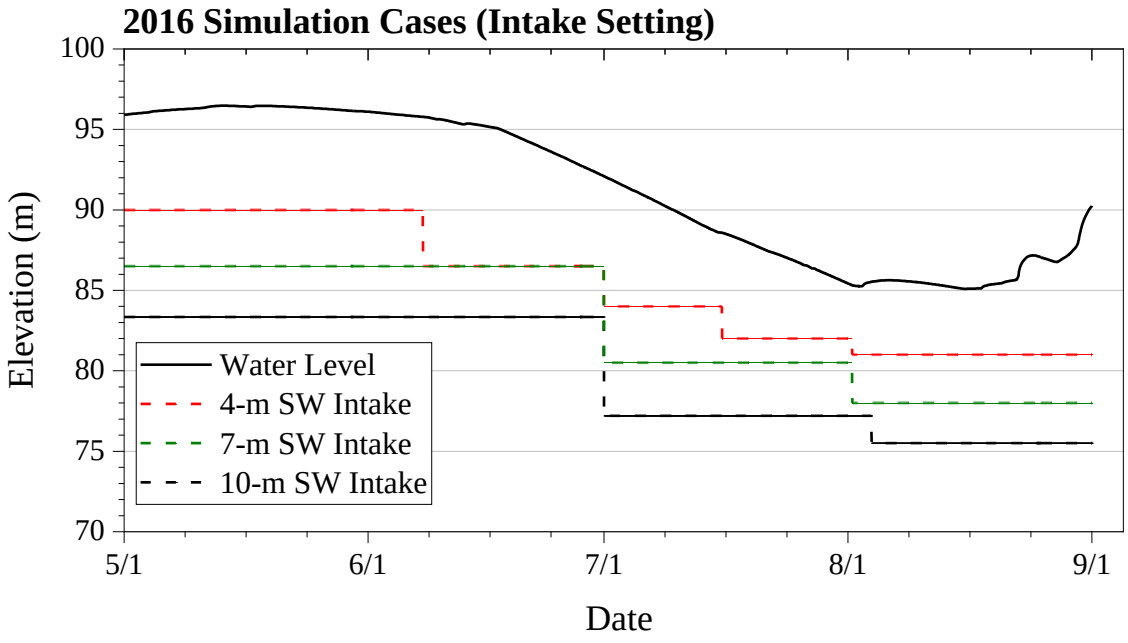

Figure 2.11 The SW intake settings for the period with long and sustained stratification.

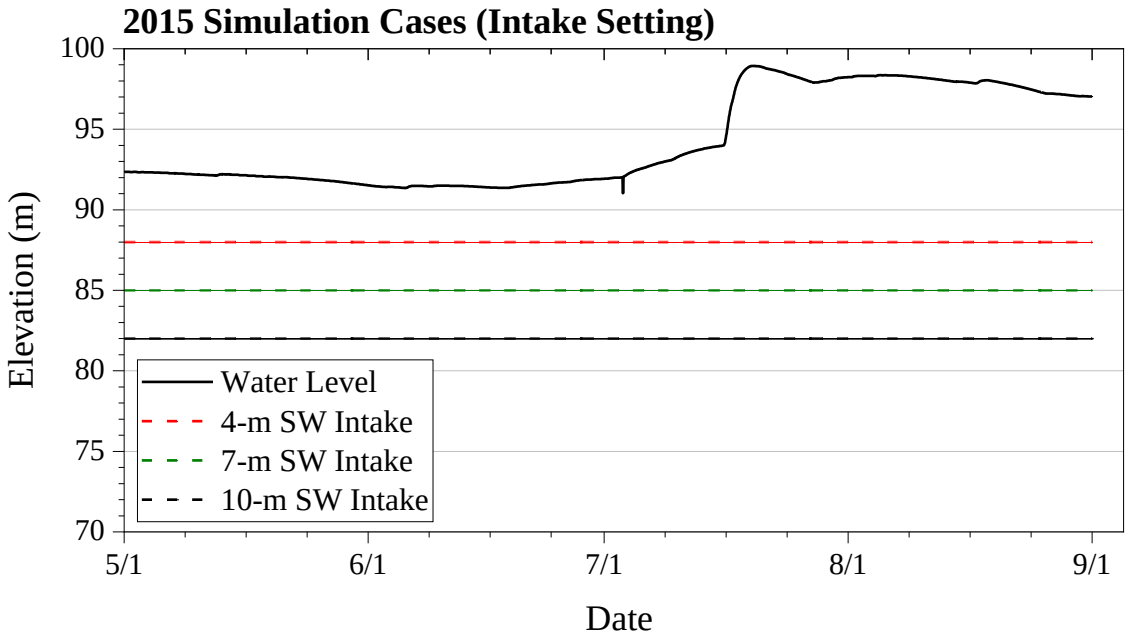

Figure 2.12 The SW intake settings for the period with a stratification affected by flood.

CHAPTER 3

Effect of Climate on Reservoir Temperatures

3.1 Introduction

The temperatures of lakes and reservoirs are known to respond to the changes in atmospheric conditions (Hondzo and Stefan, 1993). In order to understand the thermal conditions of the reservoir, it is necessary to first identify and examine several climate drivers such as solar radiation, air temperature, wind speed and rainfall. Solar radiation directly affects the reservoir's water temperature particularly during the heating seasons. Furthermore, air temperature is commonly used as the main indicator of climate change, which can greatly affect the long term trends of water temperature. Higher air temperatures are associated with higher surface temperatures and greater summer thermal stability (Wang et al., 2012). Likewise, one study showed that rising air temperatures could result in warmer overall lake temperatures by offsetting the cooling effects of increased rainfall and river inflows (Bayer et al., 2013). On the other hand, wind generally supplies the energy for mixing and surface cooling. Wind is also responsible for the formation, stability and depth of thermoclines (Edlund et al., 2017). Further, rainfall is the main source of river inflow, which then produces horizontal currents affecting vertical stratification.

This study aims to determine the effects of climate on the temperatures of the reservoir with varying operations. This chapter focuses on the analysis of trends of air temperature, rainfall and wind speed in comparison with the trends of water temperatures. Further, the temperature profiles and heat content of the reservoir for the varying periods of operation are evaluated. The Ogouchi Reservoir in Japan is chosen as the study site as it had apparently experienced climate warming between 1959 and 2016 and its operation had transitioned into three distinct periods within this duration with the use of deep penstock withdrawal (DPW), purely SW and combination of SW and VC.

3.2 Results

3.2.1 Climate Analysis

The recent values of these climatic drivers, from 2012 to 2016 (**Fig 3.1**) from the dam station, were examined to highlight their typical daily variations, which were later on used as a basis to identify the two seasons in a year, namely, summer half-year and winter half-year. Then, air temperatures and wind speeds were analyzed based on their annual averages and the averages for the two seasons using the dam station data; for rainfall, only the totals of the annual event and extreme events (>50 mm d−1) were analyzed for their basin averages using all six stations.

The annual average air temperature in the Ogouchi Reservoir is 15.4 °C, with a maximum of 36.3°C and a minimum of −12.8 °C between 1959 and 2016. The daily variation in air temperature (**Fig. 3.1a**) shows that peaks are prominent in August and the lows in January. A typical year can be initially subdivided into a summer half-year (April to September) and a winter half-year (October to March). The summer half-year is classified when the air temperature is equal to or greater than the annual average air temperature, while the winter half-year is when temperatures are below it. **Fig. 3.1b** shows the typical daily rainfall pattern, wherein the rainy season onsets in the late spring while the typhoon season, bringing large amounts of rainfall, occurs in summer and autumn. **Fig. 3.1c** provides the recent typical daily wind speed, where cold winds are particularly strong from November to March due to the prevalence of northwesterly winds (Japan Meteorological Agency, n.d.). Interestingly, strong rain events are mostly concentrated during the summer half-year while stronger winds occur during the winter half-year. This further justifies why this paper adopts the two specific seasons in analyzing the interaction of climate with the thermal conditions of the reservoir.

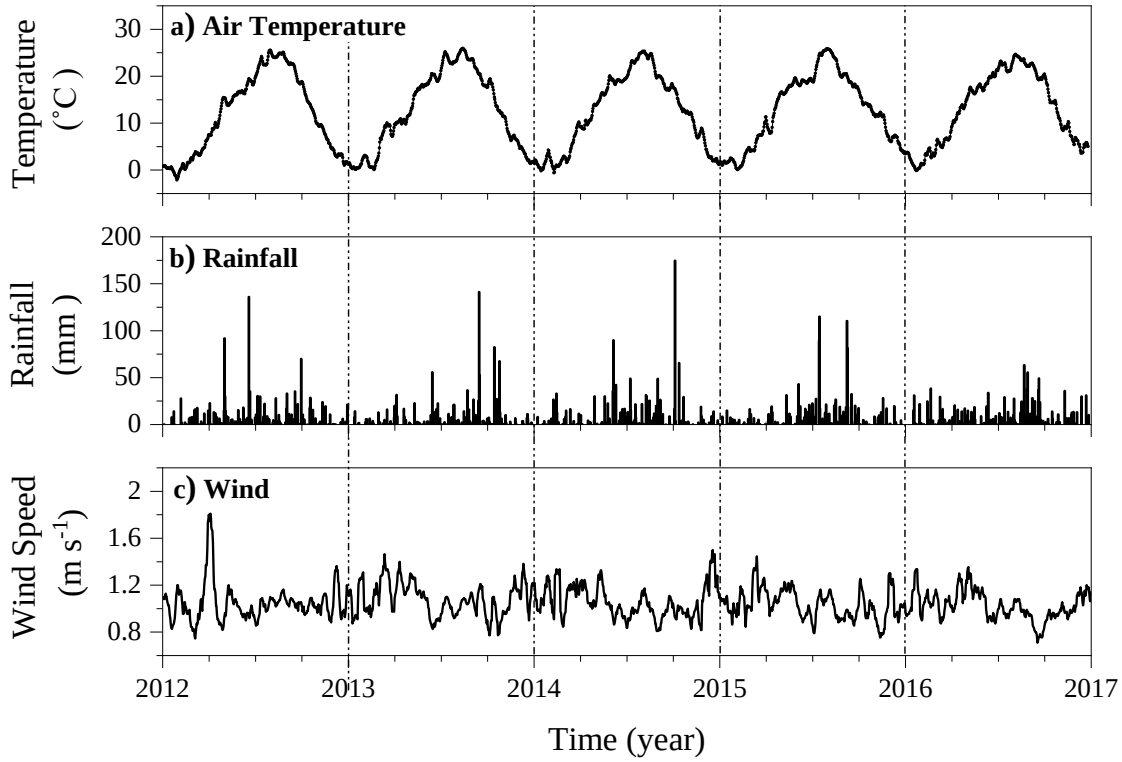

Figure 3.1 Typical variation of (a) air temperature (11-day moving average), (b) rainfall, and (c) wind speed from 2012 to 2016 from the dam station.

The plots in air temperature, wind speed, and basin-averaged rainfall for the year and the two seasons can be referred to in **Fig. 3.2**. Long-term atmospheric warming during the year and the winter half-year can be confirmed, with overall rising trends in air temperature. Besides these two, no other significant long-term trends were identified for the rest of the parameters (**Table 3.1**); however, several remarkable observations can be recognized at certain years. For the air temperature (**Fig. 3.2a**), the period from 1976 to 1993 is characterized by cold spells during the summer half-year. In terms of wind speed (**Figs. 3.2b**), the recent two decades are dominated by large values. In terms of rainfall (**Figs. 3.2c**), the wettest years (magnitudes greater than 2000 mm) were 1959, 1991, and 1998, while the driest years (below the average of 1480 mm) were 1973, 1980, 1984, and 2009. Strong rainfall events were observed in 1974, 1983, and 2011, due primarily to typhoons.

The corresponding results of the M–K test for these atmospheric parameters are presented in **Table 3.1**, where significant upward trends in air temperature are observed for the year and winter half-year at +0.15 and +0.30 °C decade^{-1}, respectively. The annual air temperature rise is consistent with the +0.12 °C decade^{-1} officially recorded increase

in Japan between 1898 and 2016 (Japan Meteorological Agency, 2017). The increase in air temperature during the winter half-year corresponds with the warmer winter and autumn, as evidenced by the documented rise of +0.11 and +0.13°C decade^{-1}, respectively. For the Tokyo metropolitan area, where the catchment belongs, a study (Matsumoto et al., 2017) revealed that the annual mean temperature increased by about +0.30°C decade^{-1} between 1901 and 2016, a value way larger than the national average of +0.12°C decade^{-1} (Japan Meteorological Agency, 2017). This could explain the higher rate of increase during the winter half-year for the Ogouchi catchment. However, no significant trend in air temperature could be detected in the summer half-year, which means that the annual trend is largely affected by the rising local temperatures during the winter half-year. On the other hand, wind speeds showed upward trends for the annual and the two seasons for the maximum (significant) and for the annual (not significant). Furthermore, the long-term trends of annual and heavy rainfall (>50 mm d^{-1}) are not statistically significant. While the country's air temperature displayed upward trends, which are likely attributed to climate change and urbanization, precipitation may be considered to be within the normal range of fluctuations (Xu et al., 2002).

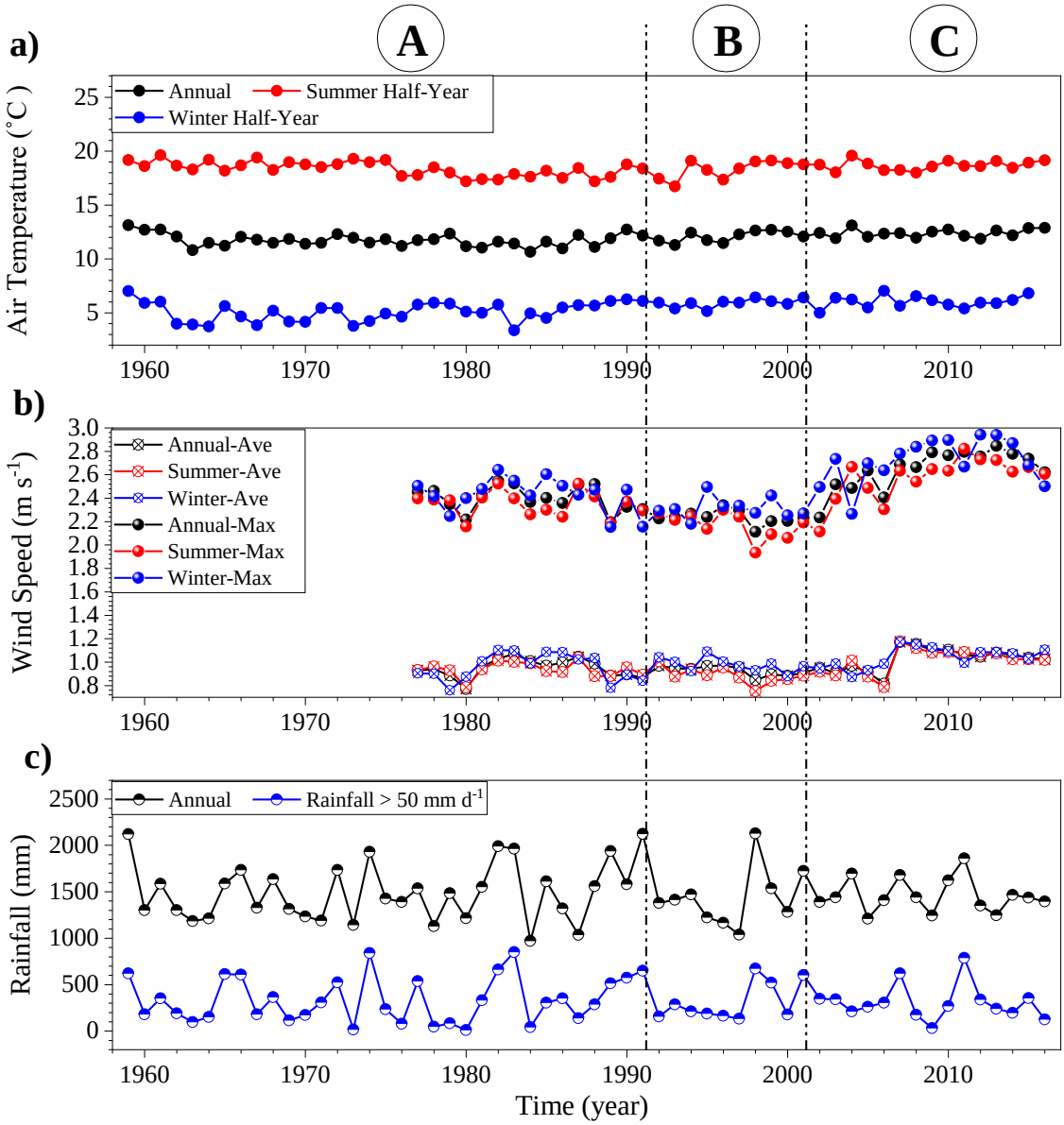

Figure 3.2. Long-term annual data of a) air temperature, b) wind speed and c) rainfall for the Ogouchi Reservoir.

Table 3.1. Results of the Mann–Kendall (M–K) test at $\alpha = 0.05$ for long-term values of air temperature, wind speed and rainfall (basin average). Significantly different p-values are in bold characters.

Parameter	Time Category	M–K z-stat	M–K p-value	Sen's Slope
Air Temperature	Annual	+2.9783	**0.0029**	+0.15 °C decade^{-1}
	Apr–Sept	−0.1610	0.8271	−0.01 °C decade^{-1}
	Oct–Mar	+4.4809	**<0.0001**	+0.30 °C decade^{-1}
Average Wind Speed	Annual	+1.8758	0.0607	+0.03 m s^{-1} decade^{-1}
	Apr–Sept	+1.4565	0.1453	+0.02 m s^{-1} decade^{-1}
	Oct–Mar	+1.8293	0.0673	+0.03 m s^{-1} decade^{-1}
Maximum Wind Speed	Annual	+2.5283	**0.0114**	+0.08 m s^{-1} decade^{-1}
	Apr–Sept	+2.1796	**0.0293**	+0.09 m s^{-1} decade^{-1}
	Oct–Mar	+2.9485	**0.0032**	+0.08 m s^{-1} decade^{-1}
Rainfall	Annual	+0.2147	0.8300	+5.02 mm decade^{-1}
	>50 mm d^{-1}	+0.2415	0.8092	+3.35 mm decade^{-1}

On **Table 3.2**, the results of the Kruskal-Wallis (KW) and rank-sum tests are provided. In terms of air temperature, significant differences are observed among periods for the year and winter half-year. For the year, Period C is significantly different (warmer) from A while for the winter half-year, both Periods B and C are significantly different (warmer) from A. In terms of wind speed, the significant differences among periods for the year and the summer half-year are brought about by Period C, having larger wind speed values than A. In terms of rainfall (annual and heavy), no significant differences were observed. On **Table 3.3**, only the wind speed for the year and the summer half-year is significantly different by rank-sum test between Periods B and C.

The short-term meteorological trends in each period are defined by the slope of the parameters using simple linear regression (**Fig. 3.3**). For Period A, air temperature, wind speed, and basin-averaged rainfall are characterized by weak slopes. On the other hand, Period B noticeably has rising trends in air temperature and basin-averaged rainfall but a decreasing one in wind speed. A limitation to estimating the trends for Period B is recognized as it covers only a relatively short duration of ten years. Furthermore, Period

C manifests a slight increase in air temperature and a strong increase in wind speed but the reverse for basin-averaged rainfall. These short-term trends are later discussed in comparison with the trends of water temperatures and heat content.

Table 3.2. Results of Kruskal–Wallis (K–W) and rank-sum tests at $\alpha = 0.05$ for the climate parameters. Significantly different p-values are in bold characters.

Parameter	Time Category	Average per Period			K–W p-value
		A	B	C	
Air Temperature (˚C)	Annual	11.7	12.1	12.4*	**1.3×10^{-3}**
	Apr–Sept	18.4	18.3	18.7	4.3×10^{-1}
	Oct–Mar	5.1	5.9*	6.0*	**4.3×10^{-4}**
Ave. Wind Speed (m s^{-1})	Annual	0.95	0.93	1.02*	**1.2×10^{-2}**
	Apr–Sept	0.94	0.89	1.02*	**2.5×10^{-3}**
	Oct–Mar	0.96	0.98	1.04	1.1×10^{-1}
Rainfall (mm)	Annual	1496.5	1437.1	159.7	8.9×10^{-1}
	>50 mm d^{-1}	335.0	342.9	308.1	9.5×10^{-1}

*significantly different from Period A by rank-sum test

Table 3.3. Results of rank-sum tests at $\alpha = 0.05$ for the climate parameters. Significantly different p-values are in bold characters.

Parameter	Time Category	Average per Period		rank-sum p-value
		B	C	
Air Temperature (˚C)	Annual	12.1	12.4	1.8×10^{-1}
	Apr–Sept	18.3	18.7	5.0×10^{-1}
	Oct–Mar	5.9	6.0	5.3×10^{-1}
Ave. Wind Speed (m s^{-1})	Annual	0.93	1.02*	**8.0×10^{-3}**
	Apr–Sept	0.89	1.02*	**3.3×10^{-3}**
	Oct–Mar	0.98	1.04	8.0×10^{-2}
Rainfall (mm)	Annual	1437.1	159.7	6.4×10^{-1}
	>50 mm d^{-1}	342.9	308.1	5.7×10^{-1}

*significantly different from Period B by rank-sum test

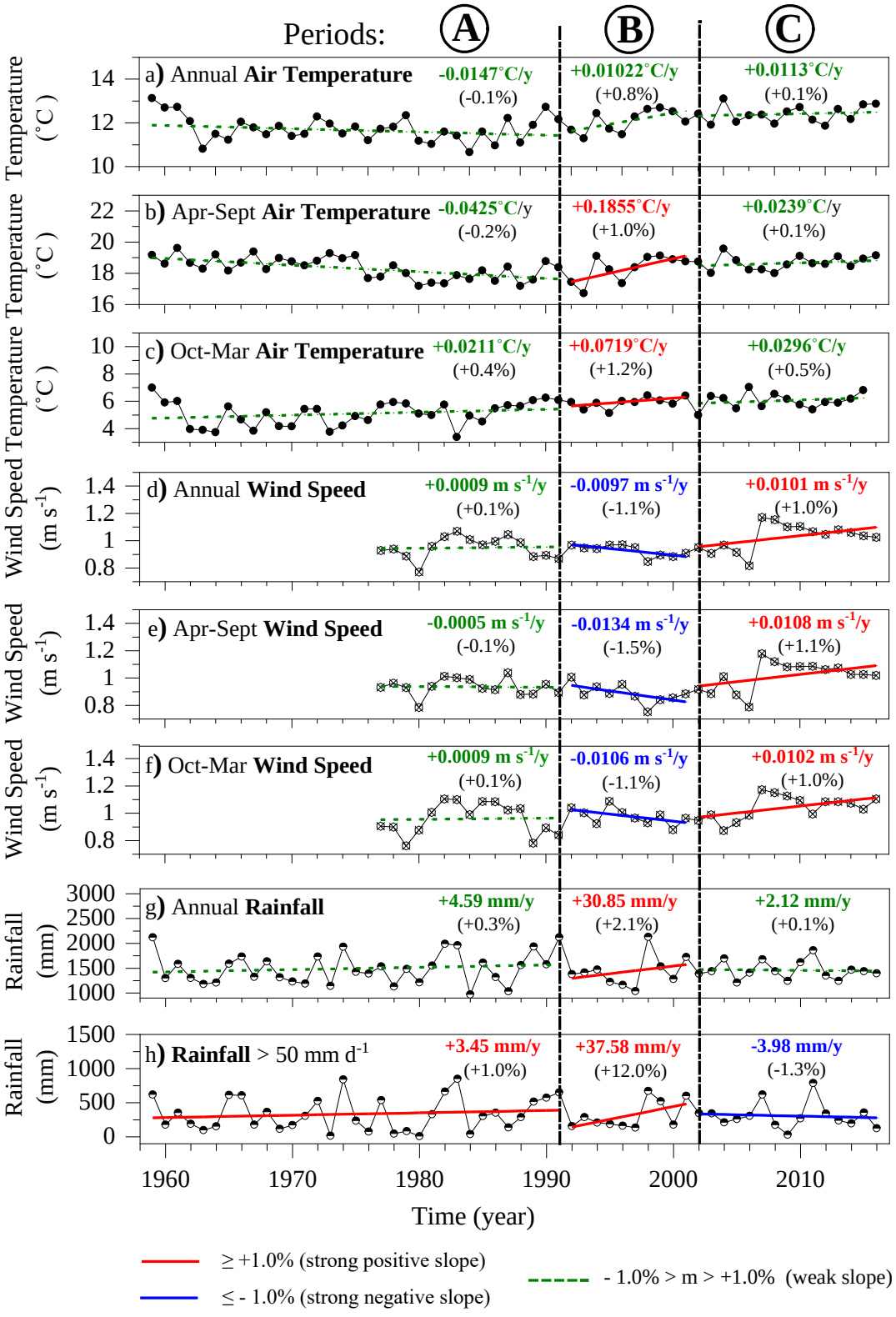

Figure 3.3. Average air temperature (a–c), average wind speed (d–f) and basin-averaged rainfall (g, h). Colored straight lines are linear fit for each period, with colored texts as slopes, while values in parentheses are slope percentages (slope value/average value for that period × 100).

3.2.2 Water Temperature Distribution and Trends

Fig. 3.4 presents the reservoir temperatures recorded at different depths from 1959 to 2016, while **Fig. 3.5** provides the average weekly temperature for the year for each period. The general pattern follows a trend where low values can be observed during winter (December to February), peaking during summer (August) and decreasing with the onset of autumn. Large fluctuations are observed for surface water temperature (0 m), with a high of 25°C and a low of 5°C for all three periods. On the other hand, Period A (**Figs. 3.4a and 3.5a**) shows warmer conditions for the 10-, 20-, 30-, and 70-m depths, while Periods B (**Figs. 3.4b and 3.5b**) and C (**Figs. 3.4c and 3.5c**) are mostly colder at these depths. Temperatures at the 70-m depth for the two latter periods are relatively flat at the 5°C level. Closer lines between depths mean a relatively mixed condition at these layers, while gaps between the layers indicate an apparent thermocline. For Period A, small temperature gaps are evident between the 30- and 70-m depths from late summer until autumn. Meanwhile, large gaps are manifested for Periods B and C between the 10-m and 30-m depths over the entire year, except during winter, where mixing occurs. Between the 30- and 70-m depths for Periods B and C, temperature gaps are larger for the latter, meaning that Period C exhibits deeper thermocline and thicker epilimnion than Period B.

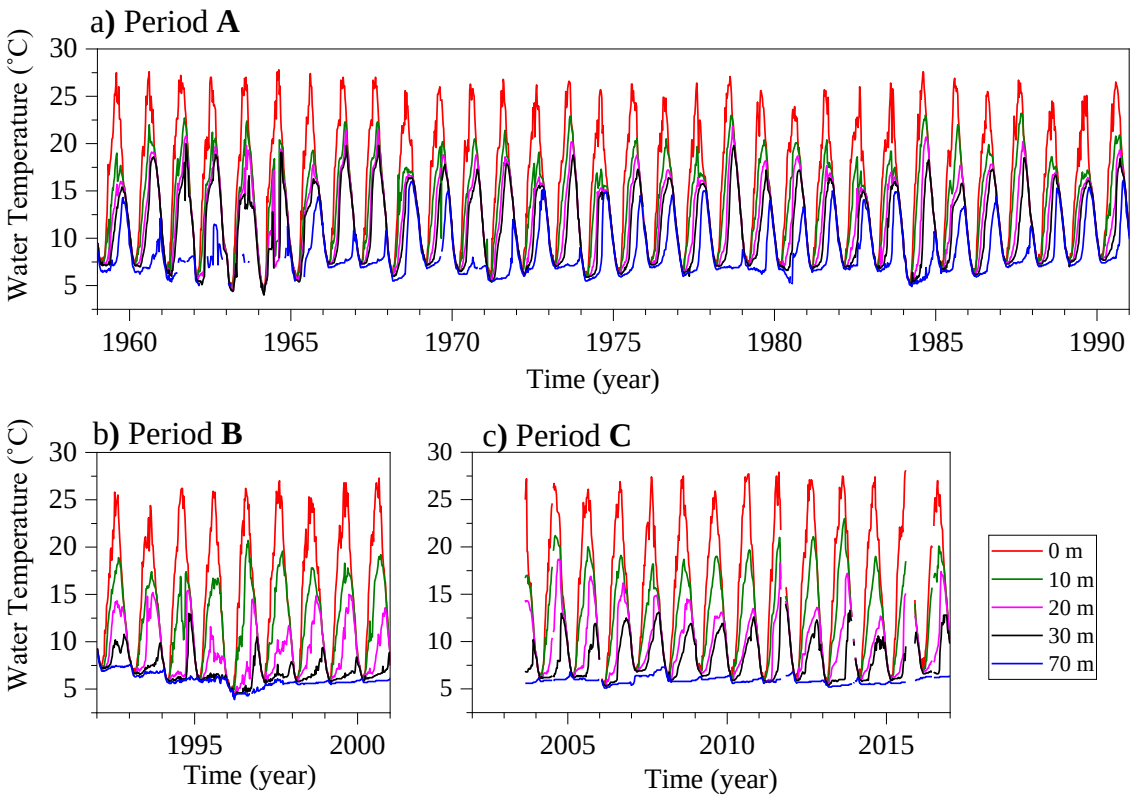

Figure 3.4. Long-term fluctuations in water temperature at different depths for the three periods (a, b and c). Data are unavailable for 2002 and largely incomplete for 2003.

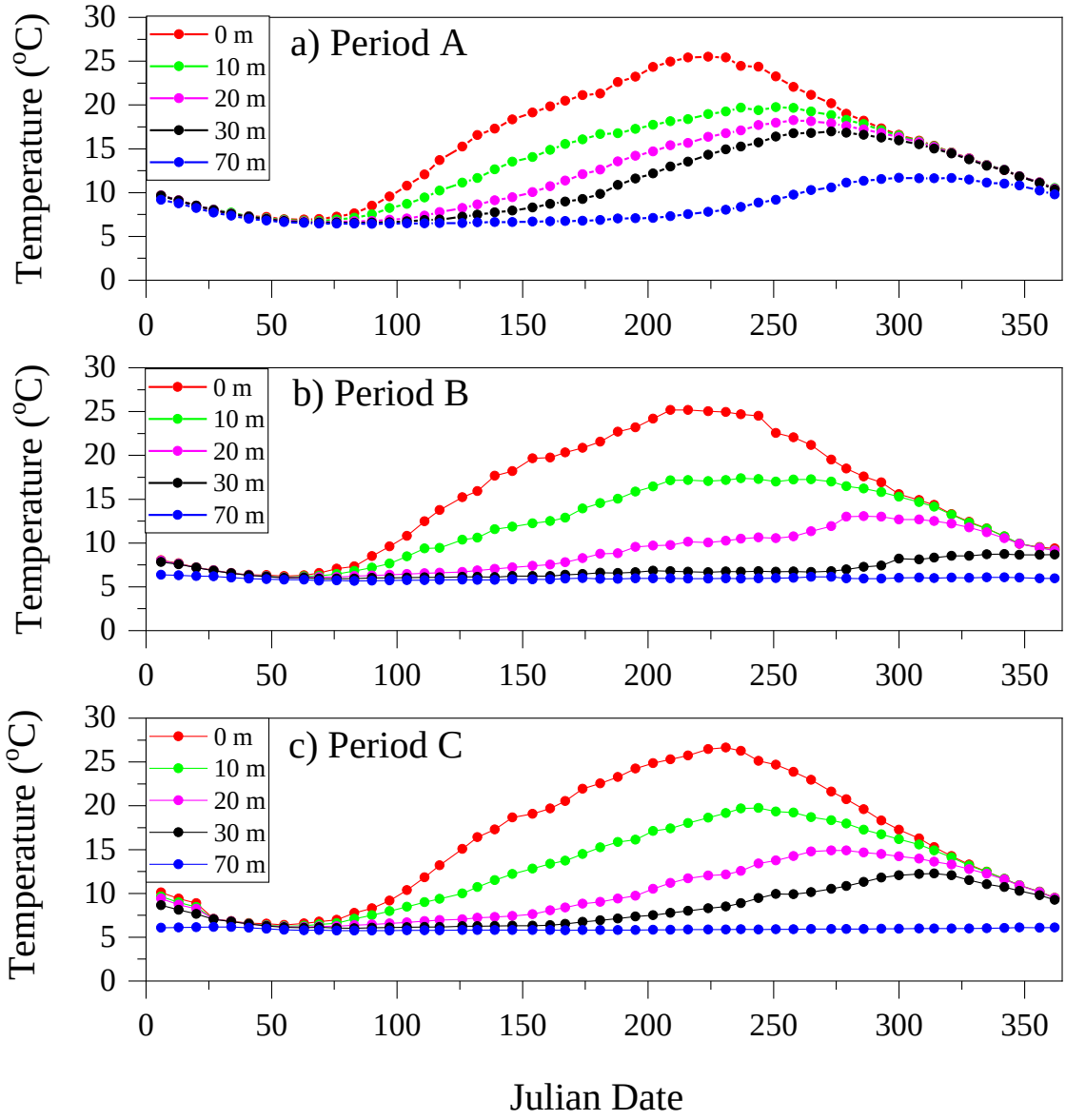

Figure 3.5. Average weekly water temperatures at different depths for different periods (a–c). To get the average per period, the transitional years between two periods are eliminated.

For the surface water temperature (SWT), no observable differences can be seen among the three periods during the summer half-year; however, the two latter periods appear to be generally colder than Period A during the winter half-year (**Table 3.4**). On average, the SWT for Periods B and C decreased relative to Period A. Kruskal–Wallis tests showed significant differences among the periods ($p = 0.0019$) for the winter half-year (October to March), while rank-sum tests further confirmed the significant differences of Periods B and C with Period A. Furthermore, based on M–K analysis

(**Table 3.5**), the SWT decreased for the year at −0.06°C decade^{-1} (nonsignificant, p = 0.2033) and for the winter half-year at −0.15°C decade^{-1} (significant, p = 0.0201), with no observable trend for the summer half-year (April to September). During the year and the winter half-year, the SWTs were decreasing, although air temperatures were significantly rising (**Table 3.1**). This surface cooling phenomenon can be strongly attributed to the change in reservoir management procedures.

For the temperatures below the water surface (10 to 70 m), Kruskal-Wallis test affirmed the significant differences among periods. Period A is generally warmer than B and C, on average (**Table 3.4**). During the summer half-year, large temperature gaps in the upper layer are observed in Periods B and C, indicating the presence of strong thermo-clines (**Fig. 3.6a**). During the winter half-year (**Fig. 3.6b**), while Period A is mostly isothermal, Periods B and C still have inherent stratification, as observed from the relatively large temperature gaps between the 20- and 70-m depths.

Table 3.4. Results of Kruskal–Wallis (K–W) and rank-sum tests at α = 0.05 for water temperatures at various depths. Significantly different p-values are in bold characters.

Depth	Season	Average per Period (˚C)			K–W p-value
		A	B	C	
0 m	Apr–Sept	20.09	20.09	20.40	3.6×10^{-1}
(SWT)	Oct–Mar	11.23	10.44*	10.73*	**1.9×10^{-3}**
10 m	Apr–Sept	15.58	13.98*	14.61*	**8.4×10^{-6}**
	Oct–Mar	11.06	10.08*	10.22*	**1.6×10^{-3}**
20 m	Apr–Sept	12.87	8.63*	9.75*	**1.9×10^{-9}**
	Oct–Mar	10.91	9.31*	9.47*	**4.7×10^{-6}**
30 m	Apr–Sept	11.14	6.40*	7.41*	**1.2×10^{-9}**
	Oct–Mar	10.76	7.46*	8.61*	**1.0×10^{-8}**
70 m	Apr–Sept	7.59	5.85*	5.79*	**1.4×10^{-7}**
	Oct–Mar	9.20	5.91*	5.97*	**7.0×10^{-9}**

*significantly different from Period A by rank-sum test

Table 3.5. Results of the Mann–Kendall (M–K) test at α = 0.05 for long-term values of surface water temperatures. Significantly different p-values are in bold characters.

Parameter	Time Category	M–K z-stat	M–K p-value	Sen's Slope
Surface Water Temperature	Annual	−1.2723	0.2033	−0.06 °C decade^{-1}
	Apr–Sept	+0.0566	0.9549	<0.01 °C decade^{-1}
	Oct–Mar	−2.3253	**0.0201**	−0.15 °C decade^{-1}

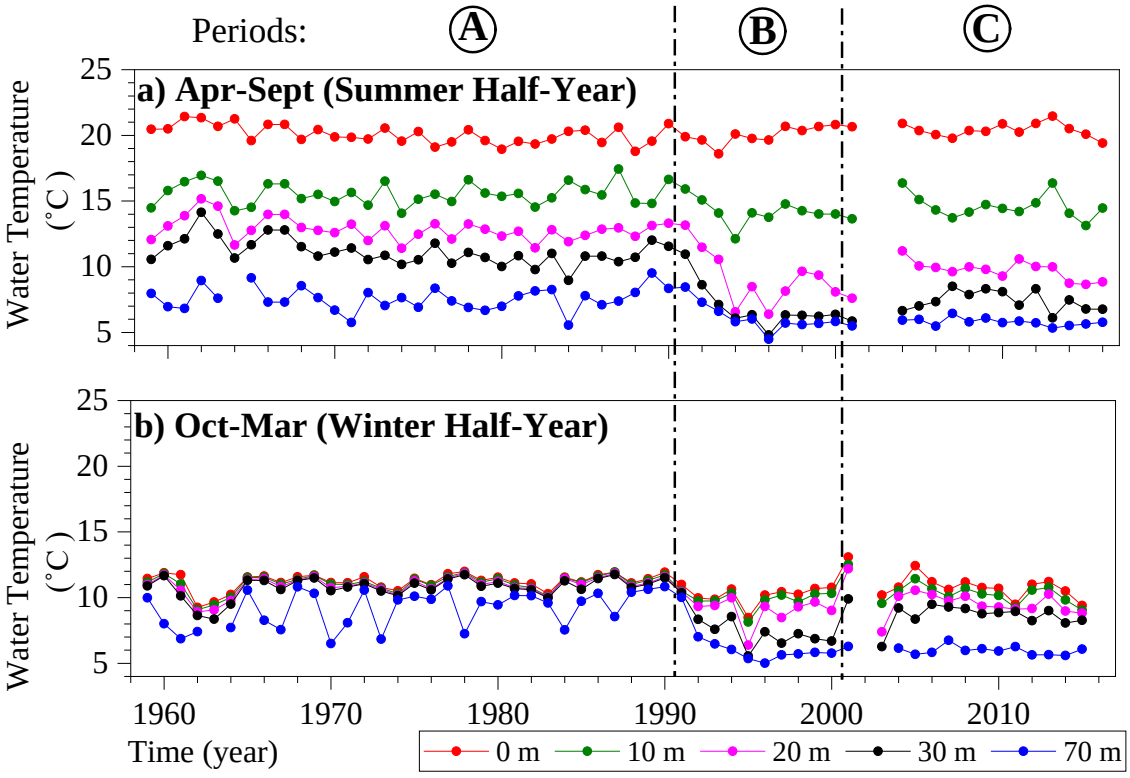

Figure 3.6. Average annual water temperatures at different depths from 1959 to 2016 for (a) the summer half-year and (b) the winter half-year.

3.2.3 Heat Content in the Reservoir

For the average weekly trends of heat content (**Fig. 3.7**), the Q peaks around Day 270 (end of September), while it is the lowest around Day 75 (mid-March) in general for the three periods. Period A consistently attained the highest amount of heat stored in the

reservoir. Periods B and C have similar trends, although Period C has relatively higher heat content than Period B. The deeper outflow level from the SW and the presence of the VC have played a role in the higher heat content of Period C. The observed differences in the plots of temperature profiles and heat content suggest that the operation of the facilities significantly influenced the thermal structure of the reservoir. This is further explained in the succeeding sections.

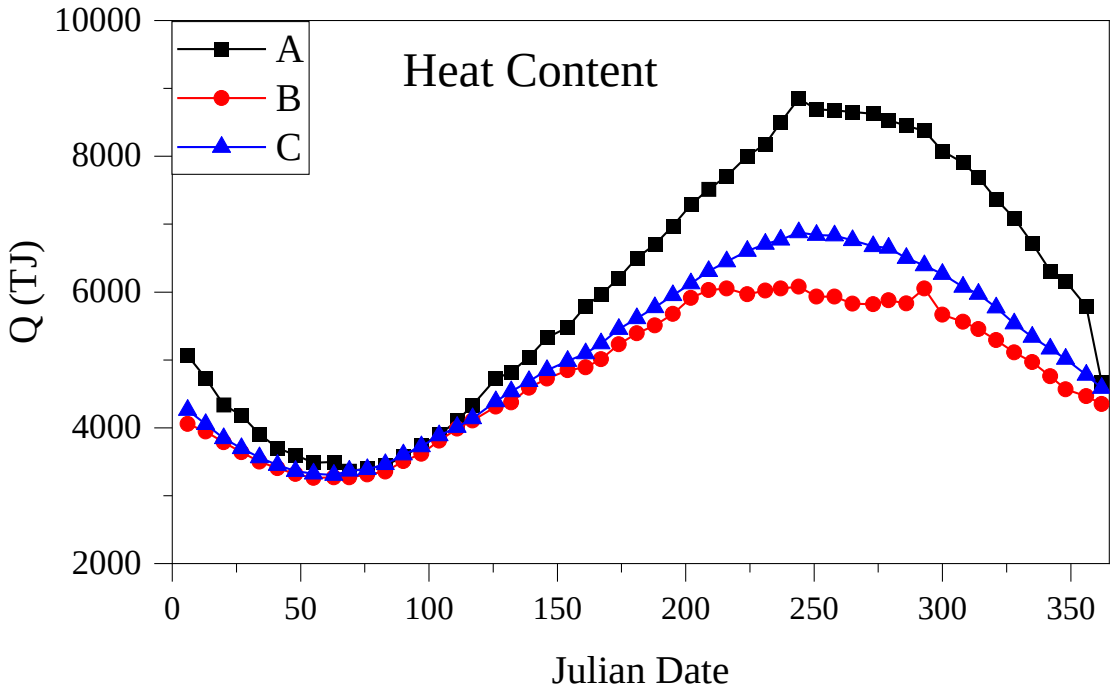

Figure 3.7. Time series plots of heat content for the three periods.

On **Table 3.6**, it shows that the heat content is significantly different among periods by K-W test for both seasons. Furthermore, the rank-sum test reveals that Period B and C are significantly different from period A, such that the two latter periods exhibit lower Q for both the summer and winter half-years. On **Table 3.7**, rank-sum test shows that Period B is significantly different from Period C based on Q.

The interannual variability of heat content is shown on **Fig. 3.8.** On average, for the summer half-year (**Fig. 3.8a**), Period A shows the highest value of Q, with 6600 TJ, followed by C with 5500 TJ, and, lastly, by B with 5200 TJ. For the winter half-year (**Fig. 3.8b**), Period A still obtains the highest average Q, followed by C and then B. In summary, Period A manifests higher Q than Periods B and C. Higher Q is observed for Period A as it has a warmer water column and thicker epilimnion.

The trend of heat content can also be compared with those of meteorological forcing. Period A, which generally exhibited weak slopes for air temperature and wind speed during both seasons, obtained relatively weak slopes for Q during the summer half-year. For Period B during both seasons, the increase in air temperature and rainfall and the decrease in wind speed (**Fig. 3.3**) are associated with the decrease in Q. On the other hand, for Period C, specifically during the winter half-year, the increase in wind speed is associated with decreasing trends in Q. To summarize, while the difference in the average values of different parameters of Q is brought largely by the varying reservoir operations, the short-term trends of Q in every period are highly associated with the trends of air temperature and wind speed.

Table 3.6. Results of Kruskal–Wallis (K–W) and rank-sum tests at $\alpha = 0.05$ for heat content (Q) for the two seasons. Significantly different p-values are in bold characters.

Parameter	Season	Average per Period (TJ)			K–W p-value
		A	B	C	
Q	Apr–Sept	6.6	5.2*	5.5*	**3.2×10^{-6}**
	Oct–Mar	5.5	4.3*	4.6*	**1.9×10^{-6}**

*significantly different from Period A by rank-sum test

Table 3.7. Results of rank-sum tests at $\alpha = 0.05$ for heat content (Q) for the two seasons. Significantly different p-values are in bold characters.

Parameter	Season	Average per Period (TJ)		Rank Sum p-value
		B	C	
Q	Apr–Sept	5.2	5.5*	**3.5×10^{-2}**
	Oct–Mar	4.3	4.6*	**4.1×10^{-3}**

*significantly different from Period B by rank-sum test

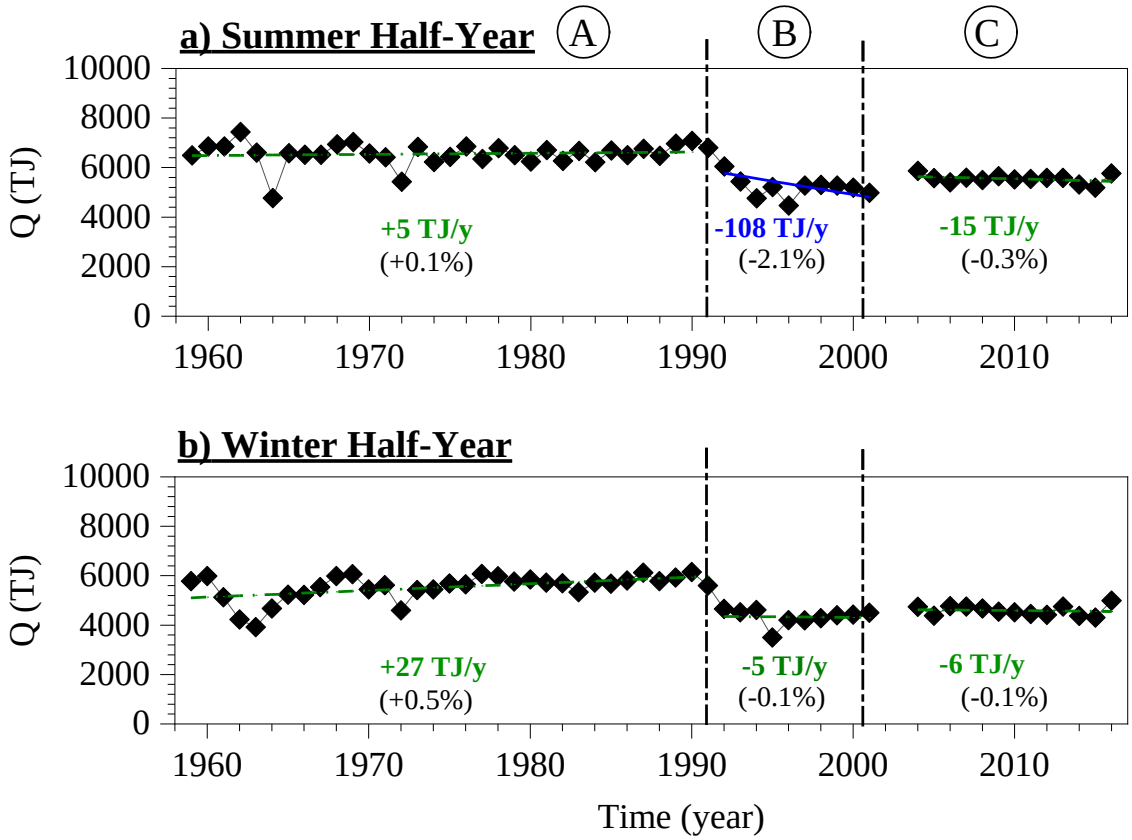

Figure 3.8. Time series plots of heat content for (a) summer half-year and (b) winter half-year. Colored straight lines are linear fit for each period, with red representing a strong positive slope ($m \geq +1\%$), blue for a strong negative slope ($m \leq -1\%$), and green for a weak slope ($-1\% > m > +1\%$). Colored texts are slopes, while values in parentheses are slope percentages (slope value/average value for that period × 100).

3.3 Discussion

3.3.1 Correlation Between Climate Forcing and Reservoir Temperatures

Pearson correlation coefficients (r) between the climate forcing and reservoir temperatures were obtained. Long-term correlation (1959-2016) was made only between climate forcing and surface water temperature (SWT), excluding the 10- to 70-m temperatures. On the other hand, all water temperatures (0 to 70 m) were included in the short-term correlation for every period.

For the long term, SWT shows a positive correlation with air temperature for the summer half-year ($r = 0.73$) and a negative one with wind speed ($r = -0.29$) for the winter half-year. Meanwhile, other meteorological parameters acquire very weak correlations for both seasons. It has to be noted that strong correlation is not evidence of a mechanistic effect, i.e., correlation is not causation. The long-term correlation established specifically between air temperature and SWT should not be confused with the long-term trends generated from the M–K test. While there is a strong positive correlation between the two parameters during the summer half-year, the M–K test showed no significant long-term trends in the same period. In the same way, while the correlation between the two parameters appeared to be weak during the winter half-year, the M-K test showed significant in-verse trends.

For the short term, SWTs for Periods A and B show positive correlation with air temperature for April to September ($r_A = 0.76$; $r_B = 0.86$) and October to March ($r_A = 0.64$; $r_B = 0.73$), with Period C exhibiting very weak correlation. The warming of the surface water occurs via downward longwave radiation, as associated with the increase in air temperature. SWT in Period B has a negative correlation with wind speed, specifically during the summer half-year ($r_B = -0.38$). Furthermore, a weak correlation between SWT and basin-averaged rainfall is seen for Periods A and B for both seasons, but SWT is negatively correlated with basin-averaged rainfall during the winter half-year ($r_C = -0.58$) for Period C. Considering the deeper layer of the reservoir, air temperature and wind speed have very low correlation with the temperatures at the 10- to 70-m depths. However, a positive correlation is detected between basin-averaged rainfall and the 70-m layer temperature, with r of 0.58 and 0.65 for Period A during the summer half-year and winter half-year, respectively.

This correlation tests showed that at some cases, negative correlation is found between climate and water temperature. However, in most cases, the correlation between the two parameters are extremely weak. Due to the low frequency of strong correlation between climate and water temperatures, it can be inferred that that the effect of climate is considered to be less significant.

3.3.2 Effect of Climate Warming and Facilities on Surface Water Temperatures

The phenomenon of long-term surface warming associated with climate change has been observed in many lakes. Surface temperatures of several lakes worldwide were found to significantly rise consistent with annual increases in air and ocean surface temperatures(O'Reilly et al., 2015). Furthermore, lakes in Europe, North America and Africa were identified to encounter warming trends together with varying thermal regimes (Coats et al., 2006). The increase in surface water temperatures could result to increased rates in evaporation (Helfer et al., 2012; Trumpickas et al., 2009) and in bacterial and phytoplankton activity (Woolway et al., 2019), enhanced thermal resistance to vertical mixing (Butcher et al., 2015), shorter period of ice covers specifically for dimictic lakes (Arvola et al., 2009) and proliferation and invasion of warm-water aquatic species (Trumpickas et al., 2009). In the Ogouchi catchment, climate warming indeed took place specifically during winter half-year (mid-autumn to early spring) yet no significant trend occurred in the summer half-year (mid-spring to early autumn). This means that the area has been experiencing warmer winters in recent years, which is consistent with the warming trends of the cold seasons in the country (Japan Meteorological Agency, 2017). Most sets of literature have established that long-term increasing trends in air temperatures follow the subsequent increase in surface water temperatures but the result of this study actually suggests the reverse, i.e., surface water cooling despite climate warming. While it cannot be discounted that the visible rising trends in wind speeds could have induced reservoir surface cooling during the recent years, it has to be noted that other factors could have directly caused this cooling phenomenon.

It is asserted rather that the lowering of the surface water temperatures of the reservoir is associated with the operation of certain water control facilities. Vertical curtains were specifically installed in the upstream reaches of the Ogouchi Reservoir not only to prevent the dispersion of phytoplankton into the main water body but also for the purpose of promoting surface cooling (Takahashi, 2008). Lower values of surface water

to air temperature ratios were computed for Periods B and C, confirming that the use of SW and VC facilities leads to a much lower surface temperature in the reservoir. The immediate release of reservoir water from the epilimnion during Periods B and C would limit the radiant heating of the upper layer, thereby causing the temperature drop in the surface and epilimnetic waters. The two latter periods also facilitated the creation of a strong thermocline that limits the advective heat transfer between the epilimnion and the hypolimnion. In the case of Period A, the atmosphere has more opportunity for heat transfer with the reservoir, which could have encouraged the warming of the water body as manifested in Lake Dillon (Lewis et al., 2019), with the same deep withdrawal operation as the Ogouchi Reservoir. Likewise, the negative correlation of rainfall and surface water temperatures in Period C suggests that strong rainfall is associated with the cooling of reservoir surface as induced by the VC. Furthermore, it is not only the vertical curtain alone but rather its combined operation with selective withdrawal that the reservoir surface temperatures are eventually lowered. The curtains facilitate the plunging of the colder river water, which then replenishes the epilimnion after the warm near-surface waters have been released out of the reservoir through SW. Without the VC, the SW can likewise be used alone to maintain colder surface and epilimnetic waters but the operation requires optimized withdrawal techniques at different layers to deliver the desired results. Additionally, the use of SW without the VC could be detrimental as it can create optimum conditions for eutrophication.

Some other factors that affect lake and reservoir cooling are likewise recognized. Among these are the thickness of the forest cover of the surrounding watershed and the clarity and transparency of the water body. Thicker forest covers reduce the surface winds while increased dissolved organic matter enhances light attenuation, both of which can result to the cooling of the overall water temperature profile and the rising of the thermocline (Heiskanen et al., 2015; Tanentzap et al., 2008). Increased water clarity can cause the faster warming of surface water as it influences the vertical partitioning of heat (Rose et al., 2016). Despite regional signatures of climate warming, an urban lake in Canada was identified to experience overall temperature drop as attributed to forest re-growth and increased dissolved organic matter (Tanentzap et al., 2008). In the Ogouchi catchment, reforestation efforts have been implemented since 1986 through non-clear cutting of timbers and multi-layer planting, thus reducing sedimentation rates and erodibility (Gunay et al., 2019) and increasing surface roughness as wind buffer. Likewise,

the amount of suspended sediments, nutrients and phytoplankton together with runoff and erosion patterns that influence the overall water quality and clarity of the reservoir (Point, 2016) might have changed over the years. While it is true that the reduction in surface winds and water clarity may facilitate reservoir cooling, their effects may be considered minimal as the process involved is slow in the long term and is greatly affected by high climate variability. The operation of SW and VC arguably has far stronger and more direct effects on lowering water temperatures versus the two other aforementioned factors as these facilities can alter outright the hydrodynamics of the reservoir.

3.3.3 Effect of Facilities on the Overall Thermal Regime

The downstream outflow control by DPW and SW and the upstream inflow interception by VCs can explain the significant differences in water temperature distributions among the three periods for both the summer half-year and winter half-year, as shown in **Fig. 3.9**.

In Period A, the river water largely disperses and remains for a longer period within the reservoir and replaces the colder water in the deep zone. This subsequent interaction of river water with the hypolimnetic water could explain the high correlation in Period A between bottom water temperatures and rainfall, wherein the latter serves as the primary source for river inflow. On the other hand, in Period B, the abstraction of water through SW leads the inflow to follow a narrow path along the upper layer and encourages most of the river water to be released directly out of the dam. The apparent thermocline formation during Period B not only limits the thermal advection between the upper and lower layers of the reservoir (Zouabi-Aloui et al., 2015) but further shields the radiant heat transfer from the atmosphere to the hypolimnion (Lewis et al., 2019). This can further reaffirm why air temperature is highly correlated with SWT but not with the temperatures at the deeper layers. Furthermore, shallow withdrawals can diminish the internal heat in the reservoir over the summer and can offset the effect of further warming (Mi et al., 2019).

Meanwhile, during Period C, the curtains facilitated the plunging of the river water underneath it, limiting the flow to a layer way below the level of inflow and making a slightly wider epilimnion than in Period B. The two curtains acted as hydraulic and thermal barriers against the direct intrusion of the river water into the upper layer of the reservoir. River water has relatively larger velocity and different temperatures than the

reservoir, and its manner of dispersion in the reservoir, as affected by the VC, essentially influences the thermal structure of the water body.

Looking at **Fig. 3.9**, higher heat was stored in the reservoir during Period A, compared to Periods B and C. In the case of the two latter periods, the heat exchange between the epilimnion and hypolimnion was strongly limited by the thermocline, hence the lower values of Q. In one study that carried out a heat budget analysis of the Sau Reservoir, it was found that hypolimnetic withdrawals increased the reservoir's annual Birgean heat budget (ABHB) while intermediate withdrawals produced stronger thermoclines and decreased both Q and ABHB (Moreno-Ostos et al., 2008). Eventually, that study concluded that hydraulic management can partially counteract the effects of climate warming.

This present study strongly establishes that the different behaviors of the thermal structure of the reservoir in the three periods are mainly caused by management and not climate warming and that some management strategies can be used to mitigate certain climate impacts. Nevertheless, this only generalizes the effects of surface releases with the use of the SW facility but has not yet explored the effect of withdrawals at different depths. The operation of the Ogouchi Reservoir can still be optimized in order to maintain desirable water quality not only in the main reservoir body but also with the released water downstream.

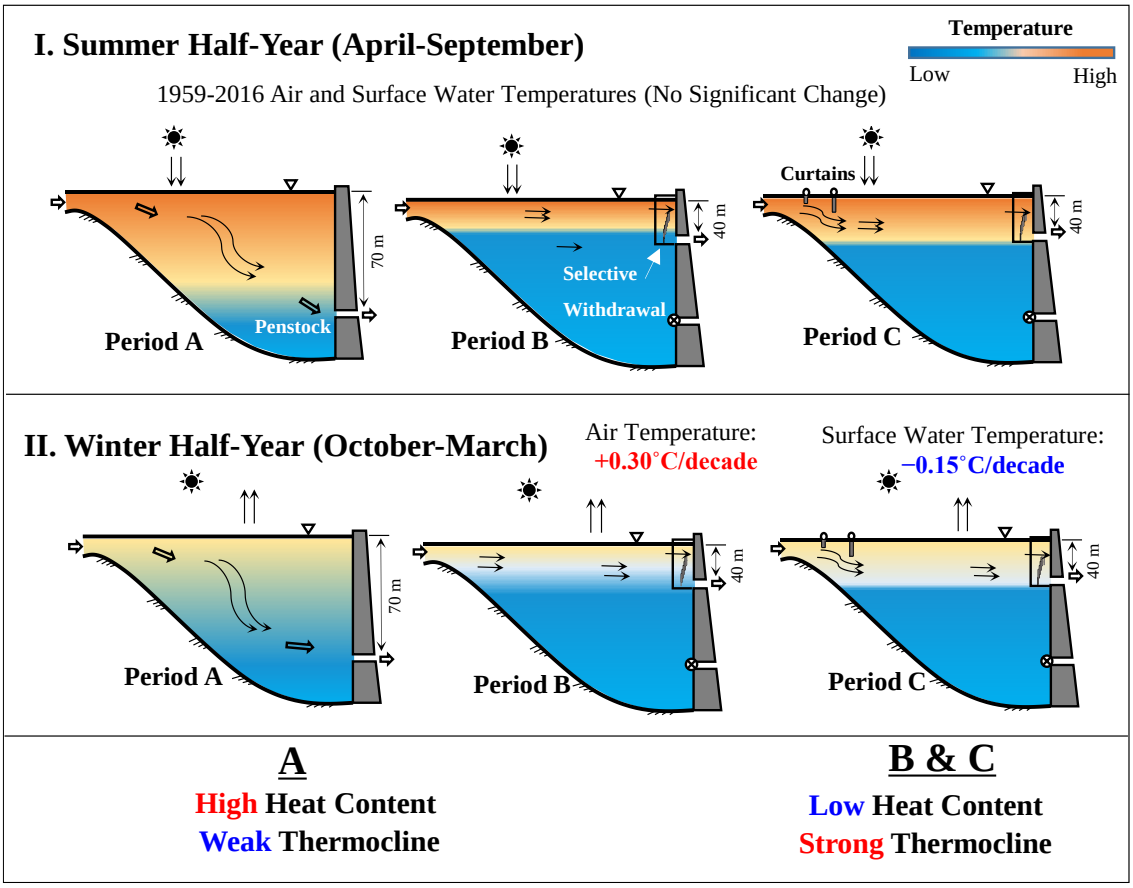

Figure 3.9. The thermal regime of the Ogouchi Reservoir as affected by climate warming and the operation of different facilities.

3.4 Conclusions

The effects of climate on the temperature and thermal structure of a warm monomictic reservoir that have varying operations are evaluated in this study. Although air temperatures were rising, surface water temperatures were found to be decreasing in the long term. Climate forcing affects the reservoir temperatures within the individual periods, but the varying reservoir operation has been identified to ultimately influence the differences in thermal responses among the periods. Kruskal-Wallis tests affirmed that the distributions of water temperatures were significantly different among the three periods, while rank-sum tests proved that Periods B and C were significantly different (colder) to Period A. The two latter periods also exhibited lower heat content due to their shallower epilimnion. Flow interception by VCs upstream and outflow control by DPW and SW downstream play a large role in either inhibiting or enhancing the radiant heat transfer from the atmosphere to the reservoir and advection between epilimnion and hypolimnion with the presence of thermocline.

This study reveals that the thermal condition of the reservoir is not significantly affected by climate warming. Reservoir operation bears a stronger influence on the temperature and thermal structure of the reservoir than climate change itself. The use of SW and VCs appears to be a promising key to mitigate the thermal impacts of climate warming.

CHAPTER 4

Seasonal Variation in Thermal Stratification

4.1 Introduction

The stratification responses of reservoirs are dependent not only on the climate but also on the operation of hydraulic facilities that particularly control the outflows and the intrusion depth of inflow. For example, conventional deep withdrawal schemes are implemented through the penstock intake such as seen in the Shasta Lake (Hanna et al., 1999), Lake Powell (Richard Marzolf et al., 2000) and Lake Dillon (Lewis et al., 2019). With this system, hypolimnetic withdrawals are facilitated, which results in the deeper migration of both the thermocline and chemocline (Hueftle and Stevens, 2001). Shallower outflows, on the other hand, can be made using selective withdrawal (SW) systems, which can enable epilimnetic water releases. A numerical simulation study (Çalişkan and Elçi, 2009) showed that near-surface releases of warm water promoted and maintained colder conditions of the hypolimnion while thermocline-level releases led to the warming of the bottom layer. In terms of other facilities, vertical curtains (VC), which are used for controlling eutrophication (Takahashi, 2008) can be installed across the river mouths in the upstream reaches to regulate the intrusion depth of inflow into the main reservoir. Using the VC modified the upstream and downstream temperature and velocity distributions of the Ogouchi Reservoir in Japan (Niiyama et al., 2010a).

It is interesting to note that the specific site for this study – the Ogouchi Reservoir – had undergone these three distinct aforementioned schemes between the years 1957 and 2016. The wealth of significant limnological data for this reservoir offers a great advantage to study in detail the effects of actual operation of the different facilities on the reservoir's thermal structure. Establishing the stratification responses for the different reservoir operations and seasons appears to be a helpful reference in further studying the stratification regimes of other water quality parameters. This study can provide reasonable inputs to the sound management of the seasonally changing water quality conditions not only for this water supply reservoir but the other monomictic reservoirs in the world.

For this study, the thermal regimes of the reservoir are evaluated during the four stages in a year, namely, 1) December-March for the mixing episode in the reservoir during winter until early spring, 2) April-July for the warming episode during spring and summer, 3) August-September for peak stratification coinciding with the typhoon season during late summer and lastly, 4) October-November as the start of cooling in preparation

for overturn in autumn. Brunt-Väisälä Frequency, thermal stability and thermocline strength are quantitatively determined in order to carry out tangible comparisons of stratification conditions among periods, rather than merely describing the differences using only temperature profiles. Likewise, this study investigates the interaction among the occurrence of notably prolonged hot or cold atmospheric conditions and the duration and the timing of onset and end of stratification, in relation to varying operation.

4.2 Results

4.2.1 Seasonal Temperature Distribution per Period

Based on **Fig. 4.1**, the temperature profiles of the reservoir significantly vary for every period and every season. In this section, every paragraph below details the discussion for every season. Data is missing for 2002 while largely incomplete for 2003 as the water quality records are unavailable at the Bureau of Waterworks. It has to be noted that these two years comprise the transition years from originally weekly measurement of water temperatures (1959-2001) to daily measurement (2004-present). During this transition, the instruments were upgraded and the VCs were also installed.

Considering Dec-Mar (**Fig. 4.1a**), Period A generally exhibits isothermal patterns at around 7-8˚C level, indicating a mixed condition in the reservoir during this cold period of the year. Meanwhile, Periods B and C show very weak stratification as indicated by a relatively small temperature gap between the 30-m and 70-m depths. Based on the average vertical profile (**Fig. 4.1e**), isothermal condition is generally confirmed for Period A showing the warmest profile. Periods B and C are weakly stratified specifically below the mid-section.

Stratification becomes strongly evident for Apr-Jul (**Fig. 4.1b**) as shown by the larger temperature gaps in the upper layers, specifically for Periods B and C. Large gaps signify the presence of a strong thermocline in that layer. The temperatures of Period A are gradually decreasing with depth. The average vertical profile in **Fig. 4.1f** confirms the stratified condition for all periods. However, Period A is relatively warmer and has a weaker thermocline than Periods B and C.

Stratification further intensifies for Aug-Sep (**Fig. 4.1c**) where peak atmospheric heating occurs. Significant differences among the temperature profiles of the three periods are observable. For Period A, large gaps are noted between 0-m and 10-m and between 30-m and 70-m intervals. Meanwhile, Period B exhibits strongly stratified condition until the 30-m depth, with a relatively mixed condition at the 70-m layer. On the other hand, Period C is consistently strongly stratified until the deepest layer. This strongly stratified condition is further shown in the average vertical profile in **Fig. 4.1g** with bottom to surface temperatures ranging from 10 to 25˚C for Period A while 5 to 24˚C for Periods B and C. Period C has a warmer profile and a deeper thermocline than B.

For Oct-Nov (**Fig. 4.1d**), isothermal conditions are observable in the upper layers of the reservoir for Period A, although the bottom layer is intermittently stratified annually. Some years where the bottom layer is stratified correspond to the years having a delayed end of stratification while those years with mixed bottom condition coincide with the years having early end of stratification. Period B, on the other hand shows a stratified condition throughout the entire vertical layer with the 20-m and 30-m layers having the largest temperature gap. For Period C, the layer between the 30- and 70-m depths of the reservoir is strongly stratified while the upper layer is relatively weaker. Based on the temperature profiles in **Fig. 4.1h**, Period A appears to approach almost isothermal conditions while Periods B and C remain stratified. Period C still has a deeper thermocline than B.

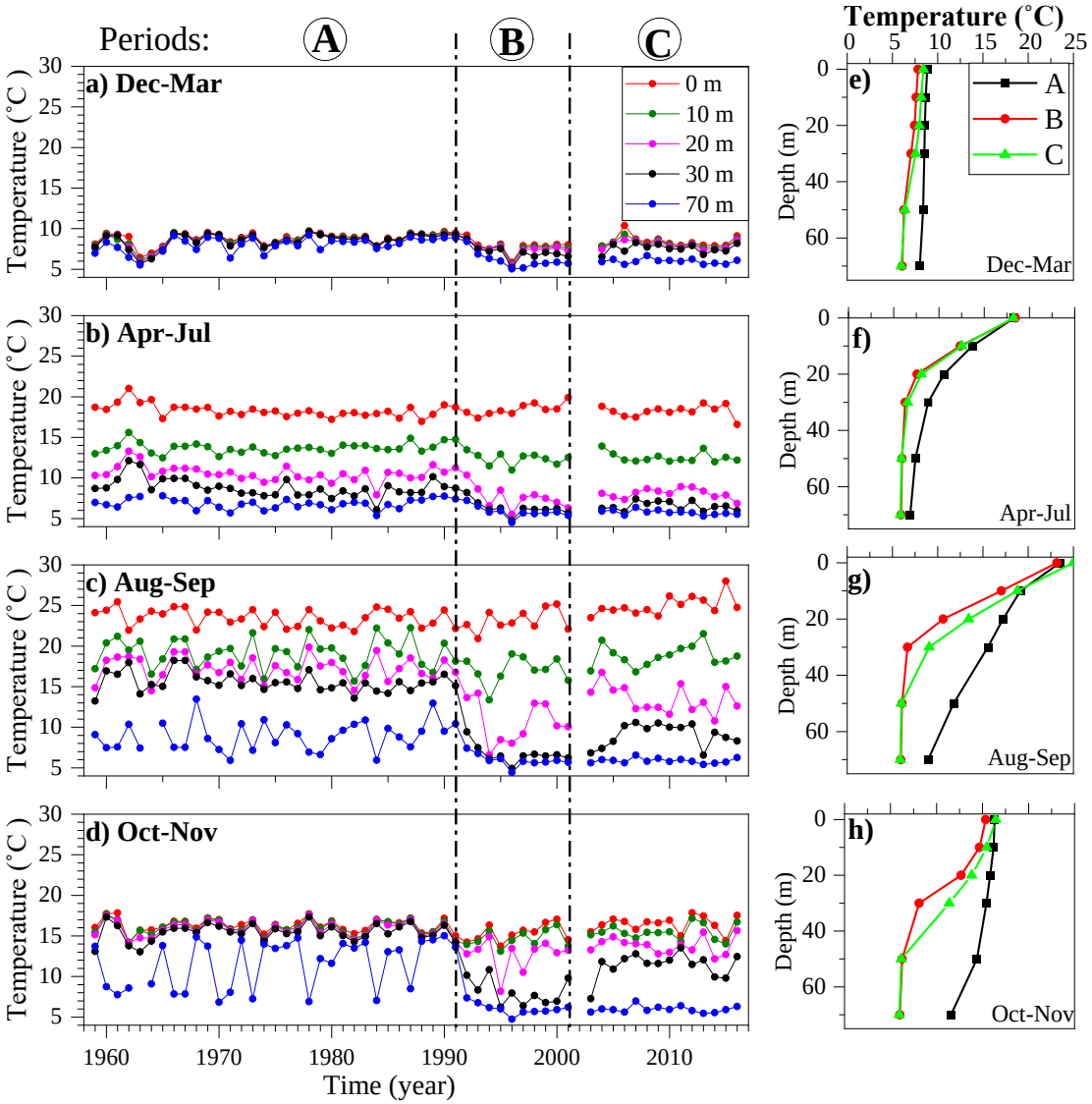

Figure 4.1. Seasonal variation in the water temperature profiles for the long term (a-d) and the average per period (e-h). Data is missing for 2002 while largely incomplete for 2003.

4.2.2 Representative Thermal Regime per Period

To compare the thermal profiles among periods, one representative year from each period was selected following certain criteria for 1) typical year, 2) cold summer year and 3) hot summer year. The year is considered typical when the annual accumulated air temperature during the heating episode (April to September) falls within +/-3% of the average for 1959 to 2016; the accumulated rainfall during the same episode is within the upper 20%, signifying a typical flood year; and that the water levels are not significantly fluctuating in that year. The selection process can be further referred to in **Fig. 4.2**. On

the other hand, a year has a cold summer when the accumulated air temperature from April to September is largely way below -3% of the long term average, while a year has a hot summer when the same atmospheric parameter is largely way above +3% of the average.

Fig. 4.3 shows the temperature contour maps of the selected representative years based on the classifications mentioned in the methods section. Considering the typical year (**Figs. 4.3a1, b1** and **c1**), the water columns for all periods are mostly isothermal from the beginning of the year until the end of March (Day 90). Meanwhile, stratification becomes evident from April (Day 91) until October (Day 273). Considering the depth of the 10˚C contour line at the end of August (Day 243), the epilimnion is widest for Period A with depth of 80 m, followed by Period C (30 m) and narrowest for Period B (15 m). This means that on average, the two latter periods have a very deep layer of the hypolimnion during the period of peak stratification. While the 10˚C contour line terminates around mid-December (Day 350) for Periods B and C, the same temperature contour line extends all the way until the beginning of the succeeding year for Period A. The dispersion of the thermal energy is more pronounced in Period A as shown by the thicker epilimnion starting from mid-July (Day 196) until almost the end of that year.

Meanwhile the cold summer years (**Figs. 4.3a2**, **b2** and **c2**) and hot summer years (**Figs. 4.3a3**, **b3** and **c3**) show almost the same pattern as the typical years, except for the fluctuating water levels and the higher water temperatures during the heating episode (April to September) for hot summer years. Same with the typical year, the cold summer years and hot summer years have Period A exhibiting a deeper epilimnion than B and C, considering the 10˚C contour line. Period C likewise has a relatively larger stratified layer compared to B. Since these profiles are based on the actual data, inherent differences are apparent among the three representative years, which can be attributed to factors other than those used in the selection criteria. To address this issue, numerical simulation was later implemented where model inputs and boundary conditions have been unified to isolate the individual effects of each operating scheme. This enables to highlight and visualize the apparent distinction of thermal stratification among periods and the direct effects of the facilities.

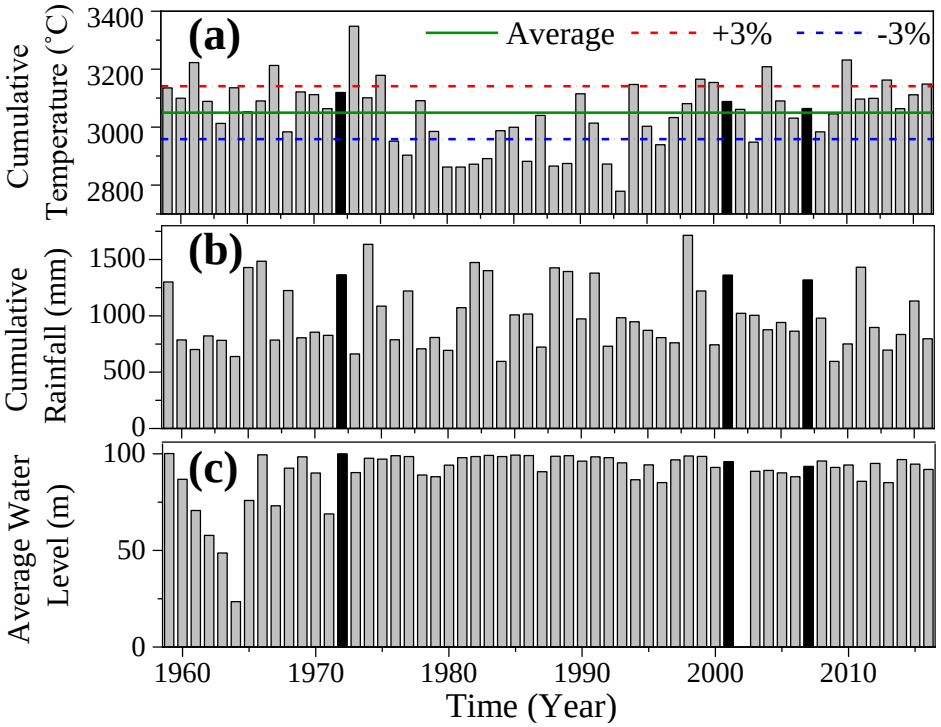

Figure 4.2 Long term values of (a) cumulative air temperature, (b) cumulative rainfall and (c) average water level for May to September. Highlighted in black bars are the chosen years (typical) for comparison, namely 1972, 2001 and 2007.

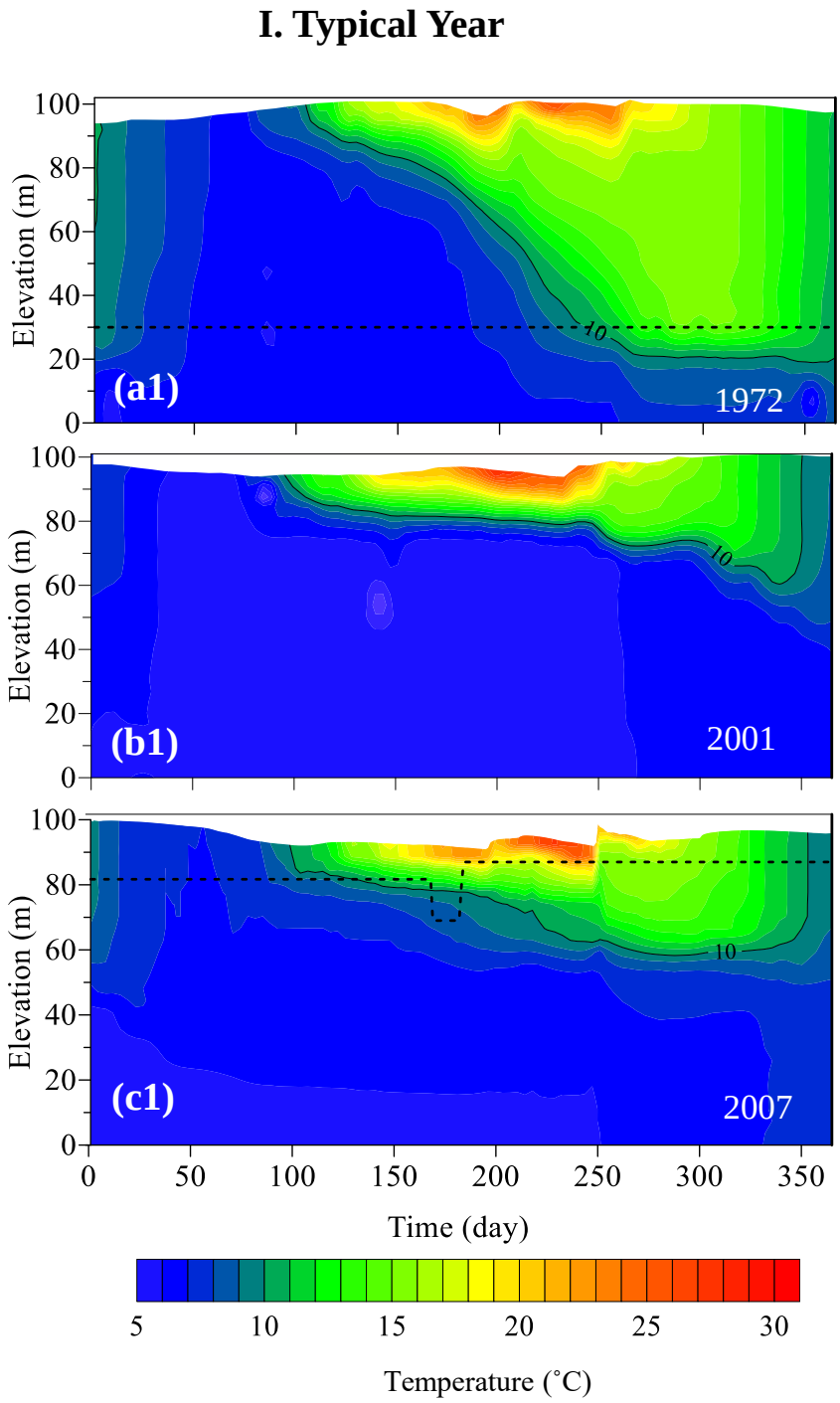

Fig 4.3. Temperature contours labelled as a1-a3 (1972, 1980, 1973), b1-b3 (2001, 1993, 1999), and c1-c3 (2007, 2008, 2004) as representative of Periods A, B and C, respectively. Dash lines indicate levels of main outflow. Actual outflow level records are unavailable except for years 1972, 1973, 1980 and 2007. However, it has to be noted that Period B was operated with 4-m deep SW intake. The thickness of the epilimnion can be visualized using the depth from the water surface of the 10˚C contour line. Selection criteria for the typical year and cold summer and hot summer years are discussed in the methods section.

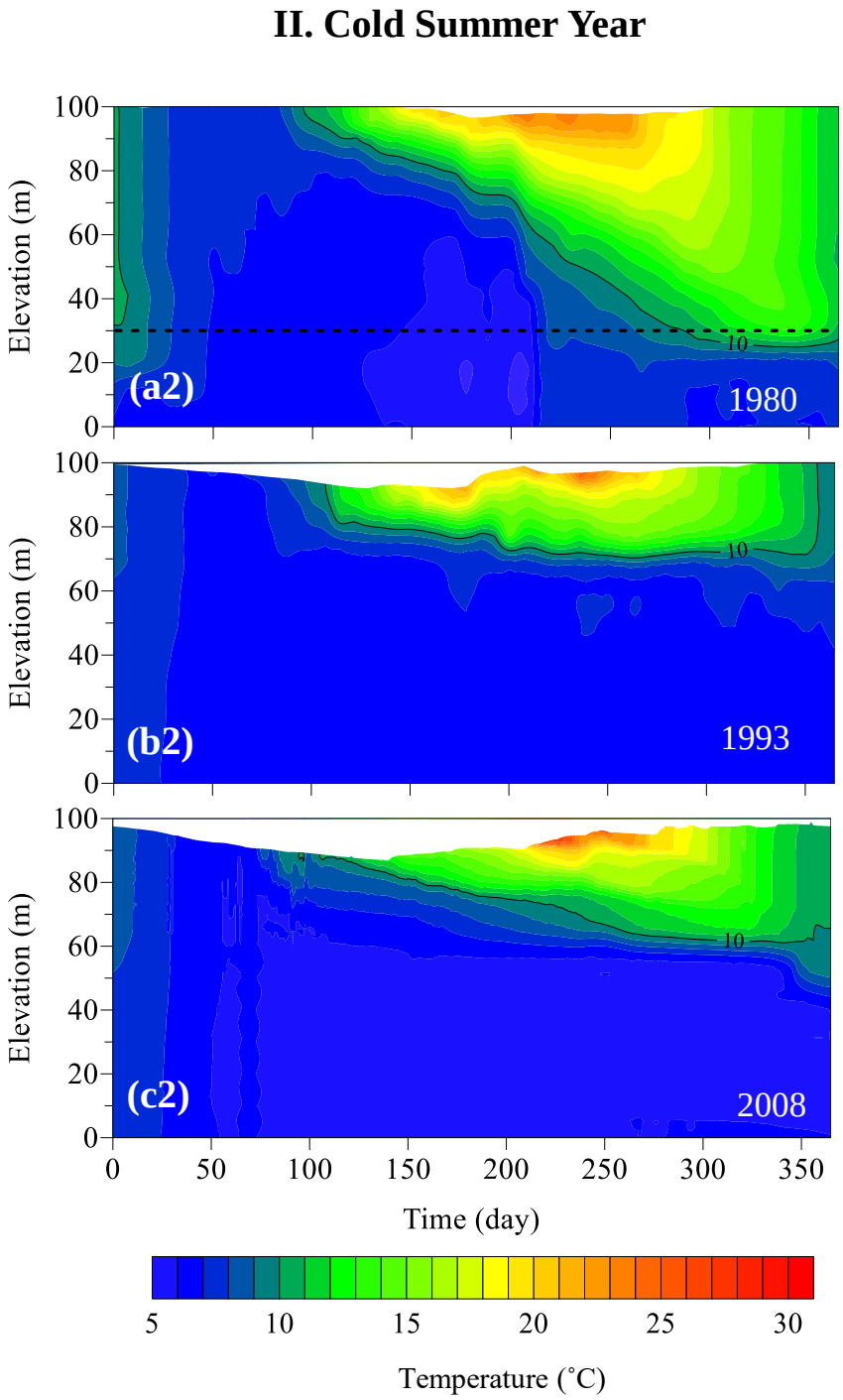

Fig 4.3. Continued…

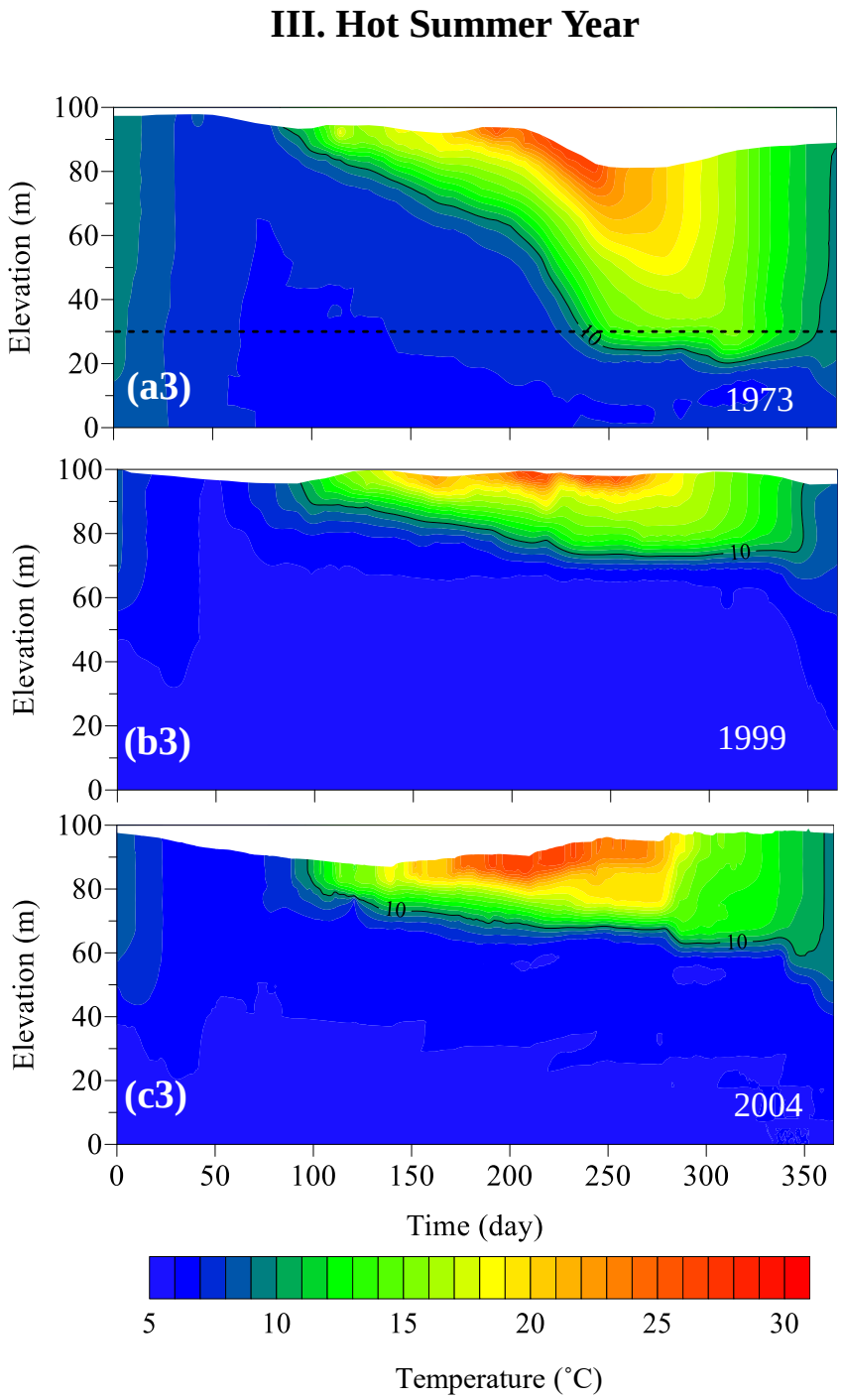

Fig 4.3. Continued…

4.2.3 Interaction of Atmosphere and River Inflows with Reservoir Temperatures

The plots of air temperature, river temperature and reservoir temperatures for the typical year of each period are given in **Fig. 4.4**. Generally for all periods, the atmosphere is much warmer than the river water from mid-March (Day 75) until mid-December (Day 350). Both the river and the atmosphere supply the additional heat in the reservoir during this warmer period. Meanwhile, the reverse happens during winter where river waters are warmer than the air. During the colder period, the river inflow provides an additional heat into the reservoir.

In terms of surface water temperatures (0-m), a similar trend is observed with air temperature from Day 75 until Day 250. However, during the rest of the year, reservoir surface waters are much warmer than the atmosphere. The drop in the air temperature during autumn causes the release of heat from the reservoir into the atmosphere, resulting in the overturning episode and the weakening of stratification.

In **Fig 4.4a**, the reservoir water temperatures at the deeper layer (30 m and 70 m) are significantly warming starting from Day 175 until Day 300. While the surface waters respond directly with the atmosphere during the entire heating period, there appears to be a delay in the warming of the deeper layer. During the cooling period, the deeper waters are much warmer than the atmosphere, which means that the reservoir could release heat into the atmosphere.

In **Fig 4.4b**, the temperatures along the 30- and 70-m depth appear to be constant at 5˚C all throughout the year, except for Day 250 to Day 365 for the 30-m layer, which is slightly warming. This means radiant and advective heat transfer could not be facilitated in the hypolimnion due to the presence of the strong thermocline developed in the upper layer.

In **Fig 4.4c**, the temperature along the 30-m depth is much higher than that of Period B but the 70-m temperatures are still constant at around 5˚C. The transfer of heat from the river inflow to the 30-m reservoir layer is possible due to the presence of the VC. This process results in the slight weakening of the thermocline at this depth.

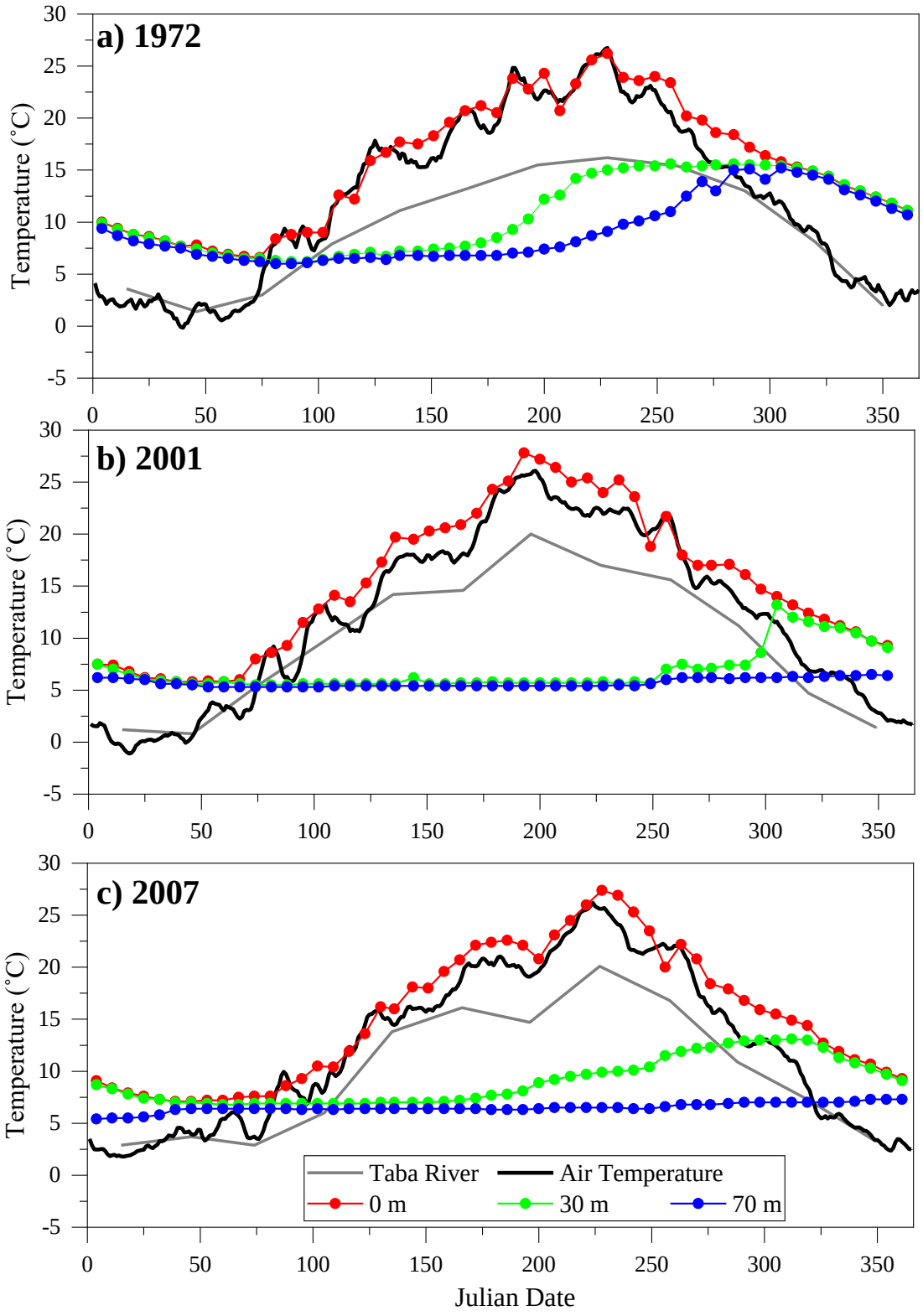

Fig 4.4. Interaction of atmosphere and river inflows with reservoir temperatures considering the typical years for the three periods: Period A-1972 (a), Period B-2001 (b) and Period C-2007 (c).

4.3 Discussion

4.3.1 Stratification in terms of the Brunt-Väisälä Frequency

The stratification of the reservoir in terms of N^2 is shown in **Figure 4.5**. For all three periods, the duration from Day 0 (1 January) until around Day 90 (31 March) is characterized by zero values of N^2. This indicates that isothermal conditions existed during this specific time range. The N^2 values are pronounced from Day 91 (1 April) to Day 273 (30 September), coinciding with spring and summer. From Day 274 (1 October) until the end of the year, the N^2 values gradually decrease as the reservoir experiences a weakening of stratification due to overturn during fall and mixing during winter.

Focusing on the peak of the summer season, stratification is more intense in August for Periods B and C compared to A. Stronger thermoclines were produced during Periods B and C because of the shallow withdrawals through the SW facility. Comparing the two latter periods with the 0.0001 contour line, stratification extends deeper for C due to the deeper SW intake and the presence of the VC.

Period A, on the other hand, has weaker stratification, as attributed to hypolimnetic withdrawals by penstock. Considering the 0.0001 contour line, the stratification extends to the deepest part of the reservoir, specifically near year-end. This means that thermoclines are developed at the deeper portions of the reservoir during the start of the cooling season.

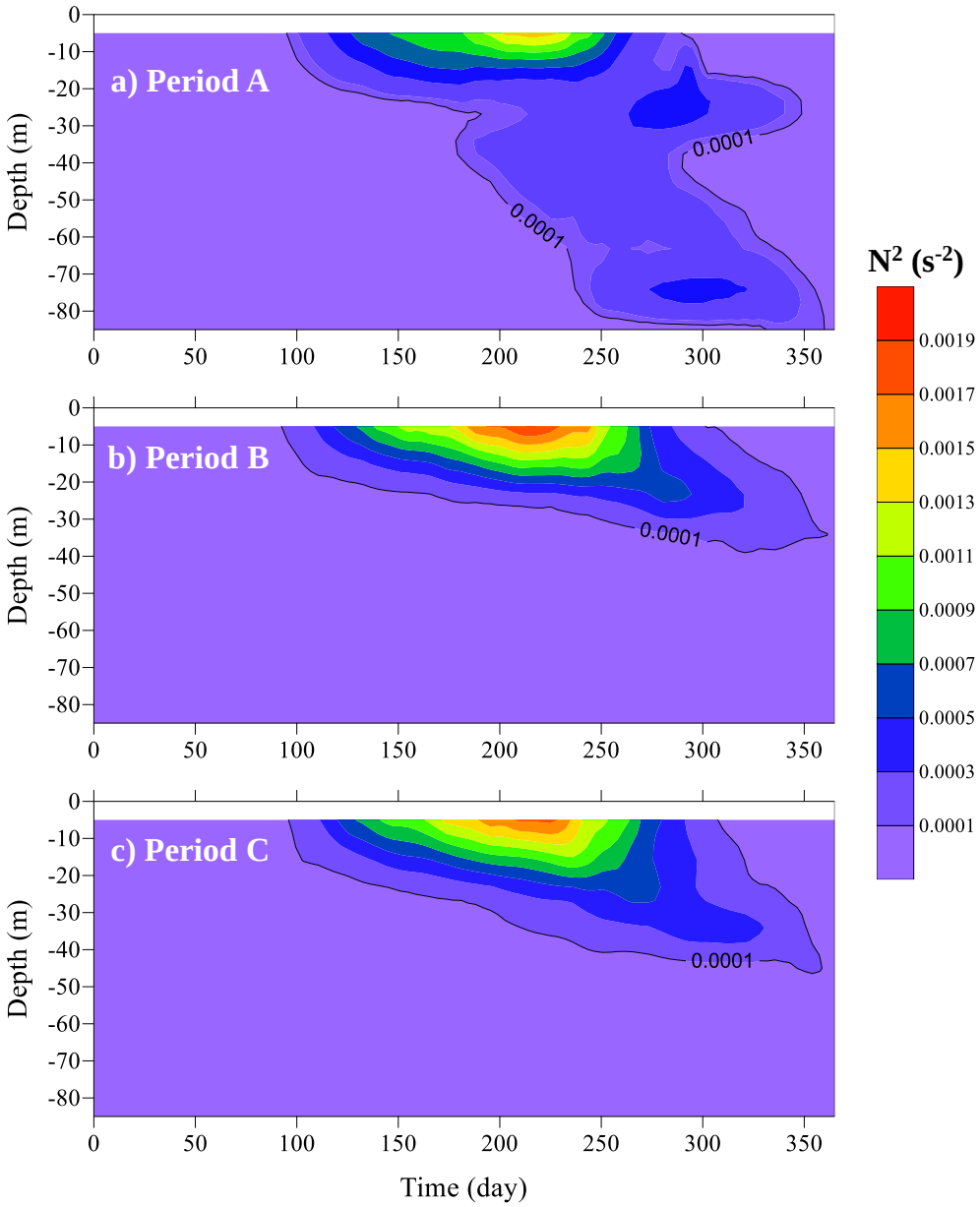

Figure 4.5. Contour plots of average N^2 for the three periods (a–c).

4.3.2 Decadal Averages of SSI and TSI

The time-series of *SSI* and *TSI* were subjected to linear regression to examine the trend in each period. The decadal averages of *SSI* and *TSI* considering the four seasons were also computed and compared.

Average values of SSI and TSI in **Fig. 4.6** were subdivided into five decadal groups where the first three decades all represent Period A while the remaining two represent Periods B and C, respectively. For Period A, the seasonal average values of SSI for the first three decades are not significantly different from each other, suggesting that

the stratification conditions as indicated by SSI during this period are likely consistent until 1991. However, in terms of TSI for Period A, significant differences occur for Aug-Sep and Oct-Nov for the first three decades, suggesting that the thermocline gradient is greatly varying during these seasons. For Periods B and C, SSI values are consistently higher during Oct-Nov when compared to Period A; however, in terms of TSI, Periods B and C have higher values during Apr-Jul and Aug-Sep. During peak stratification, Period C has the largest SSI while Period B manifests the largest TSI, in general.

In **Fig. 4.6a**, average SSI distributions for all five decades are not significantly different from Dec-Mar and Apr-Jul where SSI mildly varies from 0.2 to 0.4 kJ m^{-2} for Dec-Mar while 3.2 to 3.5 kJ m^{-2} for Apr-Jul. The obvious distinction for each period appears during Aug-Sep where the highest SSI is 7.2 kJ m^{-2} for Period C, followed by A (5.8 to 6.2 kJ m^{-2}) with B as the lowest (5.7 kJ m^{-2}). For Oct-Nov, thermal stability decreases for all periods, with C still maintaining the highest SSI (3.7 kJ m^{-2}), followed by B (3.1 kJ m^{-2}) and then lastly by A (1.9 to 2.3 kJ m^{-2}).

In **Fig. 4.6b**, the average TSI for all periods are relatively smallest for Dec-Mar for all the five decades with values ranging from 0.08 to 0.15˚C m^{-1} but the TSI distributions become distinct from the rest for the other seasons. For Apr-Jul, TSI is highest for Period B (0.52˚C m^{-1}) followed by C (0.48˚C m^{-1}), having A as the lowest (0.34 to 0.37˚C m^{-1}). This is consistent with Aug-Sep pattern where the highest peak TSI for the year belongs to B (0.64˚C m^{-1}), followed by C (0.55˚C m^{-1}) with A having the lowest (0.30 to 0.39˚C m^{-1}). The effect of withdrawal location to thermal stratification can be clearly visualized with emphasis on larger TSI for Periods B and C (shallow withdrawals) than Period A (deep withdrawals) during this heating period. The order of magnitude is reversed for Oct-Nov where TSI is highest for Period A (0.40 to 0.50˚C m^{-1}), followed by C (0.38˚C m^{-1}) and lastly by B (0.37˚C m^{-1}). Stronger thermoclines are developed in the deeper layers of the reservoir for Period A during Oct-Nov.

It can be inferred from this long term analysis that having the strongest thermocline does not necessarily translate to largest thermal stability. Stratification as a phenomenon may be subjectively classified to have varying strength depending on the index being utilized to describe it. For example in Aug-Sep (**Figs. 4.6a, b**), Period C has the largest SSI among all periods but its TSI is smaller than Period B. The magnitude of thermal stability is rather found to be related to the total depth of the thermocline and the thickness or volume of the stratified layer. In **Fig. 4.1g**, the bottom edge of the

thermocline of Period B is at the 30-m depth while Period C is at 50-m depth. The stratified layer is much thicker in Period C, hence larger energy is required to fully mix or destratify this column, resulting in the high value of SSI.

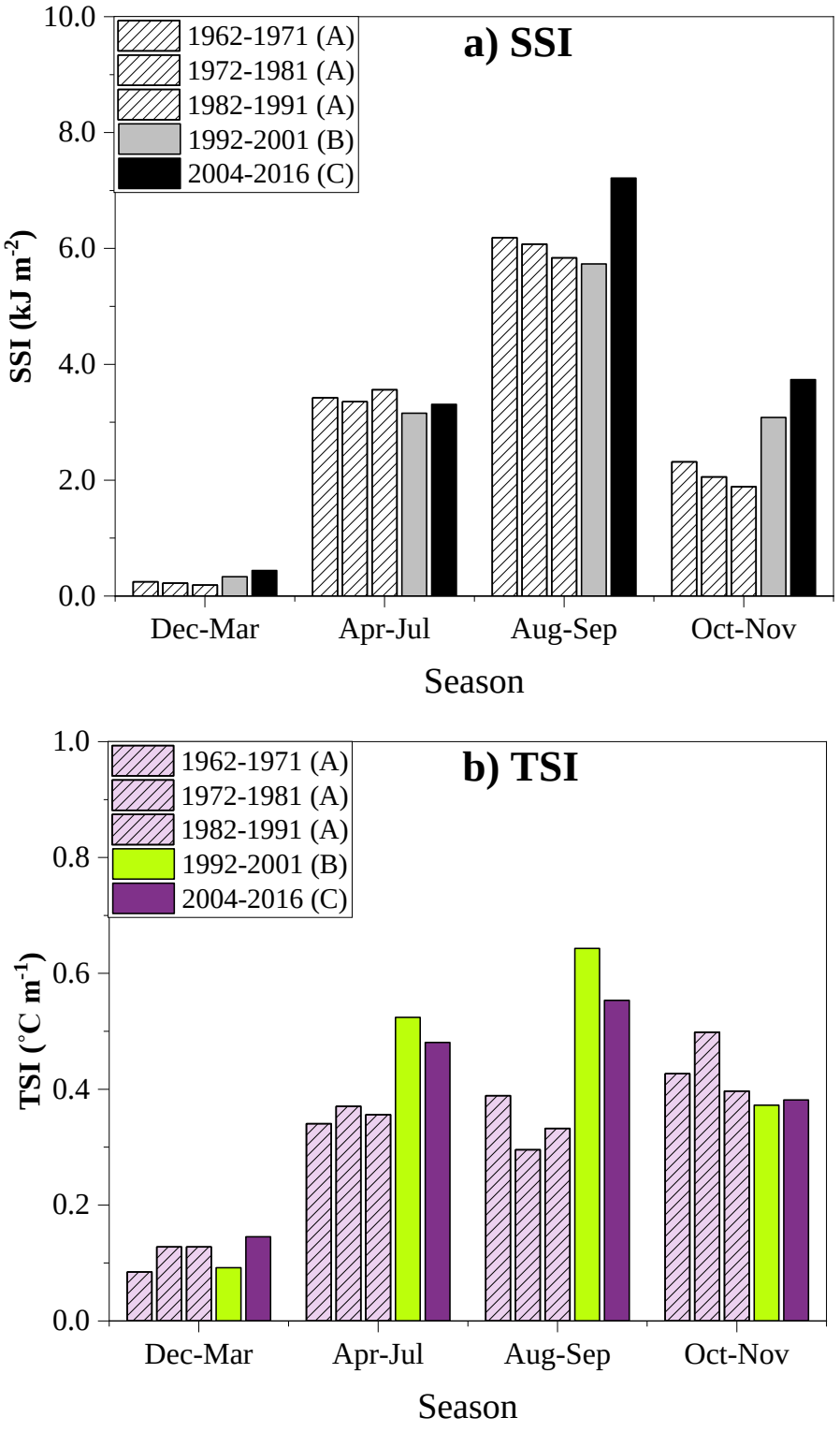

Figure 4.6. Bar graphs of decadal averages of a) SSI and b) TSI for different seasons.

4.3.3 SSI Trends

Table 4.1 shows the results of the Kruskal-Wallis (K-W) and rank-sum tests of the seasonal values of SSI per period. The SSI values are found to be significantly different among periods for all the four seasons. For Dec-Mar, Periods B and C are significantly different (more thermally stable) from Period A. For Apr-Jul, B is significantly different (lower stability) from A while for Aug-Sep and Oct-Nov, C is significantly different (more thermally stable) from A. On **Table 4.2**, Period C is significantly different from Period B for Aug-Sep and Oct-Nov.

In terms of the short-term trends per period, the SSI distributions are shown in **Fig. 4.7.**

For Dec-Mar (**Fig. 4.7a1**), constantly near-zero values of SSI are shown for Period A, affirming that a mixed condition exists in the reservoir during this coldest part of the year. The SSI patterns are consistent with the mostly isothermal profiles as shown in **Figs. 4.1a and 4.1e**, hence the very low values of SSI. On the other hand, Periods B and C obtain relatively larger values and increasing slope for their annual SSI. This can be attributed to the apparently weak stratification during the two latter periods specifically around the bottom layer of the reservoir. The increasing slope in the two latter periods may also be attributed to the significant atmospheric warming during Dec-Mar.

The SSI patterns for Apr-Jul (**Fig. 4.7a2**) are not significantly different among the three periods. Interannual variability is not visible during this warming episode, consistent with the gradually stratified temperature patterns as shown in **Fig. 4.1b** for all periods. Period B, although exhibiting a strong positive slope, has the least values of SSI among the three periods.

Annual SSI values are the largest during Aug-Sep (**Fig. 4.7a3**). Large interannual variability is evident specifically in Period A where SSI values fluctuate between 3.0 to 9.0 kJ m-2. While Period B has its annual SSI values converging closely to the 5.7-kJ m-2 average, Period C has its annual SSI values mildly fluctuating between 5.6 to 8.5 kJ m-2. This inherent variability is consistent with the oscillation in the temperature profiles for Periods A and C as shown in **Fig. 4.1c**.

Mild interannual variability is also observed during Oct-Nov (**Fig. 4.7a4**), mainly for Period A. This could be attributed to the large long term water temperature variations at the 70-m depth level of the reservoir (**Fig. 4.1d**). Period A also exhibits a strong downward slope, which can be associated with the sharp decline in the atmospheric

temperature during Oct-Nov from 1959 to 1991. On the other hand, the sharp increase in the slope in Period B is evident while Period C manifests a weak upward slope. This is consistent with the upward slope of air temperature from 1992 to 2016.

Table 4.1. Results of Kruskal–Wallis (K–W) and rank-sum tests at $\alpha = 0.05$ for SSI. Significantly different p-values are in bold characters.

Parameter	Season	Average per Period			K–W p-value
		A	B	C	
SSI (kJ m^{-2})	Dec-Mar	0.22	0.33*	0.44*	**5.7×10^{-6}**
	Apr-Jul	3.44	3.16*	3.31	**2.4×10^{-2}**
	Aug-Sep	6.06	5.73	7.21*	**4.8×10^{-3}**
	Oct-Nov	2.20	3.08	3.74*	**8.1×10^{-6}**

*significantly different from Period A by rank-sum test

Table 4.2. Results of rank-sum tests at $\alpha = 0.05$ for SSI. Significantly different p-values are in bold characters.

Parameter	Season	Average per Period		Rank-Sum p-value
		B	C	
SSI (kJ m^{-2})	Dec-Mar	0.33	0.44	1.7×10^{-1}
	Apr-Jul	3.16	3.31	6.0×10^{-1}
	Aug-Sep	5.73	7.21*	**1.7×10^{-4}**
	Oct-Nov	3.08	3.74*	**3.0×10^{-2}**

*significantly different from Period B by rank-sum test

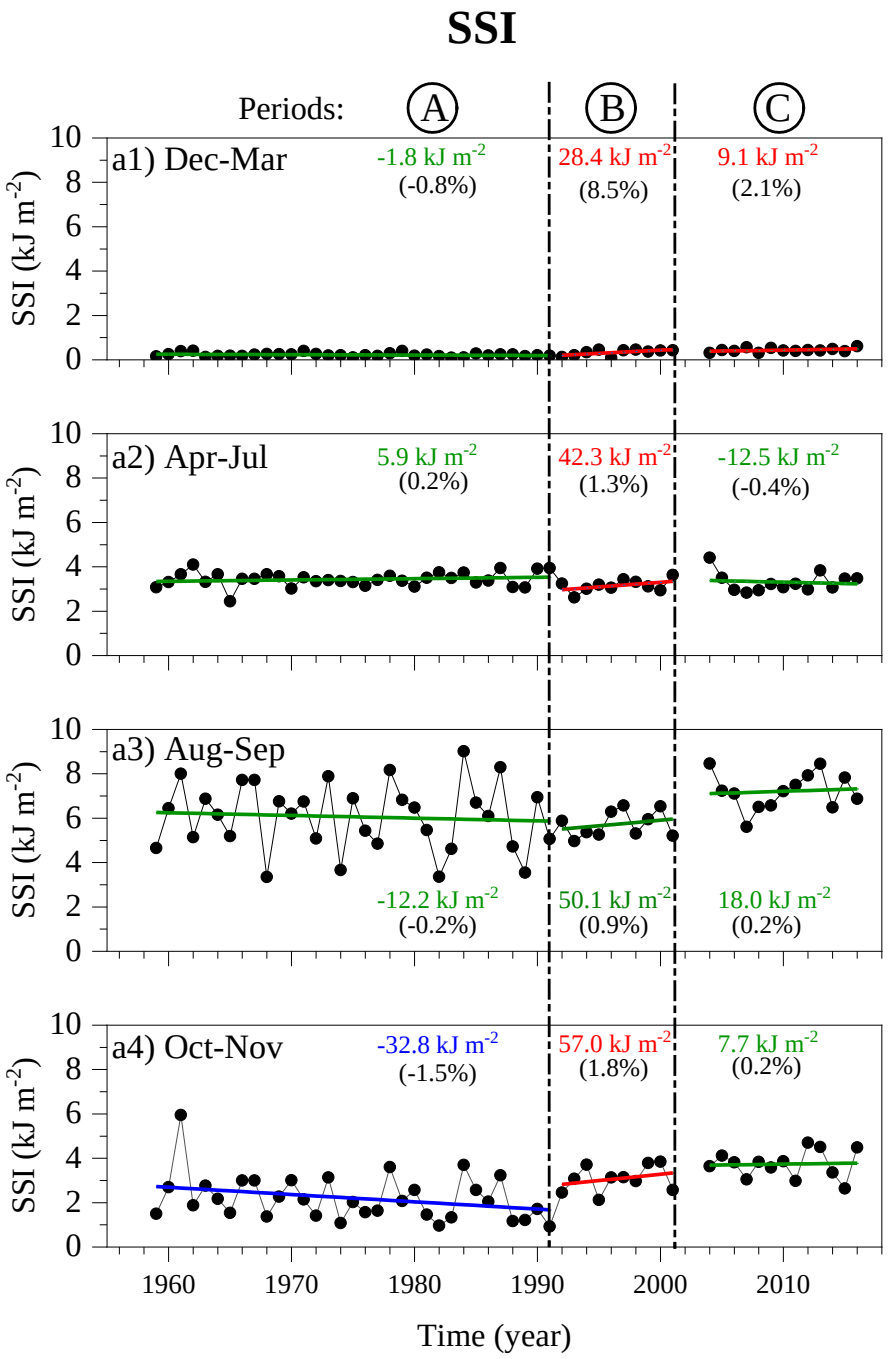

Figure 4.7. Line graphs are time-series of stratification indices with a1-a4 for different seasons. Colored straight lines are linear fit for each period with colored texts as slopes, m (unit/year) while values in parentheses are slope percentages (slope value/average value for that period x 100). Red represents strong positive slope (m ≥+1%), blue represents strong negative slope (m ≤-1%) while green for weak slope (-1%> m >+1%). Data is missing for 2002 while largely incomplete for 2003.

4.3.4 TSI Trends

Table 4.3 shows the results of the Kruskal-Wallis and rank-sum tests of the seasonal values of TSI per period. Significant differences are observed among periods for all seasons, except Oct-Nov. For Dec-Mar, Period C have stronger thermoclines than Periods A and B. Meanwhile, both Periods B and C are significantly different (stronger thermocline) compared to A. On **Table 4.4**, Period C is significantly different from Period B for Dec-Mar.

Seasonal time-series trends of TSI are provided in **Figs. 4.8**, with slopes indicated for each of the distinct periods.

For Period B, the strong upward trend in the annual TSI is evident for all the four seasons (**Fig. 4.8a1-a4**). Correspondingly for this particular period, the air temperature showed a strong increasing trend with the wind speed having a strong decreasing trend from 1992 until 2001. It appears that higher air temperatures and weaker wind speeds are associated with stronger thermocline for this period. Conversely, stronger winds can destratify and weaken the thermocline (Magee and Wu, 2017).

For Periods A and C, the TSI trends for the rest of the seasons are characterized by weak slopes, except for the sharp increase in the slope during Dec-Mar for Period A as seen in **Fig 4.8a1**. In this particular case, the increase in slope is not found to be correlated with any trends in air temperature and wind speed. Only Period B has the clearest relationship between the trends of TSI and atmospheric parameters.

Interannual variability in TSI is largely pronounced during Oct-Nov for Period A (**Fig. 4.8a4**), where values range from 0.19 to 0.80˚C m-1. TSI is particularly very high for the years 1961, 1968 and 1978 but low for 1962, 1963, 1965 and 1966. This TSI variability, same with SSI, is dependent on the behavior of the water temperature profiles, as seen in **Fig. 4.1**.

Table 4.3. Results of Kruskal–Wallis (K–W) and rank-sum tests at $\alpha = 0.05$ for SSI and TSI. Significantly different p-values are in bold characters.

Parameter	Season	Average per Period			K–W p-value
		A	B	C	
TSI (°C m^{-1})	Dec-Mar	0.11	0.09	0.15*	**6.0×10^{-3}**
	Apr-Jul	0.35	0.52*	0.48*	**1.2×10^{-7}**
	Aug-Sep	0.34	0.64*	0.55*	**3.0×10^{-8}**
	Oct-Nov	0.45	0.37	0.38	8.6×10^{-2}

*significantly different from Period A by rank-sum test

Table 4.4. Results of rank-sum tests at $\alpha = 0.05$ for TSI. Significantly different p-values are in bold characters.

Parameter	Season	Average per Period		Rank-Sum p-value
		B	C	
TSI (°C m^{-1})	Dec-Mar	0.09	0.15*	**7.9×10^{-5}**
	Apr-Jul	0.52	0.48	2.8×10^{-1}
	Aug-Sep	0.64	0.55	7.7×10^{-2}
	Oct-Nov	0.37	0.38	7.8×10^{-1}

*significantly different from Period B by rank-sum test

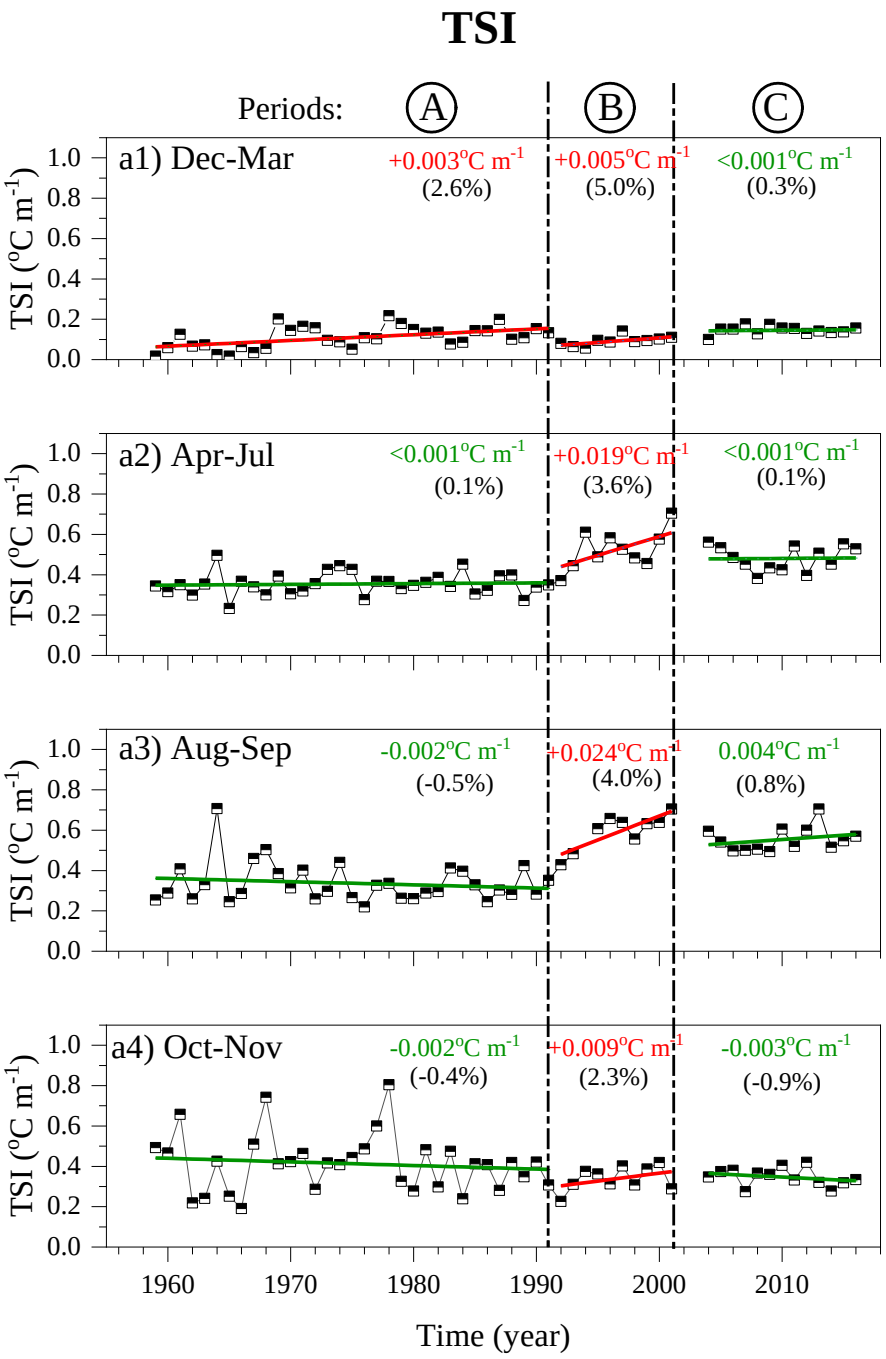

Figure 4.8. Line graphs are time-series of stratification indices with a1-a4 for TSI for different seasons. Colored straight lines are linear fit for each period with colored texts as slopes, m (unit/year) while values in parentheses are slope percentages (slope value/average value for that period x 100). Red represents strong positive slope (m ≥+1%), blue represents strong negative slope (m ≤-1%) while green for weak slope (-1%> m >+1%). Data is missing for 2002 while largely incomplete for 2003.

4.3.5 Timing of Onset and End of Stratification

The timing of onset and end of stratification for each year was analyzed. The occurrence of this timing can be identified based on subjective threshold value in terms of *SSI* (Engelhardt and Kirillin, 2014); hence SSI was adopted as the main selection criterion for this study. In examining the long-term data, it was found that the onset typically happens around spring time with a corresponding threshold value of 500 J m^{-2}. The same threshold value was used to signify the end of stratification, knowing that stratification is a binary process i.e. stratified when above the threshold and mixed when below it (Stainsby et al., 2011). This same paper used a threshold value as high as 800 J m^{-2} to characterize the timing of stratification for Lake Simcoe.

On average considering all three periods, the stratification in the reservoir onsets around early April (Day 97) using a minimum SSI threshold of 500 J m^{-2} (**Fig 4.9**). However, the timing of the end of stratification varies depending on the period. The numerical difference between the timing of onset and end of stratification is equal to the total length of stratified days in a year. In this case on the average, Period C exhibits the longest stratification at 266 days, followed by B (259 days) with A as the shortest with 246 days. Longer stratification appears to be associated with shallower withdrawals. This is particularly attributed to the sustained stratified condition until almost the year end in Periods B and C.

The timing of onset of stratification for a particular year can also be related to the atmospheric condition in that year and/or of the previous year. Here, the years with notably late or early onset of stratification are highlighted. For this paper, prolonged winter for a year means that the average air temperature for Dec-Mar is relatively smaller than its preceding and succeeding years while a prolonged summer has larger air temperatures for Aug-Sep extending until Oct-Nov.

For example, in Period A, it was observed that an onset of stratification for a particular year is likely late or extended if that year is preceded by a very hot and prolonged summer. High temperatures were recorded in the prolonged summers of 1964, 1969, 1971, 1973, 1975, 1977, 1982, 1983 and 1985, and correspondingly, the stratification started late the following year at around Day 102 until 109. Furthermore, early onset (around Day 91 to 97) likely occurred during the same year with a very cold and prolonged winter specifically during the years 1967, 1970 and 1976.

For Periods B and C, the onset of stratification around the springtime of a particular year is observed to be likely late or extended when that year is preceded by a very hot and prolonged summer. Late onset occurred in 1996 and 2000 for B and in 2006 and 2008 for C. What is interesting to note is that an early onset likely occurs in a year for Periods B and C, if that particular year is preceded by a very cold and prolonged winter. Correspondingly, late onset occurred in 1995 and 1997 for B and in 2007, 2009 and 2013 for C.

In summary, the timing of onset of stratification is both largely affected by the atmospheric condition and the withdrawal operation scheme as provided in **Fig. 4.9**. For Period A (deep withdrawal), early onset in a year likely happens if that year has a prolonged winter; meanwhile for Periods B and C (shallow withdrawal), if that year is preceded by a prolonged winter. Late onset in a year likely happens for all three periods especially if that year is preceded by a prolonged summer.

For the timing of end of stratification, the case appears to be different between the deep withdrawal scheme and the shallow one. For Period A, early termination corresponds to the year having early onset while late termination occurs in a year where there is also a late onset. However, the case is different for Periods B and C. While the timing of onset may be associated with a very hot summer or very cold winter for Period A, the timing of end of stratification for B and C appears to be shifted late until the end of the year, regardless of the atmospheric condition. As mentioned earlier, the two latter periods exhibit a sustained stratification until the end of the year. The strength of the thermocline is maintained due to this shallow withdrawal scheme, largely limiting the thermal advection and mixing between the epilimnion and hypolimnion. The thermoclines developed for Periods B and C remain almost constantly in the upper layer, unlike in Period A where the thermocline migrates deeper into the reservoir and further weakens until the year end. This phenomenon is further investigated using the numerical simulation as discussed in the next section.

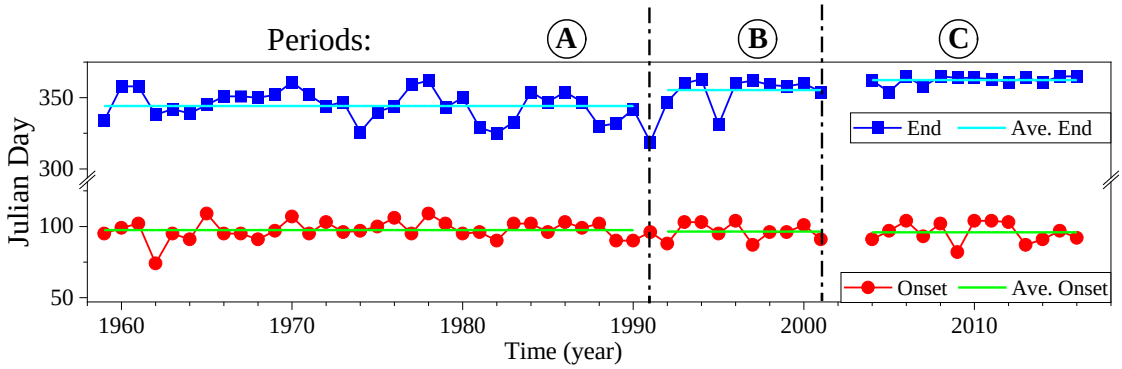

Outflow Setup	Deep Withdrawal	Shallow Withdrawal	
Curtain	None	None	**Yes**
Ave. Timing of Onset	Day 97.3	Day 96.4	Day 95.9
Ave. Timing of End	Day 344.2	Day 355.4	Day 362.4
Ave. Stratified Duration	246 days	**259 days**	**266 days**
Early Onset Case	*on a year* with *very cold & prolonged winter*	if *previous year* had *very cold & prolonged winter*	
Late Onset Case	if *previous year* had *very hot & prolonged summer*	if *previous year* had *very hot & prolonged summer*	

Figure 4.9. The timing of onset and end of stratification as determined based on SSI.

4.4 Conclusions

This study successfully evaluated and described in detail the seasonal long-term patterns of thermal stratification of a monomictic reservoir, which had undergone three distinct periods of operation. In general, the reservoir is mostly isothermal during winter (Dec-Mar) while stratification onsets in spring (starting Apr), intensifies in summer (Aug) and weakens during fall (Oct-Nov). During the peak of stratification, penstock outflows (Period A, deep withdrawal) allowed larger thermal dispersion in the reservoir, rendering a thicker epilimnion and a weaker thermocline; hence the low SSI and TSI values. The operation of SW alone (Period B, shallow withdrawal, no curtain) created a thick layer of hypolimnion and promoted a very strong thermocline (high TSI). Meanwhile, the combined operation of SW and VC (Period C, shallow withdrawal, with curtain) increased the thermal stability (high SSI) and the thickness of epilimnion relative to Period B, due to the mixing process as induced by the VC and the deeper level of the SW intake. Hence, having the strongest thermocline does not necessarily mean the largest thermal stability. Period B and C also exhibited stronger stratification in terms of the Brunt-Väisälä Frequency (N^2). Depending on the outflow depth and the occurrence of prolonged hot or cold atmospheric conditions, the onset of stratification could be likely shifted early or late. On average, stratification duration is shortened with deep withdrawals.

Based on the results of the analysis from Chapters 3 and 4, it further reinforces the earlier claim that reservoir operation bears a stronger influence on the reservoir's thermal structure than the climate itself due to the following reasons:

1. Surface water temperatures decreased in the long term with the shift of operation from DPW to SW and VC.
2. Period A has higher heat content but Periods B and C have higher stability and stronger thermocline.
3. Periods B and C exhibit longer duration of stratification and earlier onset than Period A.

These findings are summarized in **Fig. 4.10**.

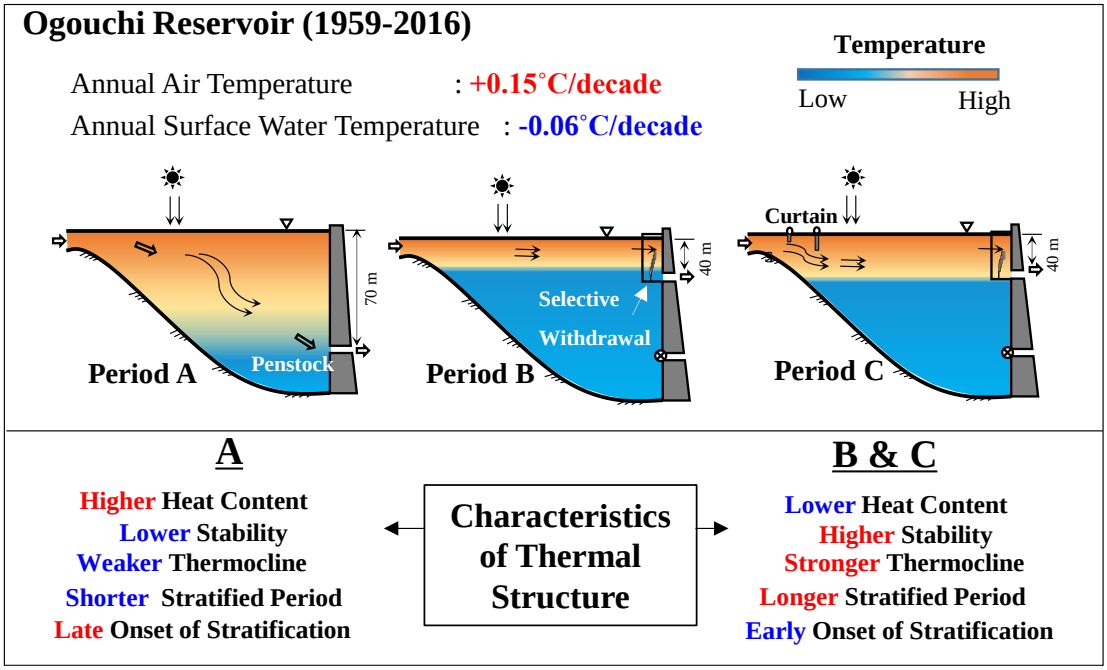

Figure 4.10. Effect of varying facilities on the thermal structure of the Ogouchi Reservoir.

CHAPTER 5

Management of In-Reservoir and Outflow Temperatures

5.1 Introduction

Chapters 3 and 4 have shown that the deep penstock withdrawal (DPW) operations in the Ogouchi Reservoir resulted in warmer water profiles and lower thermal stability. On the other hand, shallow withdrawals through the selective withdrawal (SW) facility promoted narrower warm upper layer (epilimnion), higher stability and stronger thermoclines. Additionally, it was found that shifting the operations of the reservoir from the conventional DPW to the use of SW and vertical curtains (VC) can potentially mitigate the effects of climate warming. These previous chapters however, did not elaborate much on the effect of the facilities on released water temperatures. Further, the operation of the SW together with the presence of the VC can still be evaluated to recommend the best management practice for regulating the reservoir temperatures.

This study therefore aims to evaluate the effects of varying the operation of the facilities on the thermal structure and the released water temperatures of the reservoir. Numerical simulation is employed by replicating the three periods of operation. The simulation focuses on the period from May 1 to August 31, 2016 during which a long and sustained stratification is observed, free from the interference of floods. Simulation studies usually assign uniformly distributed points for the outflow opening along the location of the intake. For this chapter, the main distinguishing feature is that this applies the velocity field for the outflow as derived from actual field observations (Niiyama et al., 2010b) in the SW of this reservoir. This study therefore evaluates the applicability of the two SW outflow models on the released water and in-reservoir temperatures. These two methods specifically are the Uniform Distribution Method (UDM) and the Modified Gaussian Distribution Method (MGDM).

After evaluating the suitable outflow model for the SW, sensitivity analysis is made. Several cases are developed by varying the SW intake depths by 4, 7 and 10 m, with or without the VC to evaluate their effects on the thermal structure and released water temperatures. These are done for both the years 2015 and 2016. While 2016 has long and sustained operation, the year 2015 is characterized by a flood in the middle of the period. The plots of temperature contours, N^2 and outflow temperatures are provided for comparison and the results are analyzed.

5.2 Applicability of the Modified Gaussian Profile

5.2.1 Vertical Temperature Profiles

Figure 5.1 shows the comparison of temperature contour maps of the actual 2016 data (**Fig. 5.1a)** and the simulation results from UDM (**Fig. 5.1b**) and MGDM (**Fig. 5.1c**). The black rectangle in the actual plot indicates the lack of data during that period. UDM and MGDM can reproduce reasonably the first half of the simulation period from Day 122 to 190 compared with the actual. However, during the second half of the period (Day 191-245), UDM tends to deviate largely from the actual trend of the measured data. UDM exhibits a warmer upper layer considering the 25˚C level relative to the actual. Strong thermocline is also observed along EL 70-75 m where the gaps between the 7-15˚C levels are rather narrow. With regards to MGDM, the warmer upper layer around the 25˚C level is narrower and the thermocline along the EL 70-75 m is weaker relative to UDM.

The representative thermal profiles for each month are shown in **Figs. 5.2a1-a4** having the profiles for the MGDM while **Figs. 5.2b1-b4** for the UDM. For May, both methods exhibited a relatively good fit with the actual. However for the next months, UDM produced steeper thermoclines and narrower epilimnion than MGDM. Furthermore, UDM poorly reproduced the lower edge of the thermocline along EL 70 m relative to MGDM.

Although visually, the simulated temperature profiles from both methods may show reasonable agreement with the actual, MGDM appears to have a better fit than UDM numerically. The RMSE of MGDM ranges from 0.44 to 1.69˚C, which is way lower than UDM with RMSE of 0.49 to 2.56˚C. The error generally increases with time as shown by the increasing RMSE from May to August.

Additionally, the simulated water levels were compared with the measured data. On **Fig. 5.3**, the water levels show reasonable agreement with RMSE of 0.57 m.

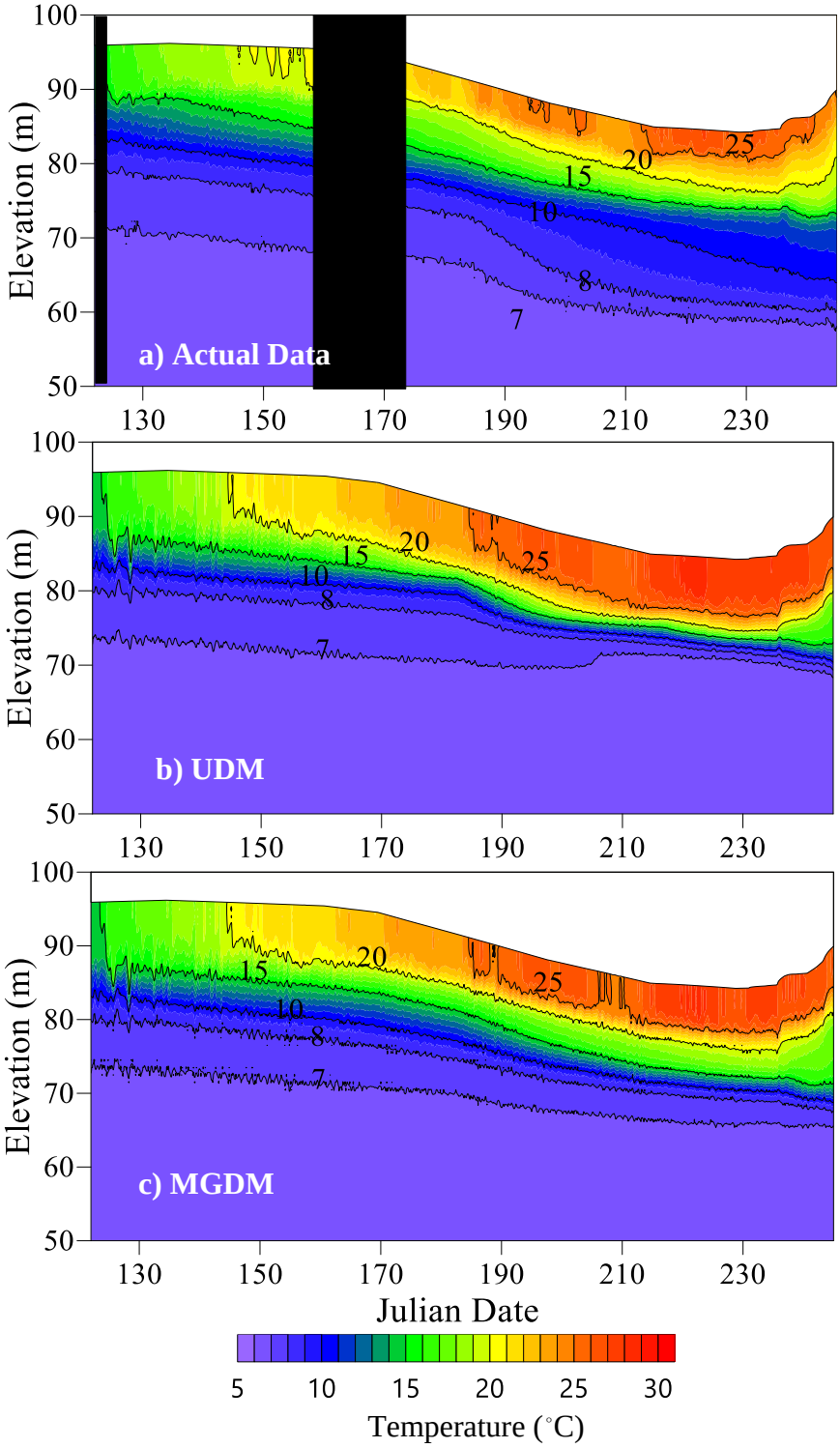

Figure 5.1. Comparison of temperature contour maps for the 2016 simulation: (a) actual data, (b) results from UDM and (c) results from MGDM.

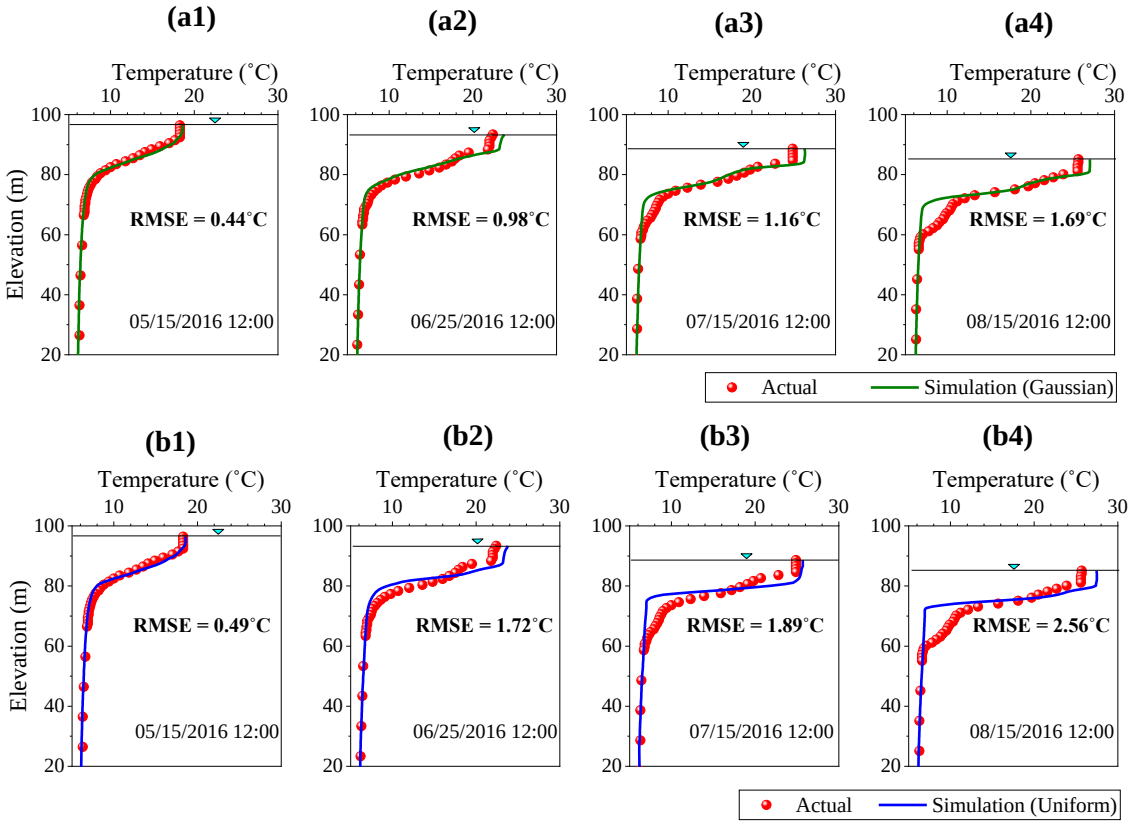

Figure 5.2. Comparison of 2016 temperature profiles between measured data and simulation results. Simulations were made by applying the outflow profiles using the (a1-a4) Modified Gaussian Distribution Method (MGDM) and the (b1-b4) Uniform Distribution Method (UDM).

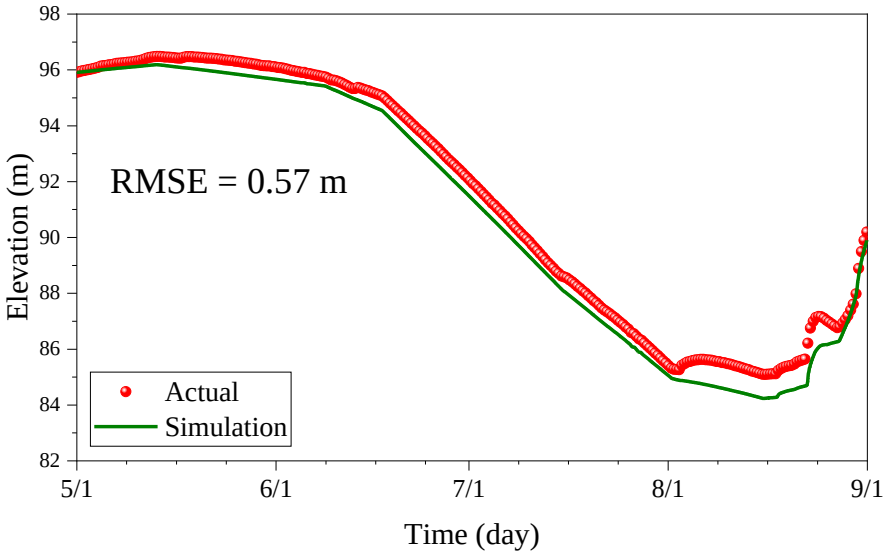

Figure 5.3. Comparison of actual and simulated water levels for 2016.

5.2.2 Outflow Temperatures

The actual temperatures (red dots) exhibit sudden dips in July 1 and in August 4, corresponding to the lowering of the SW gate intake at these dates (**Fig. 5.4**). The following are the ranges of temperatures for each month: May (9.1-12.6˚C), June (11.4-15.4˚C), July (11.8-17.1˚C) and August (15.2-19.6˚C). Daily fluctuation is apparent within a day with the maximum occurring around noontime while the minimum around midnight.

The UDM performed relatively fairly for Range 1 but poorly for Ranges 2 and 3. Meanwhile, MGDM showed very good agreement with the actual temperatures all throughout the simulation period. The oscillation is also more pronounced in UDM than in MGDM, which can be attributed to the fact that UDM averages the temperatures from only three outflow layers. UDM has its outflow located along the thermocline where strong thermal gradients are present, hence the strong fluctuation in outflow temperatures. MGDM considers the entire depth of the Gaussian profile, hence the smoother trends. The model performance of MGDM is better than UDM in terms of RMSE. Hence, MGDM was adopted for simulating the SW cases in the next section.

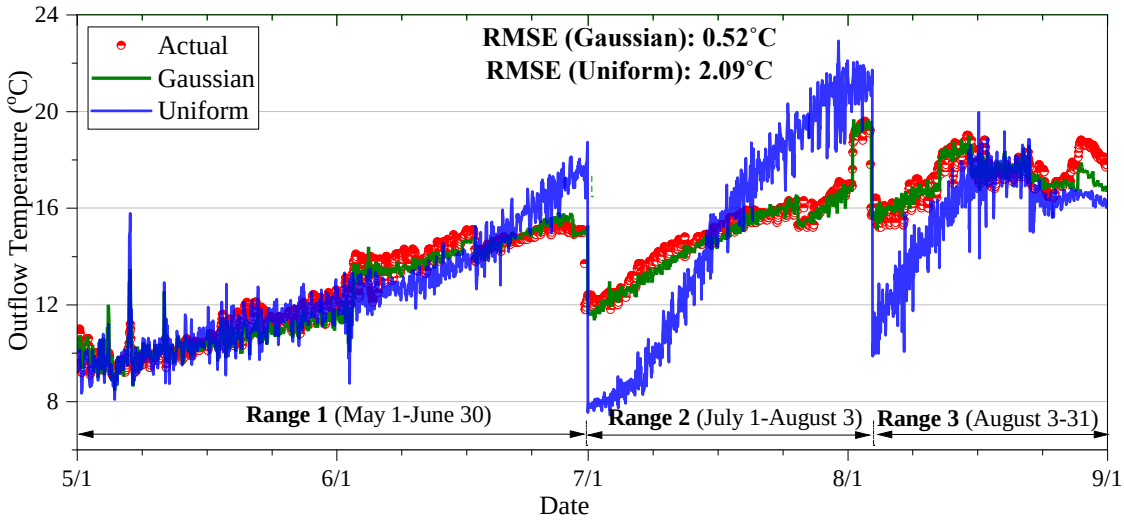

Figure 5.4. Comparison of 2016 outflow temperatures between measured data and simulation results using MGDM and UDM.

5.3 Simulation of the Three Periods

5.3.1 Thermal Structures

The in-reservoir temperature contour maps in **Fig.5.5a** show that Case A (**Fig. 5.5a1**) has a wider thermal dispersion than Cases B (**Fig. 5.5a2**) and C (**Fig. 5.5a3**). Considering the 14˚C level, Case A reaches a depth of 40 m by August 31 while B and C only reach up to 20 m on the same date.

Withdrawing water from the penstock located at a deeper layer encourages more efficient mixing of water in the reservoir, hence the wider distribution of reservoir temperatures (Case A). As a result, the thermocline for this case appears to be weaker as it migrates deeper through time. Meanwhile, the SW facility operates at shallower depths, such that a strong thermocline is created at these layers (4 m for Case C while 10 m for Case C). As a result, the reservoir appears to be generally colder, as it exhibits a very narrow epilimnion but a very wide hypolimnion. This agrees with the previous findings that deep withdrawal promotes warming of the profile and creates weaker thermoclines than shallow withdrawals in Chapters 3 and 4.

Considering Cases B and C, the thermal profiles of these two show significant differences. Case B has a narrower epilimnion compared to Case C. Likewise upon examining closely **Figs. 5.5a2-a3**, the gap between the 14 and 20˚C levels is larger in C than in B. This difference is largely attributed to the deeper intake for Case C than in Case B. Furthermore, the presence of VC in Case C enhances the widening of the epilimnion. The VC acts as a hydraulic barrier against river inflow from intruding directly into the reservoir. The river water is forced to flow under the 10-m deep VC and this action modifies the thermal structure in Case C.

The N^2 as a measure of stratification appears to strongly fluctuate between the depths of 4 and 8 m for all cases (**Fig.5.5b**). This means that the layer where stratification starts to manifest is variably migrating. Since thermal dispersion is largest in A, stratification, although weak, extends until the deeper layers of the reservoir (Fig. **5.5b1**). Meanwhile, practically zero values of N^2 were registered from the depth of 12 m below for B and from 15 m below for C due to almost isothermal conditions at these layers. The stratification of all three cases appears to be modified at the latter part of the simulation where a flood occurred.

For B (Fig. **5.5b2**), the strength of the thermocline is pronounced between the depths of 2 and 12 m. Meanwhile for C (Fig. **5.4b3**), stratification exists between 4 and 15 m but there appears to be two distinct thermoclines above and below the 10-m depth. This 10-m divide as seen in the N^2 contour plot is induced by the VC, which also has the same depth of 10 m. Overall, Case B developed a stronger thermocline than B as indicated by the stronger intensity of N^2. However Case B, appears to be more thermally stable due to the slightly deeper epilimnion. These agree with the findings obtained from Chapters 3 and 4.

In **Fig. 5.6**, the distribution of the river water along the reservoir thalweg can be visualized using tracer (**Fig. 5.6a**) as extracted from the simulation of the three cases, together with their corresponding longitudinal temperature profiles (**Fig. 5.6b**). The deep withdrawal in Case A (**Figs. 5.6a1** and **5.6b1**) encouraged the vertical mixing of water layers, thereby promoting the dispersion of thermal energy throughout the reservoir depth and the deep migration of the thermocline. The shallow withdrawal without the curtain scenario in Case B (**Figs. 5.6a2** and **5.6b2**) facilitated a flow that is directly focused along the epilimnion and eventually, a strong thermocline was created along the outflow level. Near-surface releases inhibit the further interaction of the warm water in the epilimnion with the cold water in the hypolimnion. Based from some simulation studies, it was found that deep withdrawal enhances the thermal advection in the water column, which deepens the epilimnion (Ma et al., 2008) while shallow withdrawal tends to intensify the stratification, thus inhibiting heat transfer between the epilimnion and hypolimnion (Zouabi-Aloui et al., 2015). Further, the level of the thermocline is found to correspond with the location of the outflow (Casamitjana et al., 2003), as what was similarly shown from the simulation.

Meanwhile, the shallow withdrawal with curtain scenario in Case C (Figs. **5.6a3** and **5.6b3**) shows a relatively thicker mixed layer than in Case B and this is attributed to two reasons. The first one is that Case B has deeper outflows than Case B. Secondly, the presence of the VC enhances the interaction and mixing of the river water and the reservoir water. The inflow is forced to travel under the 10-m deep impermeable fence, thus increasing the intrusion depth in Case C. This process also shifts deeper the thermocline that was originally developed along the outflow level. A previous simulation study for the Ogouchi Reservoir also provided that while the VC can effectively trap sediments upstream, it can also shift the thermocline to move into a deeper layer (Duka

et al., 2019). There are still very limited studies about the effect of VC on the hydrodynamics, sedimentation and eutrophication process not only of this reservoir but also of other reservoirs in the world. Sensitivity analysis through numerical simulation can later be made to evaluate the effect of the varying depths of VC on the thermal structure and also on the water quality regime of the reservoir.

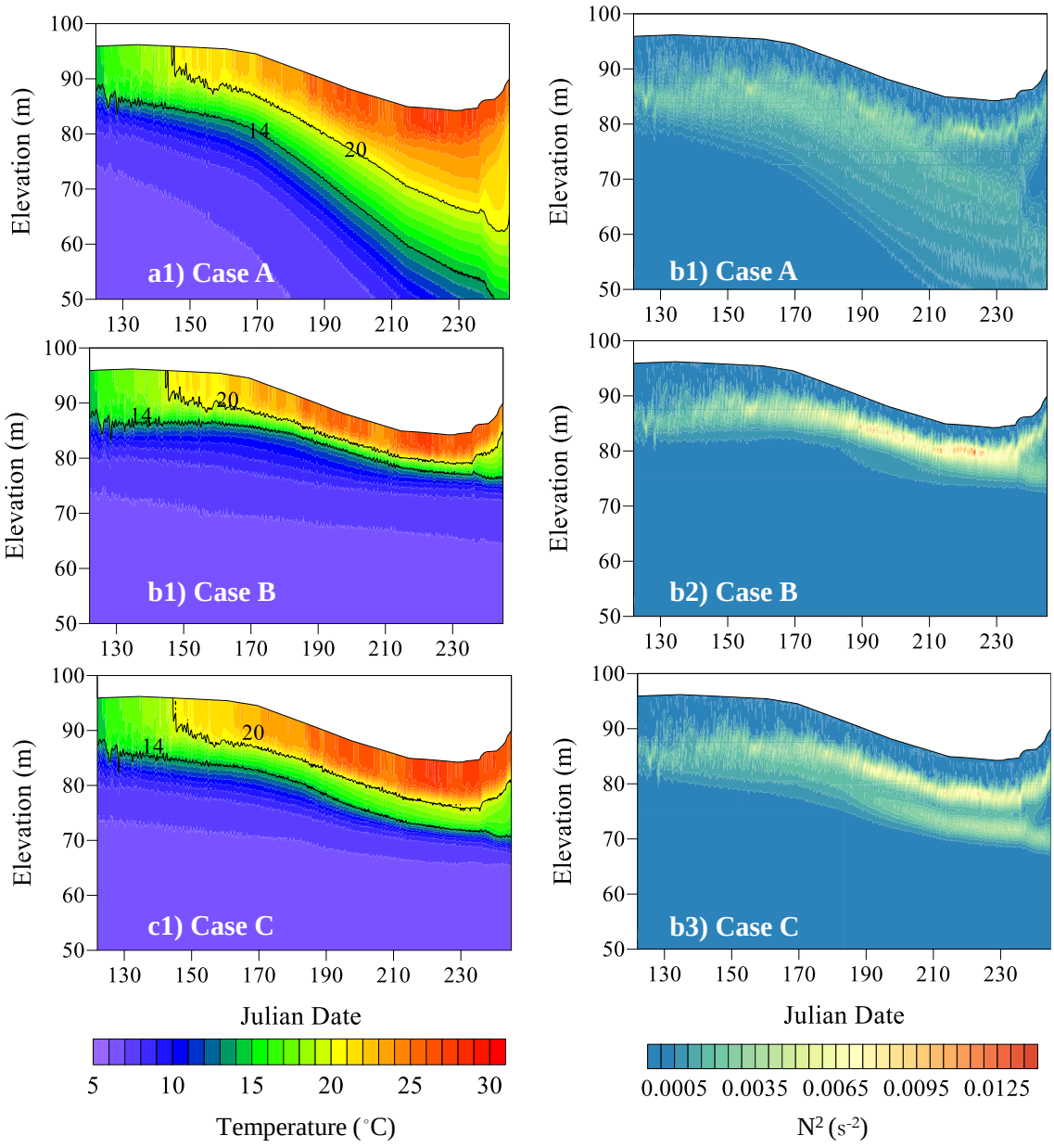

Figure 5.5. Vertical distribution of (a) in-reservoir temperatures and (b) N^2 from the simulation of the three cases from May to August 2016.

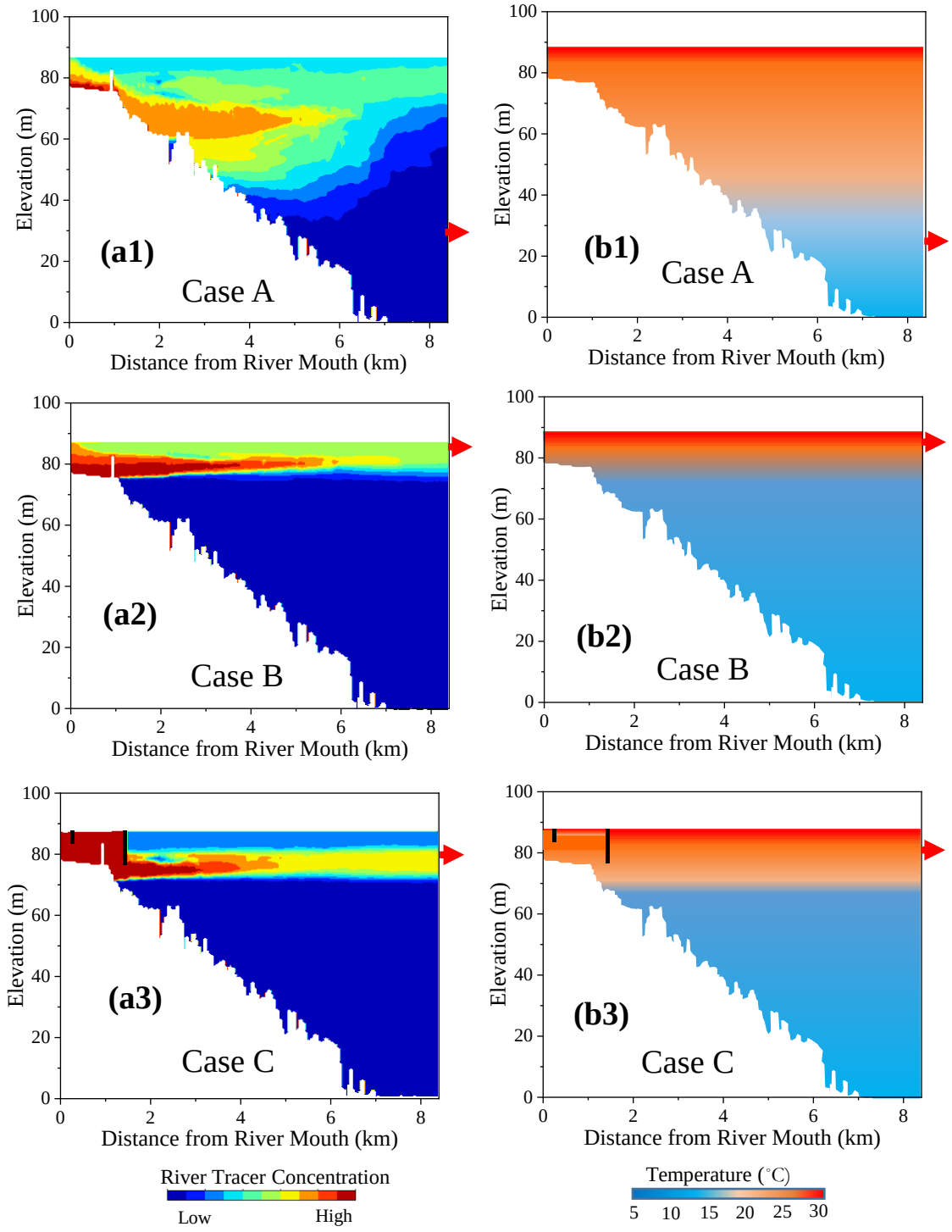

Figure 5.6. Longitudinal distribution along the thalweg of river tracer (a1-a3) and temperature (b1-b3) for the three simulation cases (sample snapshots a day after flood peak). Red arrows indicate the level of outflow.

5.3.2 Outflow Temperatures

Fig. 5.7 shows the simulation results of outflow temperatures for the three cases. Case A has a temperature range of 6 to 9˚C. Case B ranges from 14 to 25.3˚C, while Case C ranges from 8.5 to 19.7˚C. Deep withdrawals result in cold water releases as the reservoir abstracts water from the cold hypolimnion. Shallow withdrawals through the SW facility encourages warm water releases as the level of the outflow is located in the epilimnion. The significant discrepancy between Cases B and C is attributed to the shallower intake of Case B (4 m against 10 m). During stratified conditions, the near-surface layers are much warmer than the middle layer, hence the higher outflow temperatures.

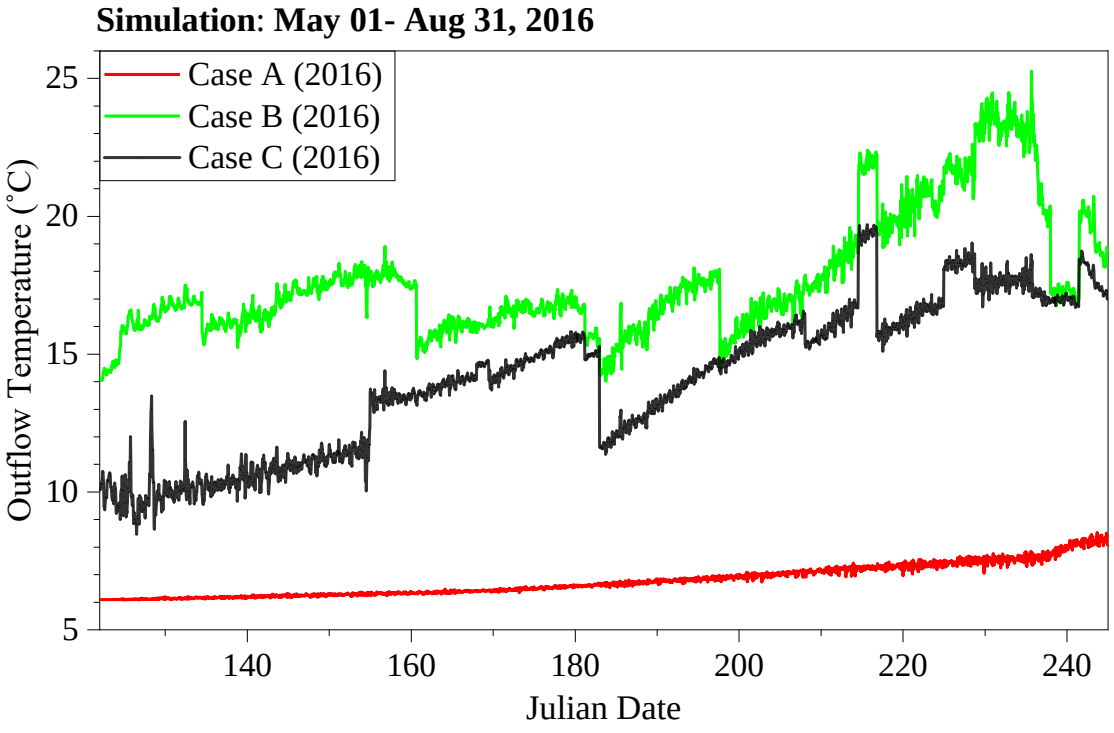

Figure 5.7. Outflow simulation temperatures for the three cases for May to August 2016.

To validate the results of simulation, the long-term weekly averages of the outflow temperatures for the different periods of operation are presented in **Fig. 5.8**. It shows that Case A follows the normal range of outflow temperatures in comparison with Period A, particularly the Decades A2 (1972-1981) and A3 (1982-1991). Decade A1 (1958-1971) shows relatively warmer outflows than the other two. Upon examining the reservoir records, Decade A1 operated on extremely low water levels during the initial stages after

the dam construction. This essentially resulted in warmer profiles of Decade A1 in comparison with the other two decades. The variability of temperatures is also more pronounced in A1 as provided by the larger error bars. Hence, Case A is more appropriately to be compared with the two latter decades of Period A.

In terms of Case B, the temperature range from the simulation (14 to 25.6˚C) is way larger than the average range in Period B (10.5 to 18.9˚C). Case C, on the other hand, produced outflow temperatures with a similar range as in Period C (9 to 18˚C). Nevertheless, the general trends of the two cases (B and C) follow that of the long-term records with Period B having warmer outflows than Period C. This simulation has proved that shallow withdrawals through the SW facility can mitigate the cold water pollution induced by penstock withdrawals. The effect of the VC is further evaluated in the section discussing sensitivity analysis.

Additionally for the long-term records, shifting the operation from deep withdrawal to the use of SW averted the cold water releases. Decades A2 and A3 have shown that during summer, the reservoir released water with temperatures not exceeding 10˚C. During winter, on the other hand, the outflow temperatures were relatively higher for Period A in comparison with Periods B and C. This likewise shows that the use of the SW facility can reverse the possible warm water releases caused by penstock withdrawals.

For the optimum operation of the facilities, it is necessary to compare the outflow temperature from the simulation with the standard temperature for release. Presently, the Ogouchi Reservoir managers are implementing an operation that would match the streamflow temperatures of the Nippara River, which is located downstream of the dam. However, at the moment, the inflow temperatures of such a river are not yet in the possession of the researcher. Hence, the succeeding section would provide recommendation of operation of the SW and VC based on sensitivity analysis.

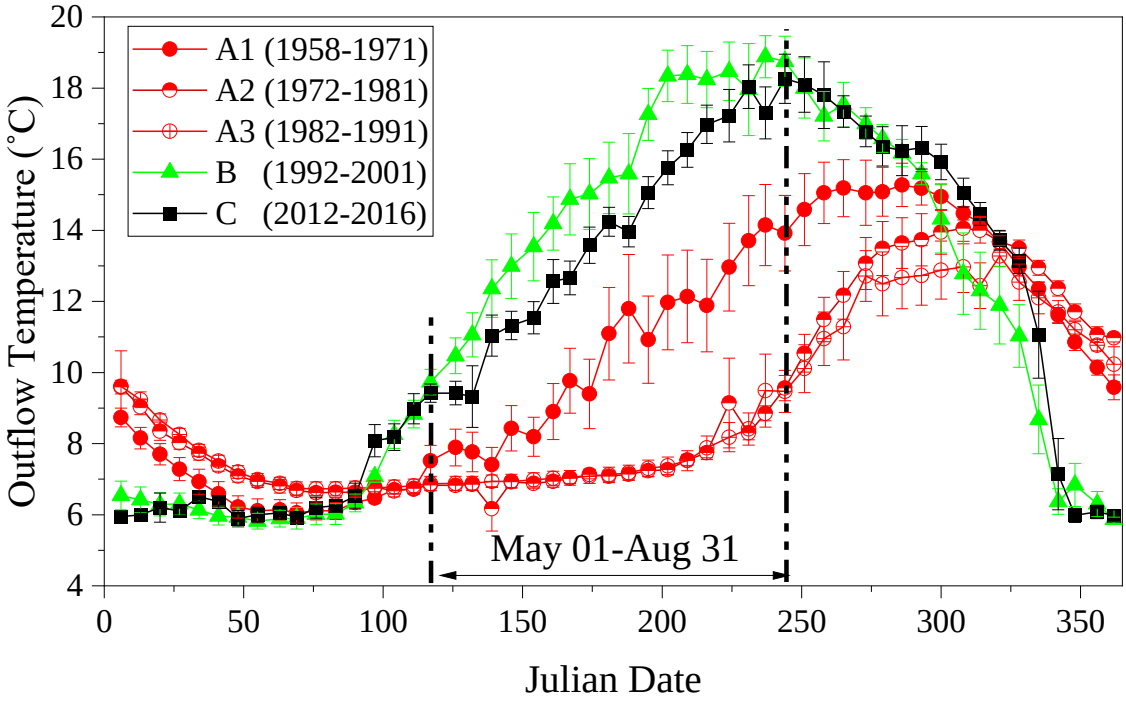

Figure 5.8. Long-term trends of outflow temperatures in the Ogouchi Reservoir from 1958 until 2016 for the different periods of operation.

5.4 Sensitivity Analysis of Thermal Structure

5.4.1 Effect of Facilities during a Period of Long and Sustained Stratification

The thermal regimes for the simulation cases considering the year 2016 are presented in **Fig. 5.9**. For both the scenarios without the VC (Case B) (**Figs. 5.9a1, b1** and **c1**) and with the VC (Case C) (**Figs. 5.9a2, b2** and **c2**), the thickness of the epilimnion increases with deeper intake levels. This trend for both cases can be easily visualized by observing the depth of the 20˚C contour line. However, Case C has wider the epilimnion than Case B, as seen by noting the differences in thickness between the 14 and 20˚C contour lines.

In terms of stratification, the distribution of the N^2 is given in **Fig. 5.10**. What may not be easily noticeable in the thermal profiles can be visible through the computation of the N^2. For Case B (**Figs. 5.10a1, b1** and **c1**), the thickness of the metalimnion increases with deeper intake levels. The intensity of thermocline strength becomes larger with shallower intakes.

For Case C (**Figs. 5.10a2, b2** and **c2**), the thickness of the metalimnion also increases with deeper intake levels. The main distinguishing feature of Case C against Case B is that the presence of the VC can produce two distinct thermoclines, as shown by the distinct gap between the upper and lower layers. Also as a result, the upper layer displays stronger intensity of stratification. The strength of the thermocline of the upper layers decreases with deeper outflows.

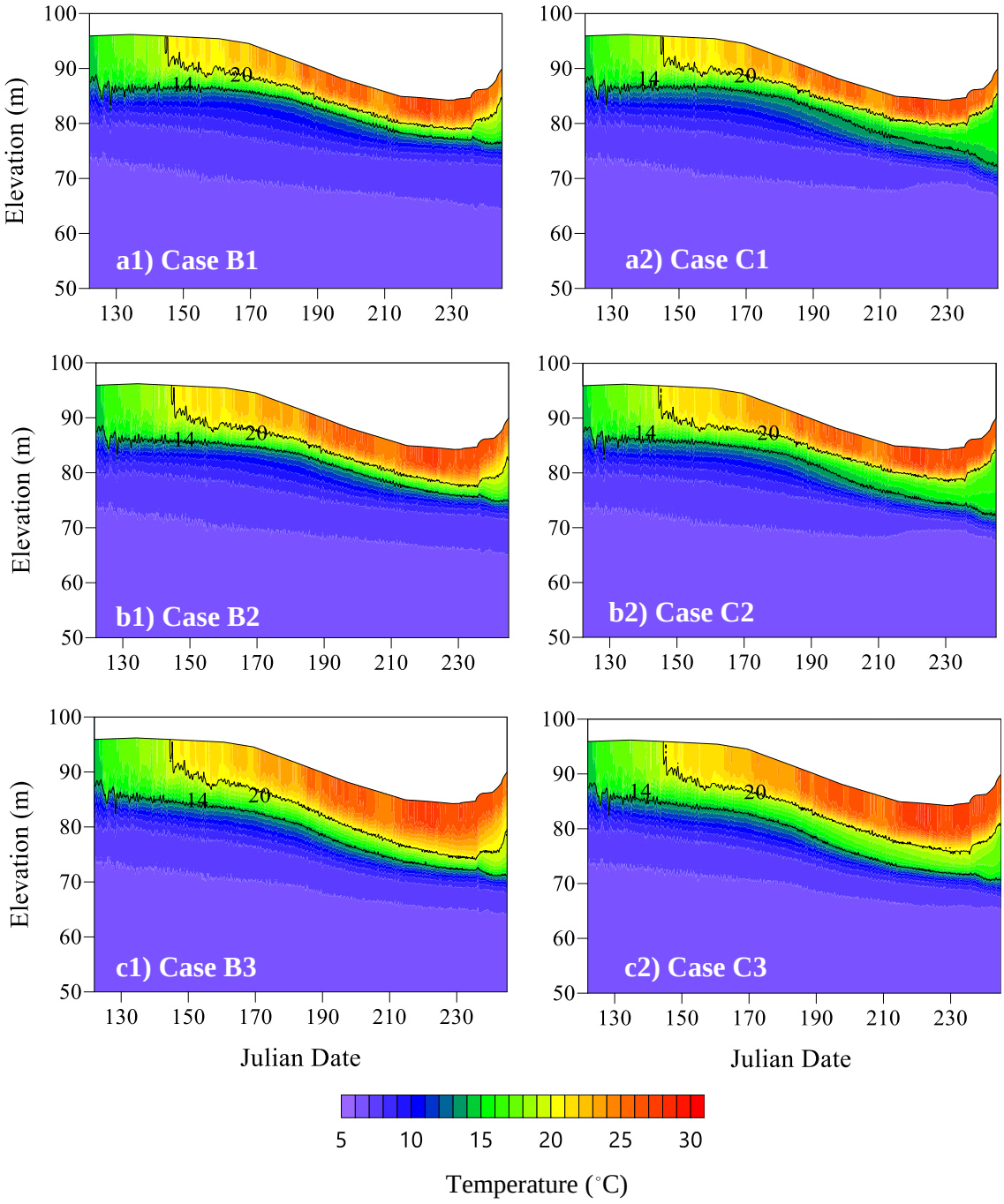

Figure 5.9. Thermal structure of the reservoir corresponding to Case B/"no VC" scenario (a1, b1 and c1) and Case C/"with VC" scenario (a2, b2 and c2) for the year 2016. B1 and C1 operate on 4-m SW intake level while B2 and C2, 7 m and Case B3 and C3, 10 m.

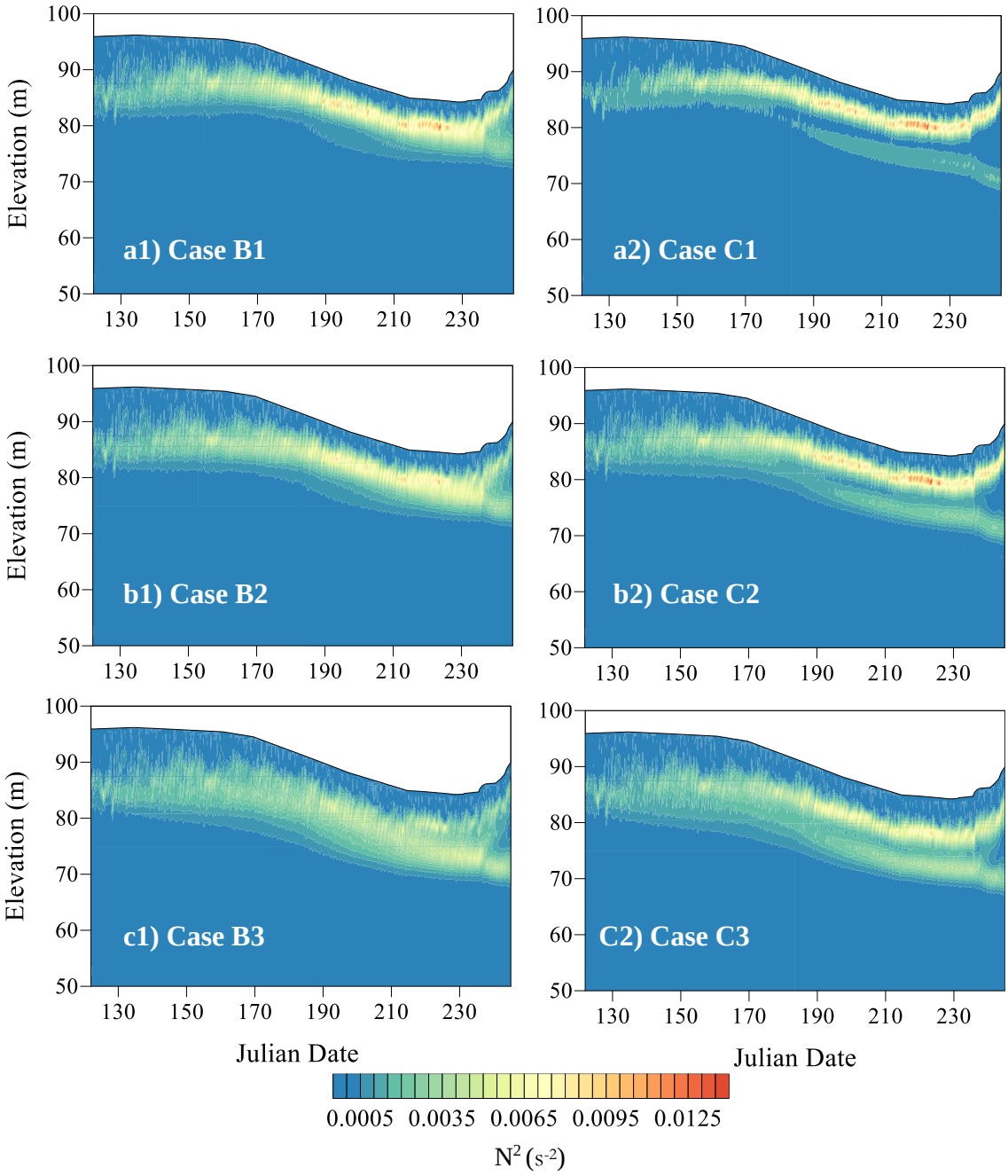

Figure 5.10. Distribution of N^2 in the reservoir corresponding to Case B/"no VC" scenario (a1, b1 and c1) and Case C/"with VC" scenario (a2, b2 and c2) for the year 2016. B1 and C1 operate on 4-m SW intake level while B2 and C2, 7 m and Case B3 and C3, 10 m.

5.4.2 Effect of Facilities during a Period with Flood Event

The thermal regimes for the simulation cases considering the year 2015 are provided in **Fig. 5.11**. For the 2015 pre-flood, Cases B (**Figs. 5.11a1, b1** and **c1**) and C (**Figs. 5.11a2, b2** and **c2**), show similar trend of thermal regimes as in no-flood scenario for the 2016 simulation. Thus, the thickness of the epilimnion increases with deeper outflow levels. However, during post-flood, the depth of the 14˚C contour lines increases with deeper outflow levels. The same is true for Case C.

The flood that occurred July 16, 2015 (Day 197) within the period of simulation has a peak discharge of about 110 m^3/s. This event has considerably affected the thermal structure of the reservoir. In terms of the effect of the VC post-flood (Case C), the warmer layer above the 20˚C contour lines is much narrower compared with the cases without the VC (Case B). Likewise, the gap between the 14 and 20˚C contour lines is wider with the VC scenario (Case C). This implies that the VC has largely influenced the dispersion of the flood waters resulting in destratification.

In terms of stratification, the distribution of the N^2 is presented in **Fig. 5.12**. The trends of stratification patterns for the 2015 pre-flood are similar with those of the 2016 simulation. For the scenario without the VC (Case B) (**Figs. 5.12a1, b1** and **c1**), the thickness of the metalimnion increases with deeper intake levels. The intensity of thermocline strength increases with shallower intakes. For the scenario with the VC (Case C) (**Figs. 5.12a2, b2** and **c2**), the thickness of the metalimnion also increases with deeper intake levels. The VC also creates two distinct thermoclines, as shown by the distinct gap between the upper and lower layers.

For the 2015 post-flood, the stratification patterns are greatly modified due to the flood event. Without the VC, the gap of the lower stratified layer increases with outflow depths. With the presence of the VC, this gap becomes much larger further as the intake level deepens. The strength of the upper thermocline increases with the presence of the VC.

It is noteworthy that the flood events could significantly shift and destratify the thermal profile. The model results showed that the occurrence of floods, apart from the facilities, can considerably increase the thickness of the epilimnion. Aside from the atmospheric drivers and reservoir operation schemes, storm inflows are considered to be another factor affecting thermal stratification. In fact, seasonal storm runoffs can

temporarily cause destratification (Huang et al., 2014) while increased inflows associated with heavy rains can totally destroy the thermocline in the riverine zone (Liu et al., 2020). Another numerical simulation study showed that extreme flood events can significantly enhance vertical mixing in the reservoir, resulting in lower thermal stability (He et al., 2019). In cases of normal inflows, it is also interesting to analyze by numerical simulation the effect of stratification to interflow travel time and the transport of sediments and nutrients as affected by the facilities.

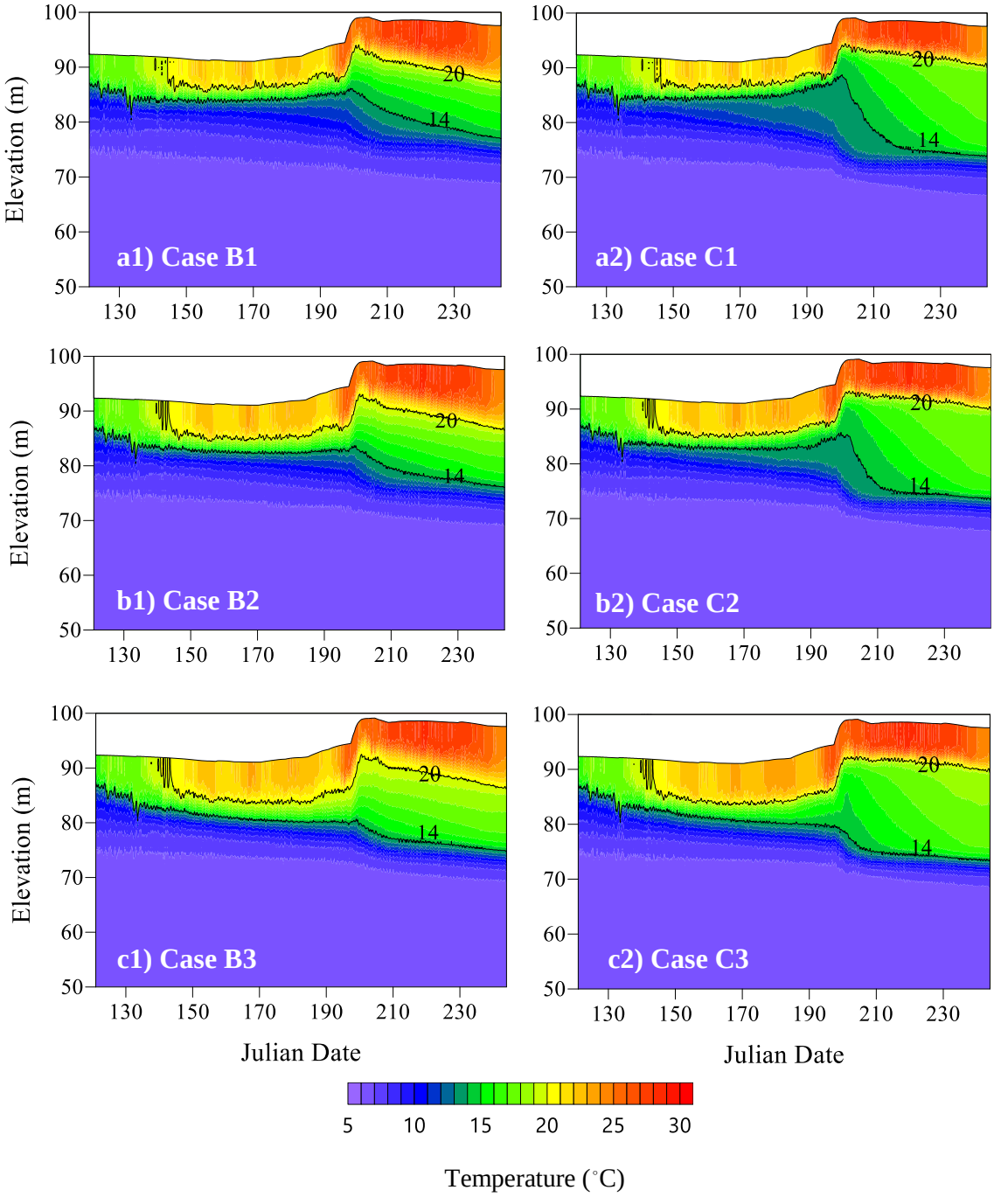

Figure 5.11. Thermal structure of the reservoir corresponding to Case B/"no VC" scenario (a1, b1 and c1) and Case C/"with VC" scenario (a2, b2 and c2) for the year 2015. B1 and C1 operate on 4-m SW intake level while B2 and C2, 7 m and Case B3 and C3, 10 m.

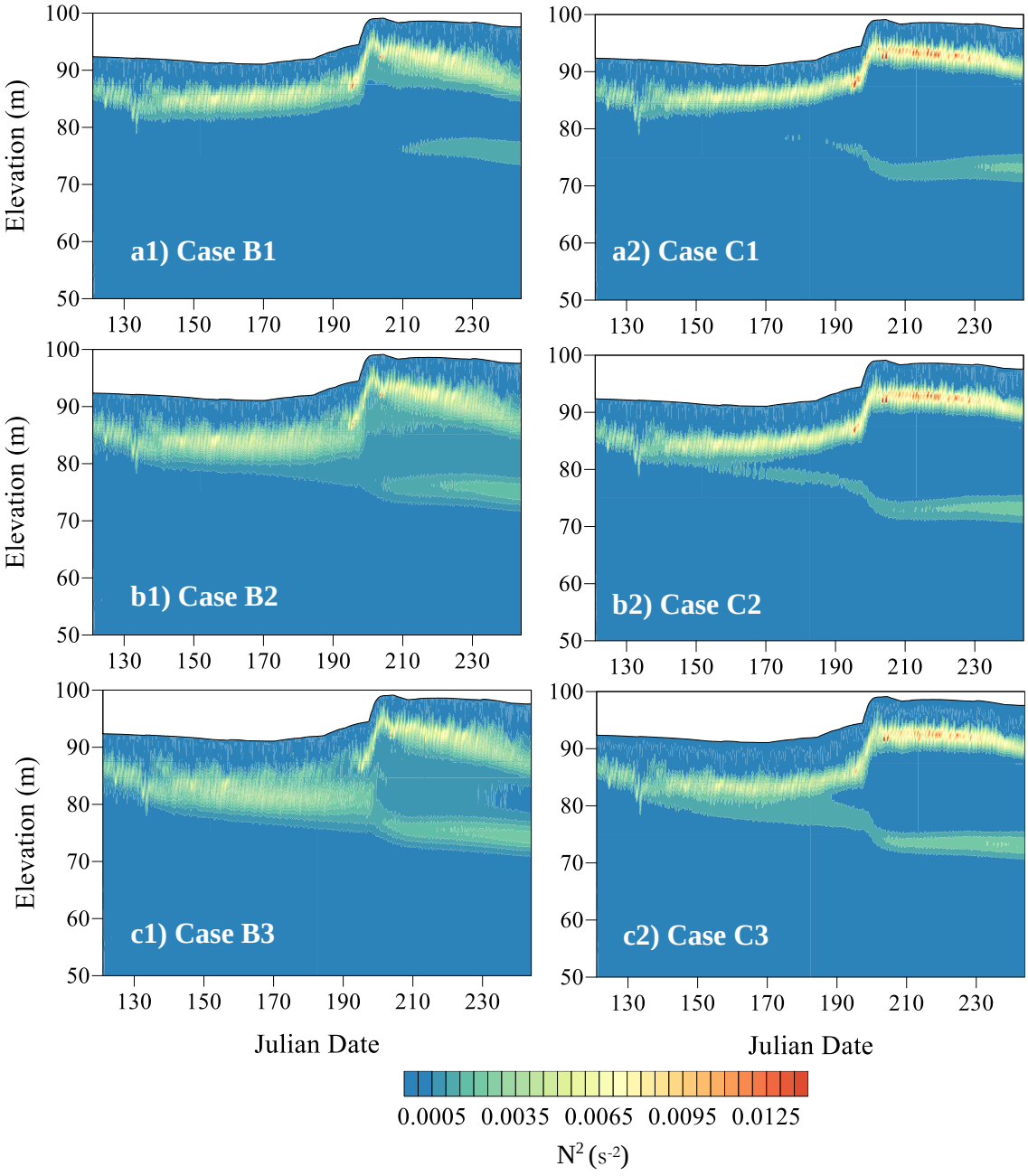

Figure 5.12. Distribution of N^2 in the reservoir corresponding to Case B/"no VC" scenario (a1, b1 and c1) and Case C/"with VC" scenario (a2, b2 and c2) for the year 2015. B1 and C1 operate on 4-m SW intake level while B2 and C2, 7 m and Case B3 and C3, 10 m.

5.5 Sensitivity Analysis of Outflow Temperatures

5.5.1 Effect of Facilities during a Long and Sustained Stratified Period

Generally, the temporal patterns of the outflow temperatures show that shallower outflows yield higher temperatures for the released water. For the without VC scenario (Case B) (**Fig. 5.13**), Case B1 (4 m) has temperatures ranging from 14 to 25.3˚C, while Case B2 (7 m) with 10.3 to 21.8˚C and Case B3 with (8.4 to 20.2 ˚C). On average, lowering the intake gate from 4 m to 7 m results in a temperature drop of 1.6˚C. Likewise, lowering the intake gate from 7 m to 10 m results in a temperature drop of 1.9˚C. For the with VC scenario (Case C) (**Fig. 5.14**), the ranges of temperatures for the individual cases (Cases C1, C2 and C3) are not significantly different from those of Case B.

Even though the thermal regime and stratification of the reservoir vary due to the VC, the resulting outflow temperatures would turn out to be the same. This does not imply however, that the VC has no effect on the outflow temperatures. The similarity of outflow temperatures for Cases B and C is attributed to the averaging of the in-reservoir temperatures through the modified Gaussian profiles. In **Fig 5.15**, although the vertical temperature profiles for both cases are inherently different, the extent of the modified Gaussian profile is large enough to offset this difference in temperature profiles, hence the similar outflow temperatures.

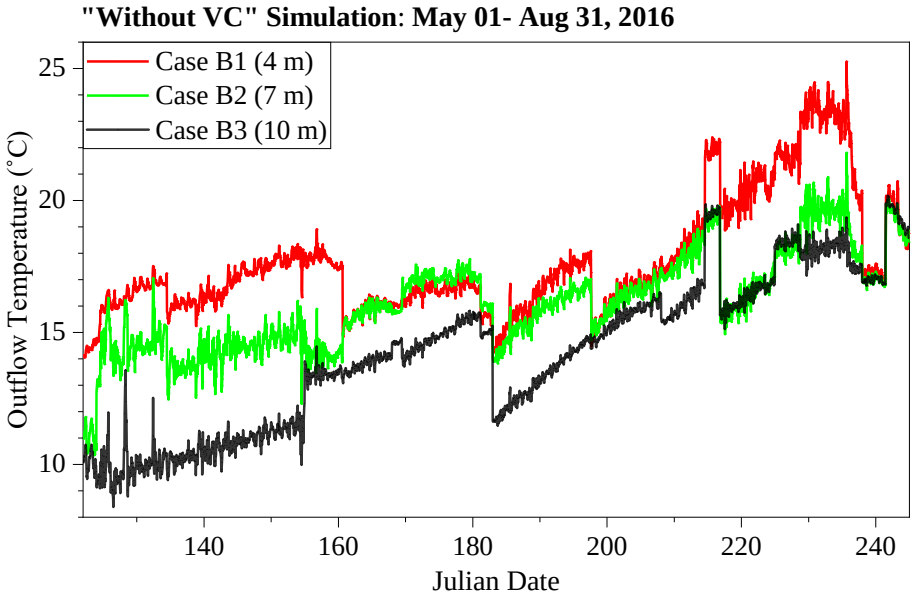

Figure 5.13. Released water temperatures corresponding to “no VC” scenario (Case B) for the year 2016.

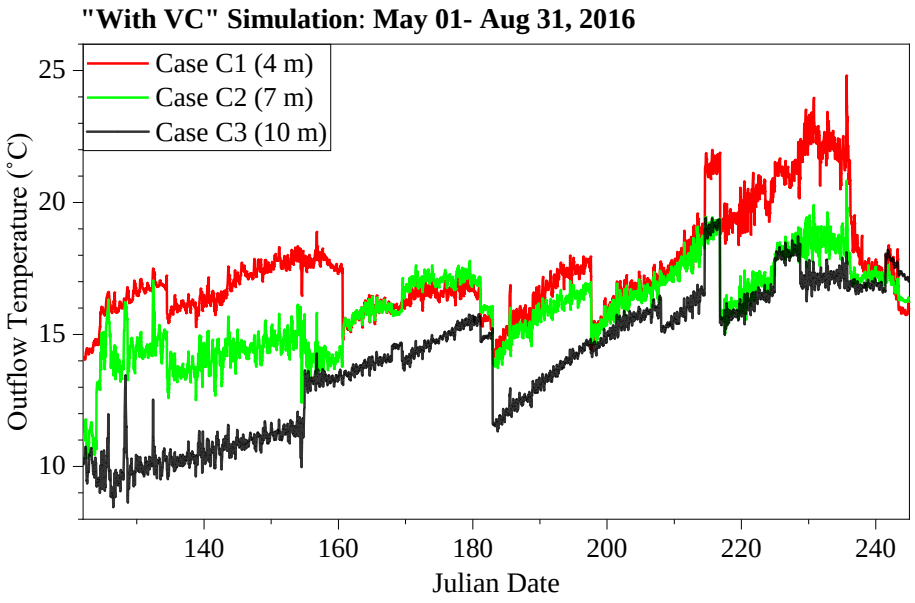

Figure 5.14. Released water temperatures corresponding to "with VC" scenario (Case C) for the year 2016.

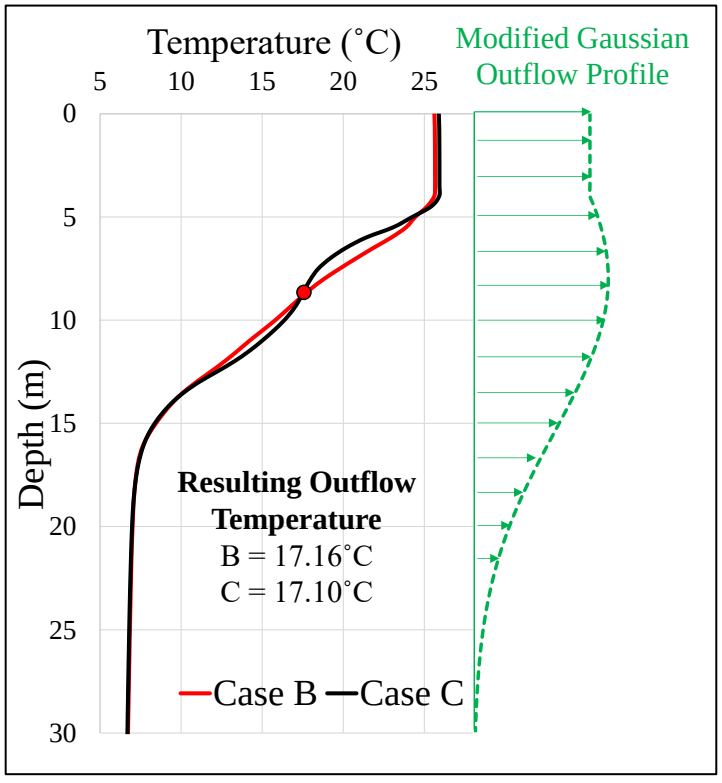

Figure 5.15. Schematic diagram of averaging of outflow temperatures for Cases B and C. Sample is for 22 July 2016 for a 10-m depth outflow.

5.5.2 Effect of Facilities during a Period with a Flood Event

Considering the pre-flood period for the 2015 simulation (**Fig. 5.16** and **5.17**), the temporal patterns of the outflow temperatures show that shallower outflows result in higher temperatures of the released water. This result is similar to the 2016 simulation. The outflow temperatures of Cases B and C are also the same, as explained **Fig. 5.15**.

However, during the post-flood period, the trends of temperatures are essentially similar for Cases B1, B2 and B3. Likewise for the "with VC" scenario, the temperature trends of Cases C1, C2 and C3 are also not significantly different. Since the flood has destratified the water column, the temperature profiles will almost be similar for Cases B1, B2 and B3 and for Cases C1, C2 and C3.

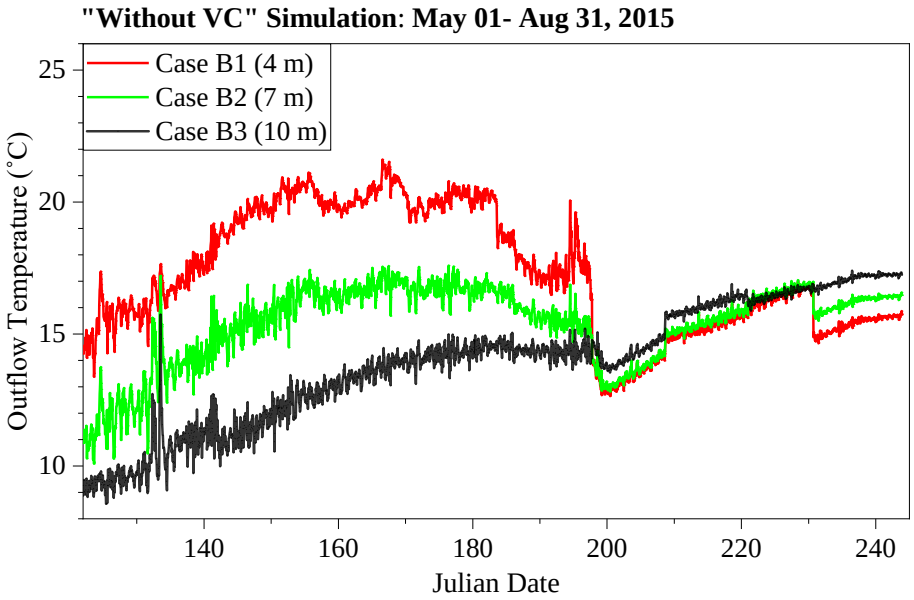

Figure 5.16. Released water temperatures corresponding to "no VC" scenario (Case B) for the year 2015.

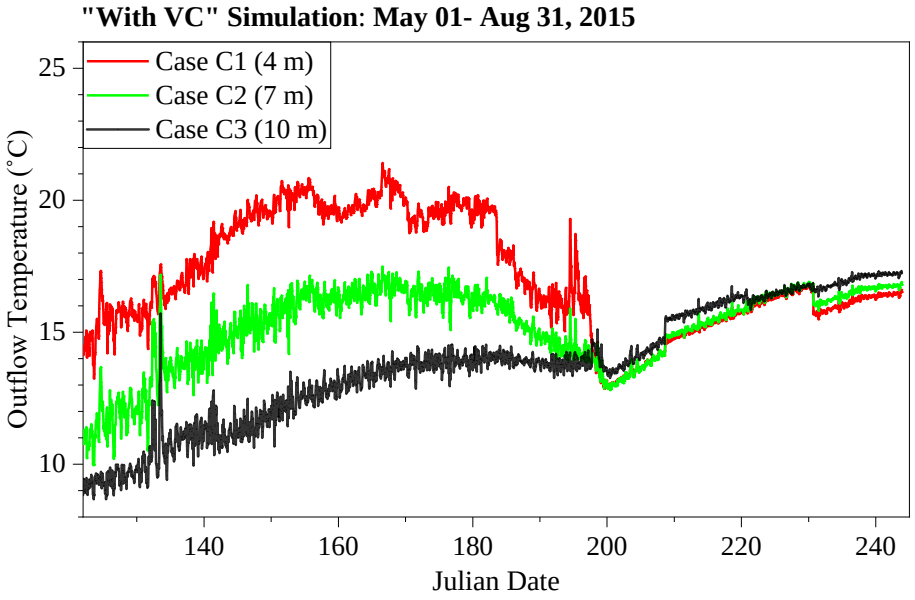

Figure 5.17. Released water temperatures corresponding to "with VC" scenario (Case C) for the year 2015.

5.6 Conclusions

Establishing the outflow profiles using the Modified Gaussian Distribution Method (MGDM) offers an advantage over the Uniform Distribution Method (UDM) in simulating both in-reservoir and outflow temperatures. MGDM is based on empirical evidence as obtained from a previous study (Niiyama et al., 2010b). MGDM accounts for the actual velocity field through the SW, which is promising in reasonably reproducing not only the reservoir temperatures but also the sediment and other water quality distributions. UDM, on the other hand, is simpler and useful in simulating concentrated flows like DPW. For SW operations, UDM can also reproduce reservoir temperature profiles comparable to MGDM, but not so reasonably for outflow temperatures. Since MGDM requires temperature profiles before simulation, UDM can approximate these temperature profiles, which can be used as input later for MGDM for prediction studies. In modeling reservoirs with SW facility, it is recommended to measure the actual velocity field of the outflow and apply these measured velocity distributions in the simulation.

Using the MGDM and UDM techniques, the thermal conditions of the Ogouchi Reservoir were established for the three periods of operation using 3-D simulation. Case A promotes wider thermal dispersion and weaker stratification while Cases B and C produce narrower epilimnion and stronger thermoclines. Simulation confirms that DPW (A) operations result in cold water pollution, which can be mitigated by SW operations (B and C). These results agree with the values of the long-term records of in-reservoir and outflow temperatures in Chapters 3 and 4.

Sensitivity analysis for the operation of the SW showed that deeper outflows yield wider epilimnion but weaker thermoclines. The VC enhances the thickness of the epilimnion and also creates two distinct thermoclines. This is particularly apparent for a period with sustained stratification. However, the presence of the flood causes destratification that widens the epilimnion and weakens the thermocline. In terms of outflow temperatures, shallower outflows result in higher outflow temperatures. Cases B and C do not have significantly different trends of outflow temperatures, as related to the effect of averaging by the modified Gaussian profile. On average, lowering the SW intake gate by three meters would result in a temperature drop of the released waters by 1.6 to 1.9°C.

CHAPTER 6

Conclusions and Recommendations

6.1 Effect of Climate on Reservoir Temperatures

Climate warming can alter the thermal conditions of reservoirs. However, some hydraulic interventions can be explored to mitigate this impact. This study investigates the long-term effects of climate on the temperature and thermal structure of a monomictic reservoir that has had varying operations from 1959 to 2016. Reservoir progressively operated through three distinct periods, namely, (A) deep penstock withdrawal (DPW; 1959–1991), (B) purely selective withdrawal (SW; 1992–2001), and (C) combination of SW and vertical curtain (VC; 2002–2016).

Although annual air temperatures are increasing (+0.15 °C decade^{-1}) in the long term, the reservoir's surface water temperatures have been found to be decreasing (−0.06 °C decade^{-1}). Periods B and C produced colder profiles and exhibited lower heat content and stronger thermoclines than Period A. Flow interception by VCs upstream and outflow control by DPW and SW downstream play a large role in either inhibiting or enhancing the radiant heat transfer from the atmosphere to the reservoir and advection between epilimnion and hypolimnion with the presence of thermocline.

Climate forcing affects the reservoir temperatures within the individual periods, but the varying reservoir operation has been identified to ultimately influence the differences in thermal responses among the periods. Mitigating the thermal impacts of climate warming in reservoirs appears promising with the use of SW and VC.

6.2 Seasonal Variation in Thermal Stratification

This study investigates the thermal stratification responses of a monomictic reservoir operated under different facilities. The analysis of 60-year long data showed that the reservoir's thermal regime varies with season and withdrawal scheme and is affected by upstream reach control through the vertical curtain. Isothermal conditions exist during winter (December-March) while stratification onsets in spring (starting April), intensifies in summer (August) and weakens during fall (October-November).

Considering summer stratification, deep hypolimnetic withdrawals through the penstock intake promoted thicker epilimnion, with low values of thermal stability (Schmidt Stability Index, SSI), thermocline strength index (TSI) and Brunt-Väisälä Frequency (N^2). Meanwhile, shallow withdrawals using selective outflow system resulted in narrower epilimnion, with larger TSI for no curtain scenario and larger SSI for with curtain scenario. Strongest thermoclines do not necessarily translate to largest magnitudes of thermal stability.

Longer duration of stratification is associated with shallow withdrawals. Depending on the outflow depth and the occurrence of prolonged hot or cold atmospheric conditions, the onset of stratification could be likely shifted early or late. Since thermal stratification directly influences the reservoir's water quality regime, this study can be a helpful reference in the water quality management of the reservoir.

6.3 Management of In-Reservoir and Outflow Temperatures

Hydrodynamic modeling in reservoirs usually implements the Uniform Distribution Method (UDM) for outflows. While this may work well in single-point portals like for deep penstock withdrawal (DPW), the case may be different for selective withdrawal (SW). Using actual observations of velocity fields through the SW facility of the Ogouchi Reservoir, a new outflow method called the Modified Gaussian Distribution Method (MGDM) was applied to simulate the in-reservoir and outflow temperatures. Results showed that MGDM can reproduce the two thermal properties more reasonably than UDM. MGDM is promising for modeling with better accuracy for the reservoir temperatures.

Using the MGDM and UDM techniques, the three periods of operation in the reservoir namely, Periods A (DPW), B (SW) and C [SW and vertical curtains (VC)] were replicated through 3-D numerical simulation. Results showed that Case A has wider thermal dispersion and exhibits cold water pollution while Cases B and C develop stronger thermoclines and can mitigate the thermal pollution. Case C has wider epilimnion due deeper SW intake and the presence of the VC. On the other hand, Case B yields warmer releases due to shallower outflows. The results of the simulation of in-reservoir and outflow temperatures agree with the long-term data in Chapters 3 and 4.

Sensitivity analyses were made for the operation of SW at different intake levels (4, 7 and 10 m) and with the presence or absence of the VC. Deeper releases result in wider epilimnion but weaker thermocline. The VC enhances the thickness of the epilimnion and also creates two distinct thermoclines. However, the presence of the flood causes destratification that also widens the epilimnion and weakens the thermocline. In terms of outflow temperatures, deeper outflows result in lower outflow temperatures.

This study has further reinforced the earlier claim of the promising potentials of operation of facilities to mitigate the effects of climate change. In managing the released water temperatures, simulation showed that on average, lowering the SW intake gate by three meters would result in temperature drop of the released waters by 1.6 to 1.9°C.

6.4 Future Work and Recommendation

1) Future studies will include numerical simulations to determine the sensitivity of the reservoir's temperature and thermal structure with varying hydro-meteorological parameters, assuming each facility is operated over the long term. It is promising to examine the effects of climate change on the long-term thermal condition of the reservoir with the aid of simulation and climate projections.

2) The effect of water level variations and floods on thermal stratification can be explored more in detail for this particular reservoir. The interaction of stratification and interflow travel time and the transport of sediments and nutrients can also be investigated using both long-term data analysis and numerical simulation.

3) The best management operation of the SW and VC facilities can be further studied by conducting optimization for the purpose of regulating the in-reservoir and downstream temperatures and other water quality parameters. The outflow temperatures should be compared against the inflow temperatures of the Nippara River.

REFERENCES

Arvola, L., George, G., Livingstone, D.M., Järvinen, M., Blenckner, T., Dokulil, M.T., Jennings, E., Aonghusa, C.N., Nõges, P., Nõges, T., Weyhenmeyer, G.A., 2009. The impact of the changing climate on the thermal characteristics of lakes, in: The Impact of Climate Change on European Lakes. pp. 85–101. https://doi.org/10.1007/978-90-481-2945-4_6

Asaeda, T., Pham, H.S., Nimal Priyantha, D.G., Manatunge, J., Hocking, G.C., 2001. Control of algal blooms in reservoirs with a curtain: A numerical analysis. Ecol. Eng. 16, 395–404. https://doi.org/10.1016/S0925-8574(00)00123-3

Azadi, F., Ashofteh, P.S., Loáiciga, H.A., 2019. Reservoir Water-Quality Projections under Climate-Change Conditions. Water Resour. Manag. 33, 401–421. https://doi.org/10.1007/s11269-018-2109-z

Bayer, T.K., Burns, C.W., Schallenberg, M., 2013. Application of a numerical model to predict impacts of climate change on water temperatures in two deep, oligotrophic lakes in New Zealand. Hydrobiologia 713, 53–71. https://doi.org/10.1007/s10750-013-1492-y

Beutel, M., Hannoun, I., Pasek, J., Kavanagh, K.B., 2007. Evaluation of hypolimnetic oxygen demand in a large eutrophic raw water reservoir San Vicente Reservoir, Calif. J. Environ. Eng. 133, 130–138. https://doi.org/10.1061/(ASCE)0733-9372(2007)133:2(130)

Boehrer, B., Schultze, M., 2008. Stratification of lakes. Rev. Geophys. 46, 1–27. https://doi.org/10.1029/2006RG000210

Brooks, N., Koh, R., 1969. Selective withdrawal from density-stratified reservoirs. Proc. Am. Soc. Civ. Eng. 95, 1369–1400. https://doi.org/https://doi.org/10.1061/JYCEAJ.0002131

Butcher, J.B., Nover, D., Johnson, T.E., Clark, C.M., 2015. Sensitivity of lake thermal and mixing dynamics to climate change. Clim. Change 129, 295–305. https://doi.org/10.1007/s10584-015-1326-1

Çalişkan, A., Elçi, Ş., 2009. Effects of selective withdrawal on hydrodynamics of a

stratified reservoir. Water Resour. Manag. 23, 1257–1273. https://doi.org/10.1007/s11269-008-9325-x

Casamitjana, X., Serra, T., Colomer, J., Baserba, C., Pérez-Losada, J., 2003. Effects of the water withdrawal in the stratification patterns of a reservoir. Hydrobiologia 504, 21–28. https://doi.org/10.1023/B:HYDR.0000008504.61773.77

Chang, C.H., Cai, L.Y., Lin, T.F., Chung, C.L., Van Der Linden, L., Burch, M., 2015. Assessment of the impacts of climate change on the water quality of a small deep reservoir in a humid-subtropical climatic region. Water (Switzerland) 7, 1687–1711. https://doi.org/10.3390/w7041687

Coats, R., Perez-Losada, J., Schladow, G., Richards, R., Goldman, C., 2006. The warming of Lake Tahoe. Clim. Change 76, 121–148. https://doi.org/10.1007/s10584-005-9006-1

Deng, Y., Tuo, Y., Li, J., Li, K., Li, R., 2011. Spatial-temporal effects of temperature control device of stoplog intake for Jinping i hydropower station. Sci. China Technol. Sci. 54, 83–88. https://doi.org/10.1007/s11431-011-4602-y

Duka, M.A., Yokoyama, K., Shintani, T., Iguchi, K., 2019. Effect of selective withdrawal and vertical curtain on reservoir sedimentation: a 3-D numerical modeling approach, in: River, Coastal and Estuarine Morphodynamics. Auckland, New Zealand. https://doi.org/10.13140/RG.2.2.13421.41442

Durran, D.R., Klemp, J.B., 1982. On the effects of moisture on the Brunt-Vaisala frequency. J. Atmos. Sci. 39, 2152–2158. https://doi.org/10.1175/1520-0469(1982)039<2152:OTEOMO>2.0.CO;2

Edlund, M.B., Almendinger, J.E., Fang, X., Hobbs, J.M.R., VanderMeulen, D.D., Key, R.L., Engstrom, D.R., 2017. Effects of climate change on lake thermal structure and biotic response in northern wilderness lakes. Water (Switzerland) 9, 1–35. https://doi.org/10.3390/w9090678

Engelhardt, C., Kirillin, G., 2014. Criteria for the onset and breakup of summer lake stratification based on routine temperature measurements. Fundam. Appl. Limnol. 184, 183–194. https://doi.org/10.1127/1863-9135/2014/0582

Feldbauer, J., Kneis, D., Hegewald, T., Berendonk, T.U., Petzoldt, T., 2020. Managing climate change in drinking water reservoirs: potentials and limitations of dynamic withdrawal strategies. Environ. Sci. Eur. 32, 1–17. https://doi.org/10.1186/s12302-020-00324-7

Ficker, H., Luger, M., Gassner, H., 2017. From dimictic to monomictic: Empirical evidence of thermal regime transitions in three deep alpine lakes in Austria induced by climate change. Freshw. Biol. 62, 1335–1345. https://doi.org/10.1111/fwb.12946

Galperin, B., Kantha, L.H., Hassid, S., Rosati, A., 1988. A quasi-equilibrium turbulent energy model for geophysical flows. J. Atmos. Sci. 45, 55–62. https://doi.org/10.1175/1520-0469(1988)045<0055:AQETEM>2.0.CO;2

Gunay, C.J.C., Duka, M.A., Yokoyama, K., 2019. Long-term analysis of sediment yield in Ogouchi watershed, in: Friedrich, H., Bryan, K. (Eds.), RCEM 2019: Book of Abstracts. International Association for Hydro-Environment Engineering and Research, Auckland, New Zealand, p. 125.

Hanna, R.B., Saito, L., Bartholow, J.M., Sandelin, J., 1999. Results of simulated temperature control device operations on in-reservoir and discharge water temperatures using CE-QUAL-W2. Lake Reserv. Manag. 15, 87–102. https://doi.org/10.1080/07438149909353954

Hayes, N.M., Deemer, B.R., Corman, J.R., Razavi, N.R., Strock, K.E., 2017. Key differences between lakes and reservoirs modify climate signals: A case for a new conceptual model. Limnol. Oceanogr. Lett. 2, 47–62. https://doi.org/10.1002/lol2.10036

He, W., Lian, J., Zhang, J., Yu, X., Chen, S., 2019. Impact of intra-annual runoff uniformity and global warming on the thermal regime of a large reservoir. Sci. Total Environ. 658, 1085–1097. https://doi.org/10.1016/j.scitotenv.2018.12.207

Heiskanen, J.J., Mammarella, I., Ojala, A., Stepanenko, V., Erkkilä, K.M., Miettinen, H., Sandström, H., Eugster, W., Leppäranta, M., Järvinen, H., Vesala, T., Nordbo, A., 2015. Effects of water clarity on lake stratification and lake-atmosphere heat exchange. J. Geophys. Res. 120, 7412–7428. https://doi.org/10.1002/2014JD022938

Helfer, F., Lemckert, C., Zhang, H., 2012. Impacts of climate change on temperature and

evaporation from a large reservoir in Australia. J. Hydrol. 475, 365–378. https://doi.org/10.1016/j.jhydrol.2012.10.008

Hondzo, M., Stefan, H.G., 1993. Regional water temperature characteristics of lakes subjected to climate change. Clim. Change 24, 187–211. https://doi.org/10.1007/BF01091829

Huang, T., Li, X., Rijnaarts, H., Grotenhuis, T., Ma, W., Sun, X., Xu, J., 2014. Effects of storm runoff on the thermal regime and water quality of a deep, stratified reservoir in a temperate monsoon zone, in Northwest China. Sci. Total Environ. 485–486, 820–827. https://doi.org/10.1016/j.scitotenv.2014.01.008

Hueftle, S.J., Stevens, L.E., 2001. Experimental flood effects on the limnology of Lake Powell reservoir, southwestern USA. Ecol. Appl. 11, 644–656. https://doi.org/10.1890/1051-0761(2001)011[0644:EFEOTL]2.0.CO;2

Idso, S.B., 1973. On the concept of lake stability. Limnol. Oceanogr. https://doi.org/10.4319/lo.1973.18.4.0681

James, S., Arifin, R., Hamlet, A., 2017. Investigating summer thermal stratification in Lake Ontario. AGU Fall Meet. Abstr.

Japan Meteorological Agency, 2017. Climate Change Monitoring Report 2016. Chiyoda, Tokyo.

Japan Meteorological Agency, n.d. Overview of Japan's climate [WWW Document]. URL https://www.data.jma.go.jp/gmd/cpd/longfcst/en/tourist_japan.html (accessed 8.15.19).

Johnson, P., LaFond, R., Webber, D.W., 1991. PAP-733 Temperature Control Device for Shasta Dam by Richard LaFond Presented to the Japan Dam Engineering Center November 1991.

Kendall, M.G., 1975. Rank Correlation Methods, Charles Griffin.

Kobler, U.G., Wüest, A., Schmid, M., 2019. Combined effects of pumped-storage operation and climate change on thermal structure and water quality. Clim. Change 152. https://doi.org/10.1007/s10584-018-2340-x

Kondo, J., 1975. Air-sea bulk transfer coefficients in diabatic conditions. Boundary-Layer

Meteorol. 9, 91–112. https://doi.org/10.1007/BF00232256

Koue, J., Shimadera, H., Matsuo, T., Kondo, A., 2018. Evaluation of thermal stratification and flow field reproduced by a three-dimensional hydrodynamic model in Lake Biwa, Japan. Water (Switzerland) 10, 1–20. https://doi.org/10.3390/w10010047

Kruskal, W.H., Wallis, W.A., 1952. Use of Ranks in One-Criterion Variance Analysis. J. Am. Stat. Assoc. 47, 583–621. https://doi.org/10.1080/01621459.1952.10483441

Kumar Dutta, R., Ma, J., Das, B., Liu, D., 2019. Modeling effects of floating curtain weirs and controlling algal Blooms in a subtropical reservoir of china. Am. J. Water Resour. 7, 42–49. https://doi.org/10.12691/ajwr-7-2-1

Lee, H., Chung, S., Ryu, I., Choi, J., 2013. Three-dimensional modeling of thermal stratification of a deep and dendritic reservoir using ELCOM model. J. Hydro-Environment Res. 7, 124–133. https://doi.org/10.1016/j.jher.2012.10.002

Lee, R.M., Biggs, T.W., Fang, X., 2018. Thermal and hydrodynamic changes under a warmer climate in a variably stratified hypereutrophic reservoir. Water (Switzerland) 10, 1–24. https://doi.org/10.3390/w10091284

Leonard, B.P., 1991. The ULTIMATE conservative difference scheme applied to unsteady one-dimensional advection. Comput. Methods Appl. Mech. Eng. 88, 17–74. https://doi.org/10.1016/0045-7825(91)90232-U

Lewis, W.M., McCutchan, J.H., Roberson, J., 2019. Effects of climatic change on temperature and thermal structure of a mountain reservoir. Water Resour. Res. 55, 1988–1999. https://doi.org/10.1029/2018WR023555

Liu, Miao, Zhang, Yunlin, Shi, K., Zhang, Yibo, Zhou, Y., Zhu, M., Zhu, G., Wu, Z., Liu, Mingliang, 2020. Effects of rainfall on thermal stratification and dissolved oxygen in a deep drinking water reservoir. Hydrol. Process. 34, 3387–3399. https://doi.org/10.1002/hyp.13826

Liu, Miao, Zhang, Yunlin, Shi, K., Zhu, G., Wu, Z., Liu, Mingliang, Zhang, Yibo, 2019. Thermal stratification dynamics in a large and deep subtropical reservoir revealed by high-frequency buoy data. Sci. Total Environ. 651, 614–624. https://doi.org/10.1016/j.scitotenv.2018.09.215

Liu, W.C., Chen, W.B., Kimura, N., 2009. Impact of phosphorus load reduction on water quality in a stratified reservoir-eutrophication modeling study. Environ. Monit. Assess. 159, 393–406. https://doi.org/10.1007/s10661-008-0637-3

Ma, S., Kassinos, S.C., Fatta Kassinos, D., Akylas, E., 2008. Effects of selective water withdrawal schemes on thermal stratification in Kouris Dam in Cyprus. Lakes Reserv. Res. Manag. 13, 51–61. https://doi.org/10.1111/j.1440-1770.2007.00353.x

Magee, M.R., Wu, C.H., 2017. Response of water temperatures and stratification to changing climate in three lakes with different morphometry. Hydrol. Earth Syst. Sci. 21, 6253–6274. https://doi.org/10.5194/hess-21-6253-2017

Mann, H.B., 1945. Nonparametric Tests Against Trend. Econometrica 70, 245–259. https://doi.org/10.2307/1907187

Mann, H.B., Whitney, D.R., 1947. On a test of whether one of two random variables is stochastically larger than the other. Ann. Math. Stat. 18, 50–60.

Martin, D.B., Arneson, R.D., 1978. Comparative limnology of a deep-discharge reservoir and a surface-discharge lake on the Madison River, Montana. Freshw. Biol. 8, 33–42. https://doi.org/10.1111/j.1365-2427.1978.tb01423.x

Matsumoto, J., Fujibe, F., Takahashi, H., 2017. Urban climate in the Tokyo metropolitan area in Japan. J. Environ. Sci. (China) 59, 54–62. https://doi.org/10.1016/j.jes.2017.04.012

Mi, C., Sadeghian, A., Lindenschmidt, K.E., Rinke, K., 2019. Variable withdrawal elevations as a management tool to counter the effects of climate warming in Germany's largest drinking water reservoir. Environ. Sci. Eur. 31, 1–15. https://doi.org/10.1186/s12302-019-0202-4

Moreno-Ostos, E., Marcé, R., Ordóñez, J., Dolz, J., Armengol, J., 2008. Hydraulic management drives heat budgets and temperature trends in a Mediterranean reservoir. Int. Rev. Hydrobiol. 93, 131–147. https://doi.org/10.1002/iroh.200710965

Muraoka, P.B., Amano, K., J., M., 2011. Effects of suspended solids concentration and particle size on survival and gill structure in fish, in: Proceedings of the 34th World Congress of the International Association for Hydro-Environment Engineering and

Research. Brisbane, Australia, pp. 2893–2900.

Niiyama, M., Kouga, K., Yokoyama, K., Koizumi, A., Yamazaki, K., Masuko, A., Kobayashi, Y., Minegishi, N., 2010a. Influence of the vertical fence on the movement of a density current in awater supply reservoir. J. JSCE, Ser. B1 (Hydraul. Eng.) 54, 1417–1422.

Niiyama, M., Tsuge, M., Yokoyama, K., Koizumi, A., Yamazaki, K., Mashiko, A., Kobayashi, Y., 2010b. Study on the Intake Flow in a Stratified Reservoir. J. JSCE, Ser. B1 (Hydraul. Eng.) 54, 1411–1416.

O'Reilly, C.M., Sharma, S., Gray, D.K., Hampton, S.E., Read, J.S., Rowley, R.J., Schneider, P., Lenters, J.D., McIntyre, P.B., Kraemer, B.M., Weyhenmeyer, G.A., Straile, D., Dong, B., Adrian, R., Allan, M.G., Anneville, O., Arvola, L., Austin, J., Bailey, J.L., Baron, J.S., Brookes, J.D., De Eyto, E., Dokulil, M.T., Hamilton, D.P., Havens, K., Hetherington, A.L., Higgins, S.N., Hook, S., Izmest'Eva, L.R., Joehnk, K.D., Kangur, K., Kasprzak, P., Kumagai, M., Kuusisto, E., Leshkevich, G., Livingstone, D.M., MacIntyre, S., May, L., Melack, J.M., Mueller-Navarra, D.C., Naumenko, M., Noges, P., Noges, T., North, R.P., Plisnier, P.D., Rigosi, A., Rimmer, A., Rogora, M., Rudstam, L.G., Rusak, J.A., Salmaso, N., Samal, N.R., Schindler, D.E., Schladow, S.G., Schmid, M., Schmidt, S.R., Silow, E., Soylu, M.E., Teubner, K., Verburg, P., Voutilainen, A., Watkinson, A., Williamson, C.E., Zhang, G., 2015. Rapid and highly variable warming of lake surface waters around the globe. Geophys. Res. Lett. 42, 10,773-10781. https://doi.org/10.1002/2015GL066235

Olden, J.D., Naiman, R.J., 2010. Incorporating thermal regimes into environmental flows assessments: Modifying dam operations to restore freshwater ecosystem integrity. Freshw. Biol. 55, 86–107. https://doi.org/10.1111/j.1365-2427.2009.02179.x

Park, C.H., Park, M.H., Kim, K.H., Kim, N.Y., Kim, Y.H., Gwon, E.M., Kim, B.H., Lim, B.J., Hwang, S.J., 2017. A physical pre-treatment method (Vertical Weir Curtain) for mitigating cyanobacteria and some of their metabolites in a drinking water reservoir. Water (Switzerland) 9, 1–12. https://doi.org/10.3390/w9100775

Point, S., 2016. Factors that Affect Water Clarity, in: Chemistry Manual. University of Wisconsin, pp. 15–20.

Ragotzkie, R.A., 1978. Heat Budgets of Lakes, in: Lerman, A. (Ed.), Lakes - Chemistry, Geology, Physics. Springer, New York, pp. 1–19. https://doi.org/10.1007/978-1-4757-1152-3_1

Rheinheimer, D.E., Null, S.E., Lund, J.R., 2015. Optimizing Selective Withdrawal from Reservoirs to Manage Downstream Temperatures with Climate Warming. J. Water Resour. Plan. Manag. 141, 04014063-1–9. https://doi.org/10.1061/(asce)wr.1943-5452.0000447

Richard Marzolf, G., Bowser, C.J., Hart, R.J., 2000. The withdrawal zone in Lake Powell reservoir during a controlled flood through Glen Canyon Dam on the Colorado River — Arizona, USA. SIL Proceedings, 1922-2010 27, 2440–2443. https://doi.org/10.1080/03680770.1998.11901679

Rose, K.C., Winslow, L.A., Read, J.S., Hansen, G.J.A., 2016. Climate-induced warming of lakes can be either amplified or suppressed by trends in water clarity. Limnol. Oceanogr. Lett. 1, 44–53. https://doi.org/10.1002/lol2.10027

Sahoo, G.B., Forrest, A.L., Schladow, S.G., Reuter, J.E., Coats, R., Dettinger, M., 2016. Climate change impacts on lake thermal dynamics and ecosystem vulnerabilities. Limnol. Oceanogr. 61, 496–507. https://doi.org/10.1002/lno.10228

Scheu, K.R., Fong, D.A., Monismith, S.G., Fringer, O.B., 2015. Sediment transport dynamics near a river inflow in a large alpine lake. Limnol. Oceanogr. 60, 1195–1211. https://doi.org/10.1002/lno.10089

Schmid, M., Hunziker, S., Wüest, A., 2014. Lake surface temperatures in a changing climate: A global sensitivity analysis. Clim. Change 124, 301–315. https://doi.org/10.1007/s10584-014-1087-2

Schneider, P., Hook, S.J., 2010. Space observations of inland water bodies show rapid surface warming since 1985. Geophys. Res. Lett. 37, 1–5. https://doi.org/10.1029/2010GL045059

Sen, P.K., 1968. Estimates of the Regression Coefficient Based on Kendall's Tau. J. Am. Stat. Assoc. 63, 1379–1389. https://doi.org/10.1080/01621459.1968.10480934

Skowron, R., 2009. Criteria of Thermal Classifications of Lakes. Bull. Geogr. Phys.

Geogr. Ser. 2, 89–105. https://doi.org/10.2478/bgeo-2009-0014

Smith, V.H., Sieber-Denlinger, J., deNoyelles, F., Campbell, S., Pan, S., Randtke, S.J., Blain, G.T., Strasser, V.A., 2002. Managing taste and odor problems in a eutrophic drinking water reservoir. Lake Reserv. Manag. 18, 319–323. https://doi.org/10.1080/07438140209353938

Stainsby, E.A., Winter, J.G., Jarjanazi, H., Paterson, A.M., Evans, D.O., Young, J.D., 2011. Changes in the thermal stability of Lake Simcoe from 1980 to 2008. J. Great Lakes Res. 37, 55–62. https://doi.org/10.1016/j.jglr.2011.04.001

Takahashi, T., 2008. The Influence of Surface Water Discharge on the Occurrence of Blue- Green Algae Water Bloom and Countermeasures to Prevent Blue- Green Algae Water Bloom from Occurring in the Ogochi Reservoir. Proc. IWA World Water Congr. Vienna, Austria. Sept. 7-12, 2008.

Tanentzap, A.J., Yan, N.D., Keller, B., Girard, R., Heneberry, J., Gunn, J.M., Hamilton, D.P., Taylor, P.A., 2008. Cooling lakes while the world warms: Effects of forest regrowth and increased dissolved organic matter on the thermal regime of a temperate, urban lake. Limnol. Oceanogr. 53, 404–410. https://doi.org/10.4319/lo.2008.53.1.0404

Trumpickas, J., Shuter, B.J., Minns, C.K., 2009. Forecasting impacts of climate change on Great Lakes surface water temperatures. J. Great Lakes Res. 35, 454–463. https://doi.org/10.1016/j.jglr.2009.04.005

Umlauf, L., Burchard, H., 2003. A generic length-scale equation for geophysical turbulence models. J. Mar. Res. 61, 235–265. https://doi.org/10.1357/002224003322005087

Veerapaga, N., Azhikodan, G., Shintani, T., Iwamoto, N., Yokoyama, K., 2019. A three-dimensional environmental hydrodynamic model, Fantom-Refined: Validation and application for saltwater intrusion in a meso-macrotidal estuary. Ocean Model. 141, 1–20. https://doi.org/10.1016/j.ocemod.2019.101425

Wang, S., Qian, X., Han, B.-P., Luo, L.-C., Hamilton, D.P., 2012. Effects of local climate and hydrological conditions on the thermal regime of a reservoir at Tropic of Cancer, in southern China. Water Res. 46, 2591–2604.

https://doi.org/10.1016/j.watres.2012.02.014

Warner, J.C., Sherwood, C.R., Arango, H.G., Signell, R.P., 2005. Performance of four turbulence closure models implemented using a generic length scale method. Ocean Model. 8, 81–113. https://doi.org/10.1016/j.ocemod.2003.12.003

Weber, M., Rinke, K., Hipsey, M.R., Boehrer, B., 2017. Optimizing withdrawal from drinking water reservoirs to reduce downstream temperature pollution and reservoir hypoxia. J. Environ. Manage. https://doi.org/10.1016/j.jenvman.2017.03.020

Wetzel, R., 2001. Limnology, Lake and River Ecosystems. Academic Press, New York.

Wilcoxon, F., 1945. Individual Comparisons by Ranking Methods. Biometrics Bull. 1, 80. https://doi.org/doi:10.2307/3001968

Woolway, R.I., Merchant, C.J., 2019. Worldwide alteration of lake mixing regimes in response to climate change. Nat. Geosci. https://doi.org/10.1038/s41561-019-0322-x

Woolway, R.I., Weyhenmeyer, G.A., Schmid, M., Dokulil, M.T., de Eyto, E., Maberly, S.C., May, L., Merchant, C.J., 2019. Substantial increase in minimum lake surface temperatures under climate change. Clim. Change 155, 81–94. https://doi.org/10.1007/s10584-019-02465-y

Xu, Z., Takeuchi, K., Ishidaira, H., 2002. Long-term trends of annual temperature and precipitation time series in Japan. J. Hydrosci. Hydraul. Eng. 20, 11–26.

Yu, H., Tsuno, H., Hidaka, T., Jiao, C., 2010. Chemical and thermal stratification in lakes. Limnology 11, 251–257. https://doi.org/10.1007/s10201-010-0310-8

Zaointz, C., 2019. Real statistics using Excel: Mann-Kendall test [WWW Document]. URL https://www.real-statistics.com/time-series-analysis/time-series-miscellaneous/mann-kendall-test/?fbclid=IwAR2FcFReolelWvgnm29hC_S0A8ClSJxUsDEQ2540K9YXkru4fe8PWNDygEY (accessed 7.15.19).

Zhang, F., Zhang, H., Bertone, E., Stewart, R., Lemckert, C., Cinque, K., 2020. Numerical study of the thermal structure of a stratified temperate monomictic drinking water reservoir. J. Hydrol. Reg. Stud. 30, 100699.

https://doi.org/10.1016/j.ejrh.2020.100699

Zhang, Y., Wu, Z., Liu, M., He, J., Shi, K., Zhou, Y., Wang, M., Liu, X., 2015. Dissolved oxygen stratification and response to thermal structure and long-term climate change in a large and deep subtropical reservoir (Lake Qiandaohu, China). Water Res. 75, 249–258. https://doi.org/10.1016/j.watres.2015.02.052

Zouabi-Aloui, B., Adelana, S.M., Gueddari, M., 2015. Effects of selective withdrawal on hydrodynamics and water quality of a thermally stratified reservoir in the southern side of the Mediterranean Sea: a simulation approach. Environ. Monit. Assess. 187, 292. https://doi.org/10.1007/s10661-015-4509-3